Supporting Information for

Azaylide-based Gemini Amphiphiles Displaying Unique Self-Assembling Behavior via Even–Odd Effect of Alkyl Linker Chain Length

Yoshimori Akiyama, Masahiro Yamashina,* and Shinji Toyota*

Department of Chemistry, School of Science, Tokyo Institute of Technology, 2-12-1 Ookayama, Meguro-ku, Tokyo 152-8551, Japan.

1. General

All reagents and solvents were purchased from commercial sources and used as received. NMR spectra were recorded using a JEOL 500 MHz JNM-ECX500 spectrometer, a 500 MHz JNM-ECZ500 spectrometer, a Bruker 600 MHz Avance III HD Smart Probe NMR spectrometer. Chemical shifts for ^{1}H, ^{13}C, and ^{31}P are reported in ppm on the δ scale; ^{1}H and ^{13}C signals were referenced to the residual solvent peak, and ^{31}P was referenced to an external standard of 85% H_3PO_4 in D_2O at 0.00 ppm. Electrospray ionization time-of-flight (ESI-TOF) was performed on a Bruker micrOTOF II mass Spectrometer. Fourier transform infrared (FT-IR) spectra were measured by a JASCO FT/IR 4100. Single crystal X-ray crystallography was carried out with a Rigaku XtaLAB Synergy R/DW HyPix diffractometer with multi-layer mirror monochromated Cu Kα radiation (λ = 1.54184 Å) and processed on a CrysAlisPro 1.171 (Rigaku Oxford Diffraction, 2018), and a diffractometer equipped in a beamline PF-BL5a at the High Energy Accelerator Research Organization (KEK), Japan with a Pilatus3 S6M detector (synchrotron, λ = 0.7500 Å) and processed on an XDS ver 2022.01.10[S1]. The structure was solved by intrinsic phasing methods using SHELXT-2018[S2] and then refined with SHELXL-2016[S3] using the Olex2.1.5[S4] as graphical user interfaces. Since some of solvent molecules were significantly disordered, the solvent mask was performed for the refinement. Powder X-ray diffraction data were collected for samples on a Rigaku MiniFlex600. Elemental analyses were performed on a Perkin-Elmer 2400 instrument. UV-visible absorption spectroscopy was performed using a JASCO V-730 UV-Vis-NIR spectrophotometer. Samples were analyzed using quartz cuvettes with optical path lengths of 2.0 mm. Fluorescence spectroscopy was performed using a JASCO FP-8550 spectrofluorometer. Samples were analyzed at room temperature using quartz cuvettes with optical path lengths of 2.0 mm. Molecular mechanics calculation was conducted by Materials Studio program (version 5.5.3, BIOVIA, USA) with the UFF force field. The MM calculation was performed without Cl^- ions, and a point charge was assigned to the nitrogen atom in the trimethylammonium group. The optimized structure of micelles was calculated from an initial state, where multiple amphiphilic molecules were arranged spherically so that the averaged distance between carbonyl groups on the hydrophilic part closely matched the value estimated by DLS analysis. DLS spectra were recorded by a Wyatt Technology DynaPro NanoStar with Nano Disp Microcuvettes at 298 K. AFM images were obtained using an Oxford Instruments Cypher S. TEM images were obtained using a HITACHI H-

7650 type zero A. TEM samples were stained by a Nissin-EM EM stainer or a Nanoprobes inc. Nano-W.

References

[S1]. W. Kabsch *Acta Cryst.* 2010, **D66**, 125–132.

[S2]. G. M. Sheldrick *Acta Cryst.* 2015, **A71**, 3–8.

[S3]. G. M. Sheldrick *Acta Cryst.* 2015, **C71**, 3–8

[S4]. O. V. Dolomanov, L. J. Bourhis, R. J. Gildea, J. A. K. Howard and H. Puschmann *J. Appl. Cryst.* 2009, **42**, 339–341.

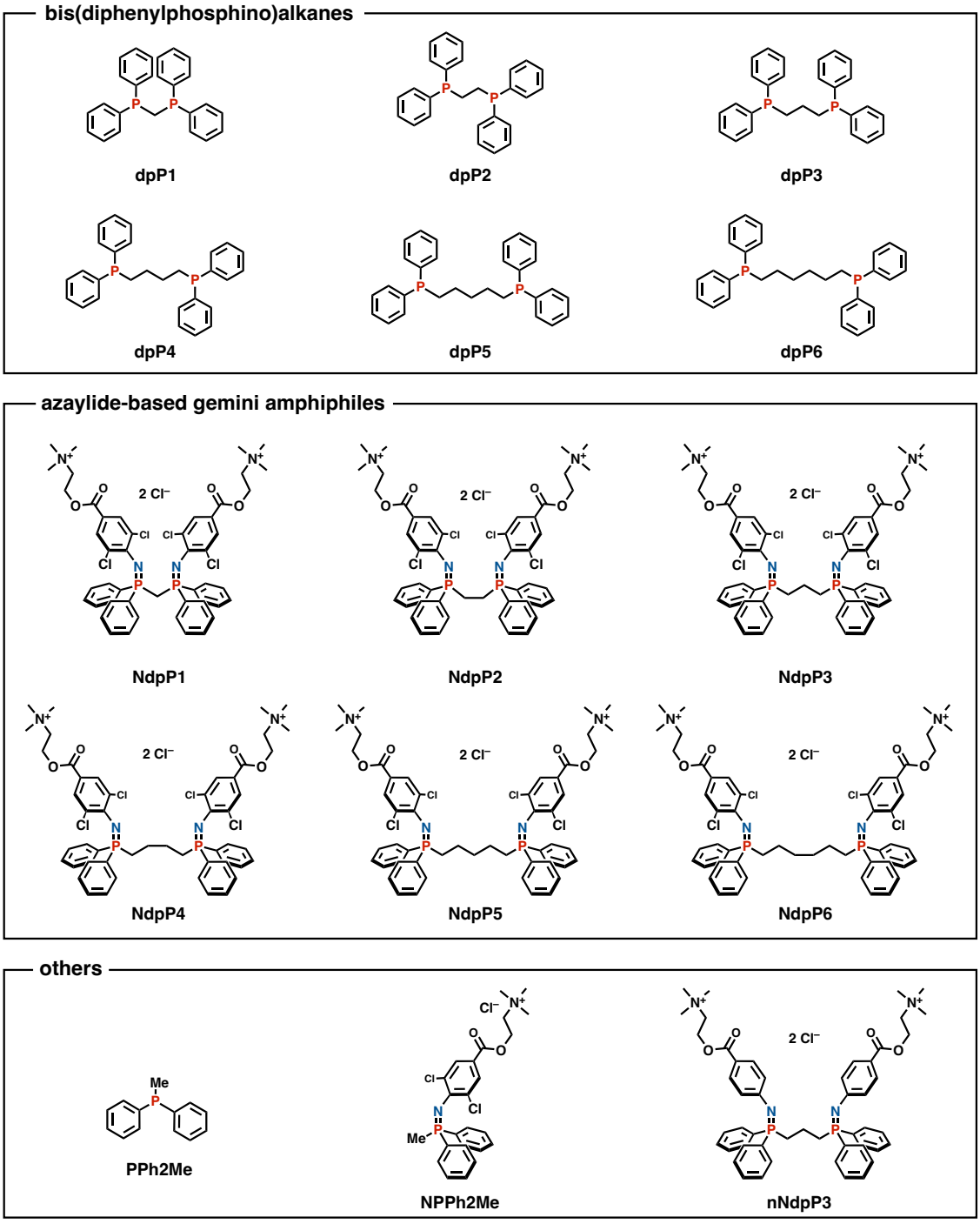

Figure S1. Chemical structures of bis(diphenylphosphino)alkanes, corresponding azaylide-based gemini amphiphiles, and related compounds used in this study.

2. Synthesis

2.1. Preparation of NdpPn via the Staudinger reaction YA1-168

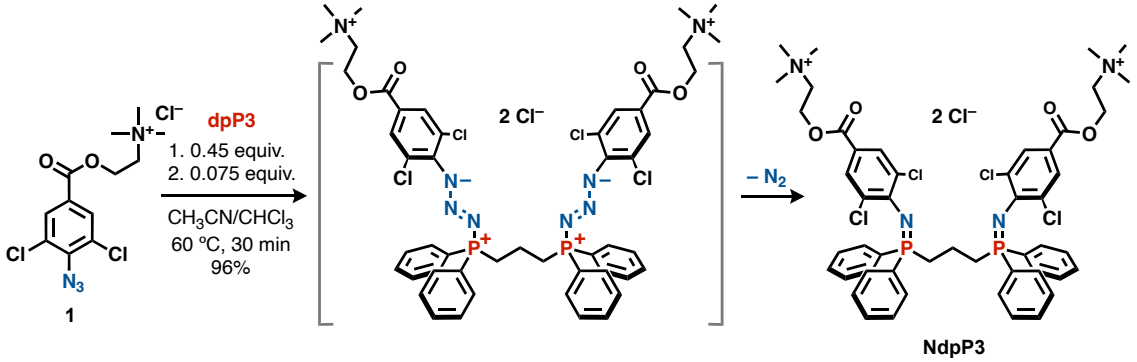

A CH_3CN solution (7.0 mL) of hydrophilic azide **1** (49.3 mg, 0.139 mmol) and 1,3-bis(diphenylphosphino)propane (**dpP3**; 26.0 mg, 0.0630 mmol, 0.45 equiv.) was added to a 25 mL glass flask, and the mixture was stirred at 60 °C for 10 min. After the solution color changed from bright yellow to colorless, a $CHCl_3$ solution (3.0 mL) of **dpP3** (4.2 mg, 0.0102 mmol, 0.075 equiv.) was added dropwise over 10 min. After stirring for 10 min, the solvent was removed under reduced pressure. The obtained solid was purified by reprecipitation (CH_3CN/Et_2O) and washed with hexane to afford **NdpP3** as a hygroscopic off-white solid (71.4 mg, 96%). Azaylide-based amphiphiles **NdpP5**, and **NdpP6** were synthesized from **dpP5** (91%) and **dpP6** (92%), respectively, in the same manner as **dpP3**.

NdpP2 and **NdpP4** were synthesized from **dpP2** (98%) and **dpP4** (93%), respectively. Obtained precipitates were washed with hexane. Due to the proximity of two phosphine sites, **NdpP1** was synthesized from **dpP1** (87%) under conditions at 80 °C for 1 h stirring time, employing higher concentration (113 mM). Non-chlorinated azaylide **nNdpP3** was also prepared using non-chlorinated **1'** (83%) in the same manner as **NdpP3**.

for **NdpP3**

^{1}H NMR (500 MHz, DMSO-d_6, 298 K): δ 7.74 (dd, $J_{H–H}$ = 7.4 Hz, $J_{H–P}$ = 11.9 Hz, 8H), 7.72 (d, $J_{H–P}$ = 1.1 Hz, 4H), 7.53 (td, $J_{H–H}$ = 7.4 Hz, $J_{H–P}$ = 1.1 Hz, 4H), 7.46 (td, $J_{H–H}$ = 7.4 Hz, $J_{H–P}$ = 2.8 Hz, 8H), 4.66 (br, 4H), 3.86 (br, 4H), 3.22 (s, 18H), 2.91 (br, 4H), 1.64 (br, 2H); ^{13}C NMR (125 MHz, DMSO-d_6, 298 K): δ 163.7 (C=O), 149.5 (C_q), 131.9 (d, C_q, $J_{C–P}$ = 103.7 Hz), 131.8 (CH), 130.7 (d, CH, $J_{C–P}$ = 9.5 Hz), 128.8 (CH), 128.7 (CH), 117.8 (C_q), 63.8 (CH_2), 58.7 (CH_2), 52.8 (CH_3), 29.9 (dd, CH_2, $J_{C–P}$ = 64.4 Hz, 13.1 Hz), 14.8 (CH_2). One C_q signal was overlapped; ^{31}P NMR (202 MHz, DMSO-d_6, 298 K): δ 7.3; FT-IR (KBr, cm^{-1}): 3054, 3025, 2967, 1713, 1635, 1578, 1498, 1437, 1377, 1253, 1180, 1117, 1026, 956, 794, 761, 716, 695, 503; ESI-TOF MS (CH_3OH/CH_3CN) *m/z*: [M − 2Cl]$^{2+}$ calcd for $C_{51}H_{56}{}^{35}Cl_4N_4O_4P_2$, 496.13; found 496.18; Elemental Analysis: calcd for $C_{51}H_{56}Cl_6N_4O_4P_2$•$(H_2O)_3$: C, 54.80; H, 5.59; N, 5.01. Found C, 54.65; H, 5.50; N, 5.22.

for **NdpP1**

^{1}H NMR (500 MHz, DMSO-d_6, 298 K): δ 7.90 (dd, $J_{H–H}$ = 7.4 Hz, $J_{H–P}$ = 12.5 Hz, 8H), 7.42 (s, 4H), 7.31–7.21 (m, 12H), 4.87 (t, $J_{H–P}$ = 13.0 Hz, 2H), 4.63 (br, 4H), 3.85 (br, 4H), 3.23 (s, 18H); ^{13}C NMR (125 MHz, DMSO-d_6, 298 K): δ 163.7 (C=O), 147.9 (C_q), 133.8 (d, C_q, $J_{C–P}$ = 114.4 Hz), 131.0 (CH), 130.7 (t, CH, $J_{C–P}$ = 4.8 Hz), 128.5 (CH), 128.1 (t, CH, $J_{C–P}$ = 7.2 Hz), 127.9 (t, C_q, $J_{C–P}$ = 7.2 Hz), 116.8 (C_q), 63.8 (CH_2), 58.5 (CH_2), 52.8 (CH_3), 34.7 (t, CH_2, $J_{C–P}$ = 52.5 Hz); ^{31}P NMR (202 MHz, DMSO-d_6, 298 K): δ −3.6; FT-IR (KBr, cm^{-1}): 3057, 3021, 2963, 1706, 1588, 1506, 1437, 1382, 1254, 1119, 1036, 955, 794, 760, 695, 500; ESI-TOF MS (CH_3OH/CH_3CN) *m/z*: [M − 2Cl]$^{2+}$ calcd for $C_{49}H_{52}{}^{35}Cl_4N_4O_4P_2$, 482.11; found 482.17; Elemental Analysis: calcd for $C_{49}H_{52}Cl_6N_4O_4P_2$•$(C_4H_{10}O)_{0.3}$•$(H_2O)_3$: C, 54.23; H, 5.53; N, 5.04. Found: C, 53.99; H, 5.50; N, 5.25.

for **NdpP2**

^{1}H NMR (500 MHz, DMSO-d_6, 298 K): δ 7.76–7.70 (m, 8H), 7.72 (s, 4H), 7.58 (t, $J_{H–H}$ = 7.4 Hz, 4H), 7.50 (t, $J_{H–H}$ = 7.4 Hz, 8H), 4.63 (br, 4H), 3.81 (br, 4H), 3.18 (s, 18H), 2.83 (br, 4H); ^{13}C NMR (125 MHz, DMSO-d_6, 298 K): δ 163.5 (C=O), 149.4 (C_q), 132.2 (CH), 130.9 (t, CH, $J_{C–P}$ = 4.8 Hz), 130.5 (m, C_q), 129.1 (d, C_q, $J_{C–P}$ = 4.8 Hz), 129.0 (t, CH, $J_{C–P}$ = 6.0 Hz), 128.8 (CH), 118.4 (C_q), 63.9 (CH_2), 58.7 (CH_2), 52.8 (CH_3), 22.7 (m,

CH_2); ^{31}P NMR (202 MHz, DMSO-d_6, 298 K): δ 7.7; FT-IR (KBr, cm^{-1}): 3081, 3002, 2962, 1712, 1577, 1483, 1361, 1251, 1173, 1120, 1034, 957, 793, 758, 727, 696, 629, 518; ESI-TOF MS (CH_3OH/CH_3CN) *m/z*: $[M - 2Cl]^{2+}$ calcd for $C_{50}H_{54}{}^{35}Cl_4N_4O_4P_2$, 489.12; found 489.17; Elemental Analysis: calcd for $C_{50}H_{54}Cl_6N_4O_4P_2 \bullet (H_2O)_{2.8}$: C, 54.59; H, 5.46; N, 5.09. Found: C, 54.61; H, 5.30; N, 5.18.

for **NdpP4**

^1H NMR (500 MHz, DMSO-d_6, 298 K): δ 7.83 (dd, J_{H-H} = 7.4 Hz, J_{H-P} = 12.5 Hz, 8H), 7.75 (s, 4H), 7.54 (td, J_{H-H} = 7.4 Hz, J_{H-P} = 1.1 Hz, 4H), 7.48 (td, J_{H-H} = 7.4 Hz, J_{H-P} = 2.8 Hz, 8H), 4.64 (br, 4H), 3.83 (br, 4H), 3.20 (s, 18H), 2.81 (br, 4H), 1.50 (br, 4H); ^{13}C NMR (125 MHz, DMSO-d_6, 298 K): δ 163.6 (C=O), 149.7 (C_q), 132.3 (d, C_q, J_{C-P} = 102.5 Hz), 131.7 (CH), 130.8 (d, CH, J_{C-P} = 9.5 Hz), 128.8 (d, CH, J_{C-P} = 6.0 Hz), 128.7 (CH), 128.6 (C_q), 117.6 (C_q), 63.9 (CH_2), 58.6 (CH_2), 52.8 (CH_3), 28.8 (d, CH_2, J_{C-P} = 65.6 Hz), 22.3 (d, CH_2, J_{C-P} = 15.5 Hz); ^{31}P NMR (202 MHz, DMSO-d_6, 298 K): δ 8.0; FT-IR (KBr, cm^{-1}): 3055, 3009, 1706, 1579, 1490, 1437, 1385, 1253, 1177, 1116, 1025, 957, 926, 835, 795, 718, 696, 536; ESI-TOF MS (CH_3OH/CH_3CN) *m/z*: $[M - 2Cl]^{2+}$ calcd for $C_{52}H_{58}{}^{35}Cl_4N_4O_4P_2$, 503.13; found 503.18; Elemental Analysis: calcd for $C_{52}H_{58}Cl_6N_4O_4P_2 \bullet (H_2O)_{3.3}$: C, 54.92; H, 5.73; N, 4.93. Found: C, 54.90; H, 5.53; N, 4.99.

for **NdpP5**

^1H NMR (500 MHz, DMSO-d_6, 298 K): δ 7.83 (dd, J_{H-H} = 6.8 Hz, J_{H-P} = 11.9 Hz, 8H), 7.76 (s, 4H), 7.55 (t, J_{H-H} = 6.8 Hz, 4H), 7.50 (td, J_{H-H} = 6.8 Hz, J_{H-P} = 2.8 Hz, 8H), 4.64 (br, 4H), 3.83 (br, 4H), 3.20 (s, 18H), 2.69 (br, 4H), 1.37–1.27 (m, 6H); ^{13}C NMR (125 MHz, DMSO-d_6, 298 K): δ 163.6 (C=O), 149.7 (C_q), 132.4 (d, C_q, J_{C-P} = 103.7 Hz), 131.7 (CH), 130.7 (d, CH, J_{C-P} = 9.5 Hz), 128.8 (d, CH, J_{C-P} = 7.2 Hz), 128.7 (CH), 128.6 (d, C_q, J_{C-P} = 10.7 Hz), 117.6 (C_q), 63.8 (CH_2), 58.6 (CH_2), 52.8 (CH_3), 30.1 (t, CH_2, J_{C-P} = 13.1 Hz), 28.6 (d, CH_2, J_{C-P} = 64.4 Hz), 20.5 (CH_2); ^{31}P NMR (202 MHz, DMSO-d_6, 298 K): δ 7.9; FT-IR (KBr, cm^{-1}): 3054, 2943, 1709, 1577, 1497, 1437, 1377, 1253, 1180, 1117, 1036, 1025, 956, 794, 761, 716, 696; ESI-TOF MS (CH_3OH/CH_3CN) *m/z*: $[M - 2Cl]^{2+}$ calcd for $C_{53}H_{60}{}^{35}Cl_4N_4O_4P_2$, 510.14; found 510.19; Elemental Analysis: calcd for $C_{53}H_{60}Cl_6N_4O_4P_2 \bullet (H_2O)_3$: C, 55.56; H, 5.81; N, 4.89. Found: C, 55.61; H, 5.65; N, 5.08.

for **NdpP6**

^{1}H NMR (500 MHz, DMSO-d_6, 298 K): δ 7.85 (dd, $J_{H–H}$ = 7.4 Hz, $J_{H–P}$ = 11.9 Hz, 8H), 7.76 (d, $J_{H–P}$ = 1.1 Hz, 4H), 7.54 (t, $J_{H–H}$ = 7.3 Hz, 4H), 7.50 (td, $J_{H–H}$ = 7.3 Hz, $J_{H–P}$ = 2.8 Hz, 8H), 4.64 (br, 4H), 3.83 (br, 4H), 3.20 (s, 18H), 2.75 (br, 4H), 1.35–1.16 (m, 8H); ^{13}C NMR (125 MHz, DMSO-d_6, 298 K): δ 163.6 (C=O), 149.8 (C_q), 132.5 (d, C_q, $J_{C–P}$ = 103.7 Hz), 131.7 (CH), 130.7 (d, CH, $J_{C–P}$ = 9.5 Hz), 128.8 (d, CH, $J_{C–P}$ = 8.3 Hz), 128.7 (CH), 128.6 (d, C_q, $J_{C–P}$ = 11.9 Hz), 117.5 (C_q), 63.8 (CH_2), 58.6 (CH_2), 52.8 (CH_3), 28.9 (d, CH_2, $J_{C–P}$ = 13.1 Hz), 28.7 (d, CH_2, $J_{C–P}$ = 64.4 Hz), 20.9 (CH_2); ^{31}P NMR (202 MHz, DMSO-d_6, 298 K): δ 7.8; FT-IR (KBr, cm^{-1}): 2931, 1715, 1577, 1506, 1437, 1376, 1253, 1117, 1025, 956, 794, 761, 695, 502; ESI-TOF MS (CH_3OH/CH_3CN) *m/z*: $[M - 2Cl]^{2+}$ calcd for $C_{54}H_{62}{}^{35}Cl_4N_4O_4P_2$, 517.15; found 517.20; Elemental Analysis: calcd for $C_{54}H_{62}Cl_6N_4O_4P_2 \bullet (H_2O)_{3.5} \bullet (CHCl_3)_{0.1}$: C, 55.03; H, 5.90; N, 4.75. Found: C, 54.74; H, 5.69; N, 4.99.

for **nNdpP3**

^{1}H NMR (500 MHz, DMSO-d_6, 298 K): δ 7.66 (dd, $J_{H–H}$ = 7.5 Hz, $J_{H–P}$ = 11.5 Hz, 8H), 7.61–7.54 (m, 8H), 7.48 (td, $J_{H–H}$ = 7.5 Hz, $J_{H–P}$ = 2.6 Hz, 8H), 6.54 (d, $J_{H–H}$ = 8.6 Hz, 4H), 4.61 (br, 4H), 3.79 (br, 4H), 3.20 (s, 18H), 2.89 (br, 4H), 1.52 (br, 2H); ^{13}C NMR (125 MHz, DMSO-d_6, 298 K): δ 165.4 (C=O), 158.1 (C_q), 132.1 (CH), 131.1 (d, CH, $J_{C–P}$ = 8.3 Hz), 130.7 (CH), 129.0 (d, CH, $J_{C–P}$ = 10.7 Hz), 122.0 (d, C_q, $J_{C–P}$ = 20.3 Hz), 116.0 (C_q), 64.2 (CH_2), 57.7 (CH_2), 52.9 (CH_3), 26.0 (dd, CH_2, $J_{C–P}$ = 65.6 Hz, 10.7 Hz), 14.8 (CH_2). One C_q signal was overlapped; ^{31}P NMR (202 MHz, DMSO-d_6, 298 K): δ 9.5; FT-IR (KBr, cm^{-1}): 3024, 2547, 2103, 1918, 1700, 1593, 1542, 1506, 1437, 1339, 1266, 1169, 1105, 1017, 949, 849, 772, 717; ESI-TOF MS (CH_3OH/CH_3CN) *m/z*: $[M - 2Cl]^{2+}$ calcd for $C_{51}H_{60}{}^{35}Cl_2N_4O_4P_2$, 427.20; found 427.20; Elemental Analysis: calcd for $C_{51}H_{60}Cl_2N_4O_4P_2 \bullet (H_2O)_{2.5} \bullet (C_2H_3N)_{0.1} \bullet (C_4H_{10}O)_{0.1}$: C, 62.76; H, 6.68; N, 6.10. Found: C, 62.82; H, 6.91; N, 6.09.

2.2. Preparation of NPPh2Me via the Staudinger reaction YA1-176

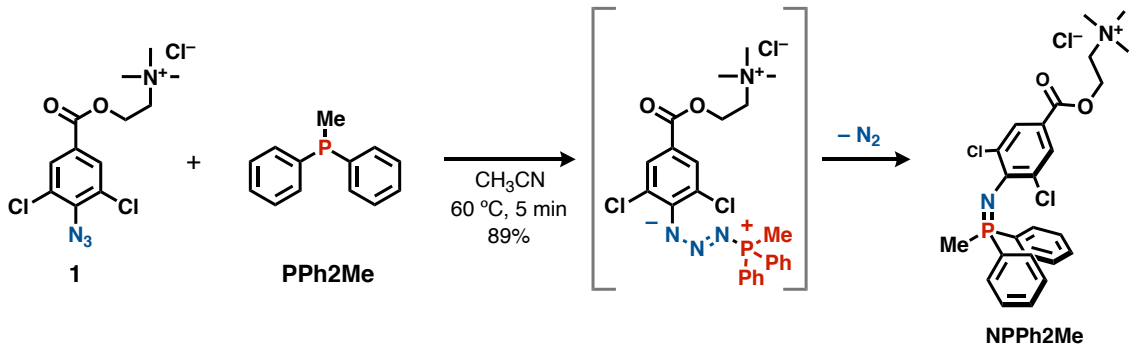

A CH_3CN solution (20 mL) of hydrophilic azide **1** (100 mg, 0.283 mmol) and methyldiphenylphosphine (**PPh2Me**; 58 μL, 0.309 mmol, 1.1 equiv.) was added to a 50 mL glass flask, and the mixture was stirred at 60 °C for 5 min. After the solution color changed from bright yellow to colorless, the solvent was removed under reduced pressure. The obtained solid was purified by reprecipitation (CH_3CN/Et_2O) and washed with Et_2O to afford **NPPh2Me** as a hygroscopic brown solid (132 mg, 89%).

^{1}H NMR (500 MHz, DMSO-d_6, 298 K): δ 7.91 (ddd, $J_{H–H}$ = 6.8 Hz, 1.7 Hz, $J_{H–P}$ = 12.5 Hz, 4H), 7.78 (d, $J_{H–P}$ = 1.7 Hz, 2H), 7.53 (td, $J_{H–H}$ = 6.8 Hz, $J_{H–P}$ = 1.7 Hz, 2H), 7.52 (td, $J_{H–H}$ = 6.8 Hz, $J_{H–P}$ = 3.4 Hz, 4H), 4.64 (br, 2H), 3.82 (br, 2H), 3.19 (s, 9H), 2.46 (d, $J_{H–P}$ = 12.5 Hz, 3H); ^{13}C NMR (125 MHz, DMSO-d_6, 298 K): δ 163.6 (C=O), 149.7 (C_q), 133.6 (d, C_q, $J_{C–P}$ = 106.9 Hz), 131.7 (CH), 130.5 (d, CH, $J_{C–P}$ = 10.3 Hz), 128.8 (d, CH, $J_{C–P}$ = 7.8 Hz), 128.7 (CH), 128.6 (d, C_q, $J_{C–P}$ = 11.5 Hz), 117.7 (C_q), 63.9 (CH_2), 58.6 (CH_2), 52.8 (CH_3), 16.8 (d, CH_3, $J_{C–P}$ = 65.6 Hz); ^{31}P NMR (202 MHz, DMSO-d_6, 298 K): δ 5.0; FT-IR (KBr, cm^{-1}): 3055, 3013, 2967, 2535, 2120, 1980, 1714, 1588, 1498, 1437, 1376, 1251, 1181, 1119, 1026, 997, 957, 881, 794, 762, 743; ESI-TOF MS (CH_3OH/CH_3CN) *m/z*: [M − Cl]$^+$ calcd for $C_{25}H_{28}{}^{35}Cl_2N_2O_2P$, 489.13; found 489.13; Elemental Analysis: calcd for $C_{25}H_{28}Cl_3N_2O_2P•(H_2O)_{1.4}•(C_2H_2N)_{0.2}$: C, 54.55; H, 5.66; N, 5.51. Found C, 54.44; H, 5.65; N, 5.42.

3. X-ray crystallography

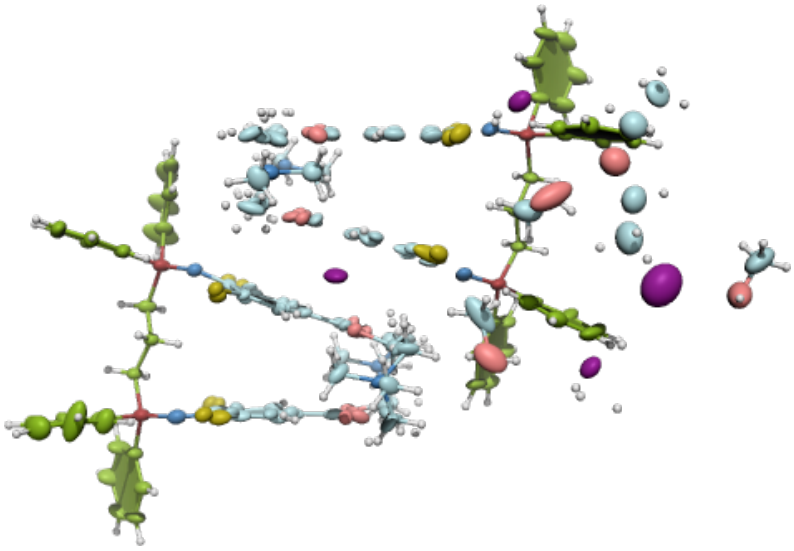

Figure S2. ORTEP drawing of **NdpP3^{I}**, an analogue of **NdpP3** (phosphorus (red), nitrogen (blue), oxygen (pink), carbon (green and light blue), chlorine (yellow), iodine (purple). The thermal ellipsoids are drawn at 50% probability.

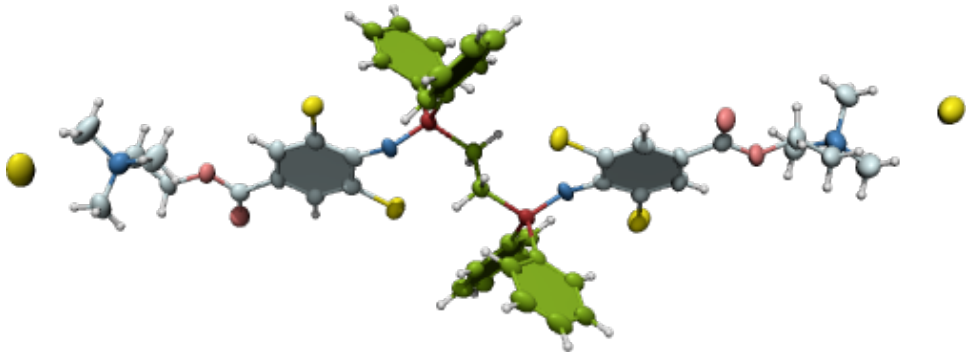

Figure S3. ORTEP drawing of **NdpP2** (phosphorus (red), nitrogen (blue), oxygen (pink), carbon (green and light blue), chlorine (yellow). The thermal ellipsoids are drawn at 50% probability.

Table S1. Crystal data and structure refinement.

Compounds	**NdpP3[1]**	**NdpP2**
Identification code	NdpP3I	NdpP2
CCDC number	2342817	2342818
Empirical formula	$C_{54.09}H_{64.09}Cl_4I_2N_4O_6P_2$	$C_{50}H_{54}Cl_6N_4O_4P_2$
Formula weight	1323.83	1049.61
Temperature (K)	93	123
Wavelength (Å)	0.750	1.54184
Crystal system	monoclinic	triclinic
Space group	$P2_1/n$	P-1
Unit cell dimensions		
a (Å)	21.492(3)	9.4418(3)
b (Å)	22.384(6)	17.2643(12)
c (Å)	26.001(4)	17.5420(10)
α (°)	90	78.146(5)
β (°)	111.870(9)	78.602(4)
γ (°)	90	81.396(4)
Volume (Å^3)	11608(4)	2725.5(3)
Z	8	2
Density (calculated)	1.515	1.279
Absorption coefficient	1.577	3.789
F(000)	5349.0	1092.0
Crystal size	0.2 × 0.1 × 0.1	0.251 × 0.133 × 0.082
2θ range for data collection	2.226 to 71.372	5.226 to 134.15
Index ranges	$-32 \le h \le 33$	$-10 \le h \le 11$
	$-33 \le k \le 32$	$-20 \le k \le 20$
	$-40 \le l \le 40$	$-20 \le l \le 20$
Reflections collected	125809	27888
Independent reflections	43115 [R_{int} = 0.0529]	9693 [R_{int} = 0.0974]
Completeness to θ	0.942	0.997
Absorption correction	multi-scan	multi-scan
Refinement method	Full-matrix least-squares on F^2	Full-matrix least-squares on F^2
Data / restraints / parameters	43115/326/1851	9693/0/601
Goodness-of-fit on F^2	1.038	1.045
Final R indices [I>2sigma(I)]	R_1 = 0.0931	R_1 = 0.1280
	wR_2 = 0.2728	wR_2 = 0.3646
R indices (all data)	R_1 = 0.1877	R_1 = 0.1725
	wR_2 = 0.3325	wR_2 = 0.3917
Largest diff. peak and hole	1.514 and −1.831 e Å^{-3}	0.855 and −0.787 e Å^{-3}

4. UV-vis and fluorescence spectra of NdpP3

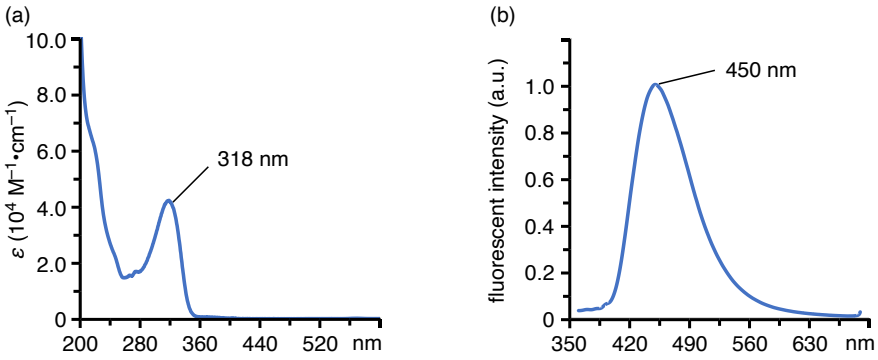

Figure S4. (a) UV-vis and (b) fluorescence spectra (CH_3CN, 298 K, 0.05 mM) of **NdpP3**.

5. Stability in water

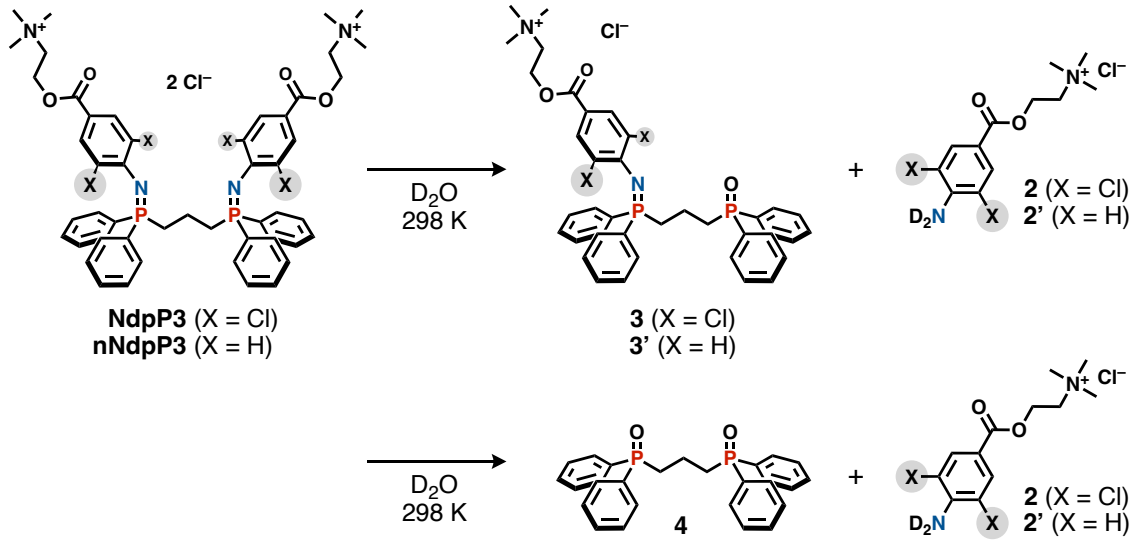

NdpP3 (X = Cl, 2.7 mg, 2.5 μmol) was dissolved in D_2O (5.0 mL). The stability of azaylides against water was monitored by ^1H NMR analysis at room temperature (298 K). The stability of **nNdpP3** (X = H) for water was also evaluated by the same procedure as **NdpP3**.

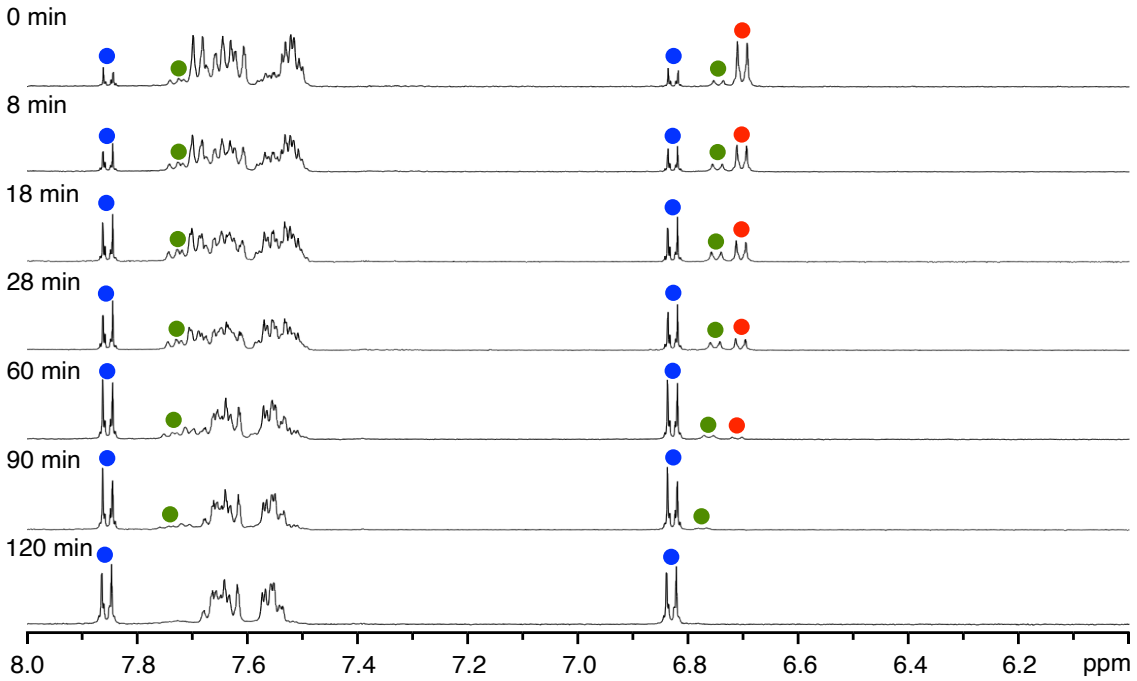

Figure S5. Time-course ^1H NMR spectra (500 MHz, 298 K, D_2O, 0.5 mM) of **nNdpP3** (red: **nNdpP3**, blue: **2'**, green: **3'**).

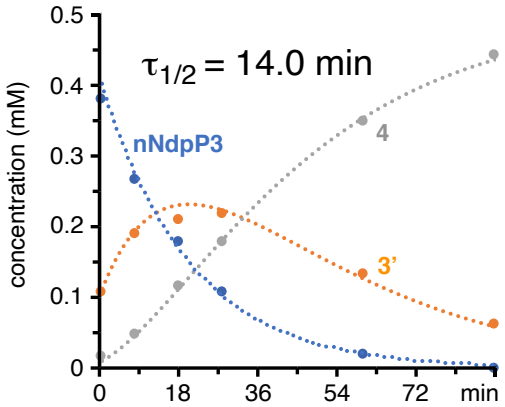

Figure S6. Changes in concentrations of **nNdpP3**, **3'**, and **4** during decomposition of **nNdpP3**.

Table S2. Changes in concentrations of **nNdpP3**, **3'**, and **4** and half-life of **nNdpP3**.

	Concentration (mM)[a]								k_1[c]	k_2[c]	$\tau_{1/2}$[d]
	0	8	18	28	60	90	120	(min)	min^{-1}	min^{-1}	min
nNdpP3	0.377	0.264	0.177	0.108	0.020	0.000	0.000				
2'	0.137	0.284	0.439	0.568	0.828	0.939	1.000		0.049	0.030	14.0
3'	0.108	0.189	0.208	0.216	0.132	0.061	0.000				
4[b]	0.015	0.048	0.115	0.176	0.348	0.439	0.500				

[a]: Calculated by NMR signal intensities. [b]: Calculated by $[\mathbf{nNdpP3}]_0-([\mathbf{nNdpP3}]+[\mathbf{3'}])$.
[c]: Decomposition rate constants of **nNdpP3** (k_1) and **3'** (k_2).
Calculated by reaction rate equation of consecutive first order reaction.
[d]: Half-life of **nNdpP3** calculated by $\tau_{1/2} = (1/k_1)\ln 2$.

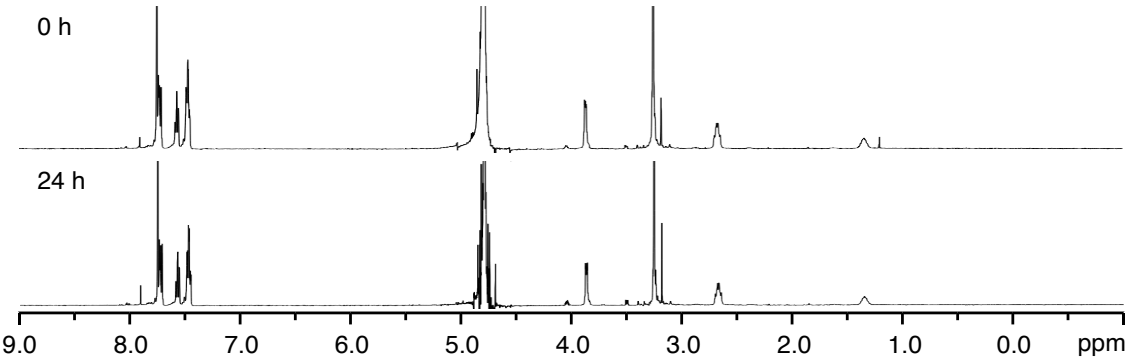

Figure S7. ^{1}H NMR spectra (500 MHz, 298 K, D_2O, 0.5 mM of **NdpP3** (0 h (top) and after 24 h (bottom)).

6. Formation of assemblies

6.1. Preparation of assemblies

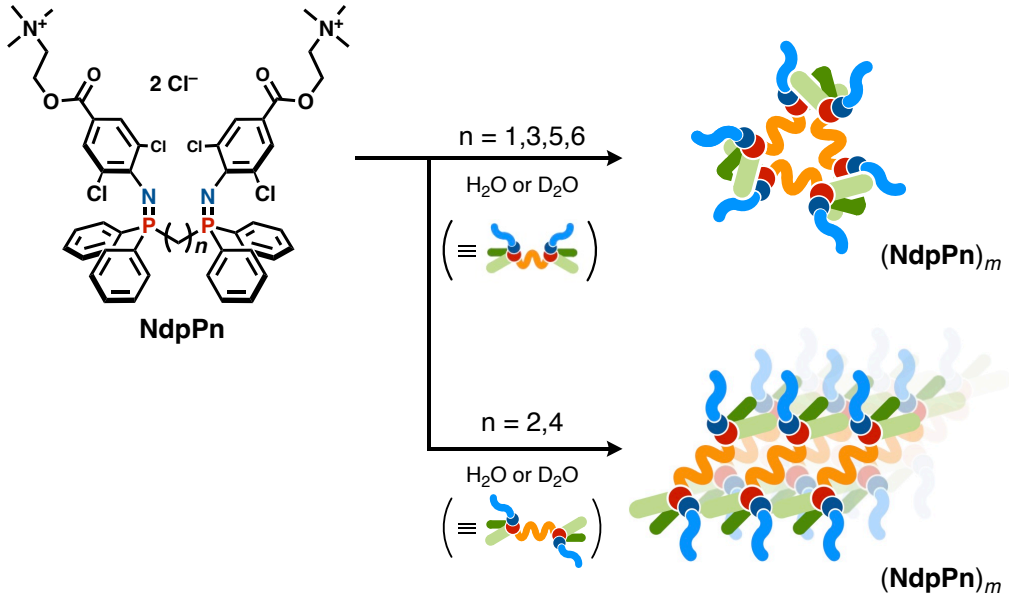

A gemini amphiphile **NdpPn** (2.0 μmol) was dissolved in H_2O or D_2O (1.0 mL). The formation of either micelles or layered structures was confirmed by NMR, DLS, and electron microscopic analyses.

for $(\mathbf{NdpP3})_m$

^{1}H NMR (500 MHz, D_2O, 298 K, 2.0 mM based on **NdpP3**): δ 7.84–7.11 (br, 24H), 4.66 (br, 4H), 3.75 (br, 4H), 3.15 (br, 18H), 2.58 (br, 4H), 1.42 (br, 2H); ^{31}P NMR (202 MHz, D_2O, 298 K, 2.0 mM based on **NdpP3**): δ 13.7.

for $(\mathbf{NdpP1})_m$

^{1}H NMR (500 MHz, D_2O, 298 K, 2.0 mM based on **NdpP1**): δ 7.78 (br, 8H), 7.45 (br, 4H), 7.19 (br, 12H), 4.60 (br, 4H), 3.72 (br, 4H), 3.15 (br, 18H). The methylene signal was overlapped with HDO signal; ^{31}P NMR (202 MHz, D_2O, 298 K, 2.0 mM based on **NdpP1**): δ −2.3.

for (**NdpP5**)$_m$

^{1}H NMR (500 MHz, D_2O, 298 K, 2.0 mM based on **NdpP5**): δ 7.82–6.84 (br, 24H), 4.52 (br, 4H), 3.64 (br, 4H), 3.05 (br, 18H), 2.29 (br, 4H), 1.09 (br, 6H); ^{31}P NMR (202 MHz, D_2O, 298 K, 2.0 mM based on **NdpP5**): δ 9.4.

for (**NdpP2**)$_m$

^{1}H NMR (500 MHz, D_2O, 298 K, 2.0 mM based on **NdpP2**): δ 7.80 (s, 4H), 7.70 (dd, $J_{H–H}$ = 7.4 Hz, $J_{H–P}$ = 12.5 Hz, 8H), 7.61 (t, $J_{H–H}$ = 7.4 Hz, 4H), 7.48 (dd, $J_{H–H}$ = 7.4 Hz, 7.4 Hz, 8H), 3.86 (br, 4H), 3.24 (s, 18H), 2.59 (br, 4H). The methylene signal was overlapped with HDO signal; ^{31}P NMR (202 MHz, D_2O, 298 K, 2.0 mM based on **NdpP2**): δ 16.0.

for (**NdpP4**)$_m$

^{1}H NMR (500 MHz, D_2O, 298 K, 2.0 mM based on **NdpP4**): δ 7.85 (s, 4H), 7.72 (dd, $J_{H–H}$ = 7.4 Hz, $J_{H–P}$ = 11.9 Hz, 8H), 7.58 (t, $J_{H–H}$ = 7.4 Hz, 4H), 7.48 (ddd, $J_{H–H}$ = 7.4 Hz, 7.4 Hz, $J_{H–P}$ = 2.3 Hz, 8H), 4.69 (br, 4H), 3.78 (br, 4H), 3.18 (s, 18H), 2.30 (br, 4H); ^{31}P NMR (202 MHz, D_2O, 298 K, 2.0 mM based on **NdpP4**): δ 15.6.

for (**NdpP6**)$_m$

^{1}H NMR (500 MHz, D_2O, 298 K, 2.0 mM based on **NdpP6**): δ 7.80–6.93 (br, 24H), 4.50 (br, 4H), 3.62 (br, 4H), 3.03 (br, 18H), 2.32 (br, 4H), 1.27–0.54 (br, 8H); ^{31}P NMR (202 MHz, D_2O, 298 K, 2.0 mM based on **NdpP6**): δ 9.5.

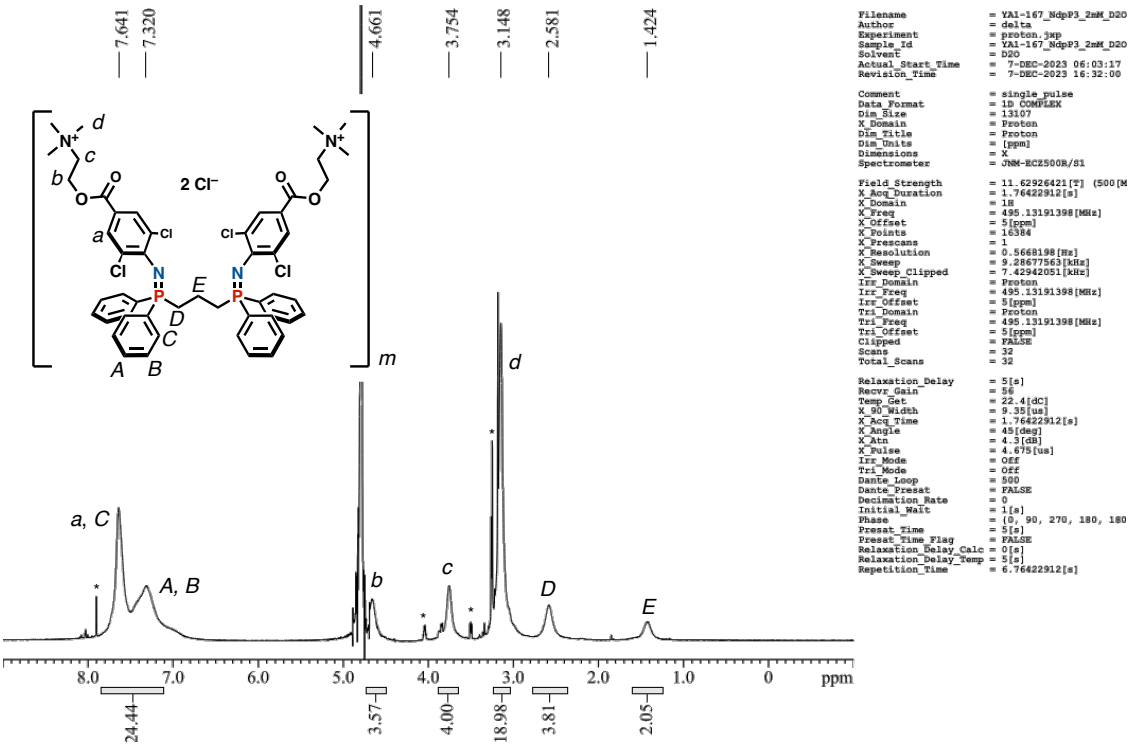

Figure S8. ^{1}H NMR spectrum (500 MHz, D_2O, 298 K, 2.0 mM based on **NdpP3**) of $(\mathbf{NdpP3})_m$.

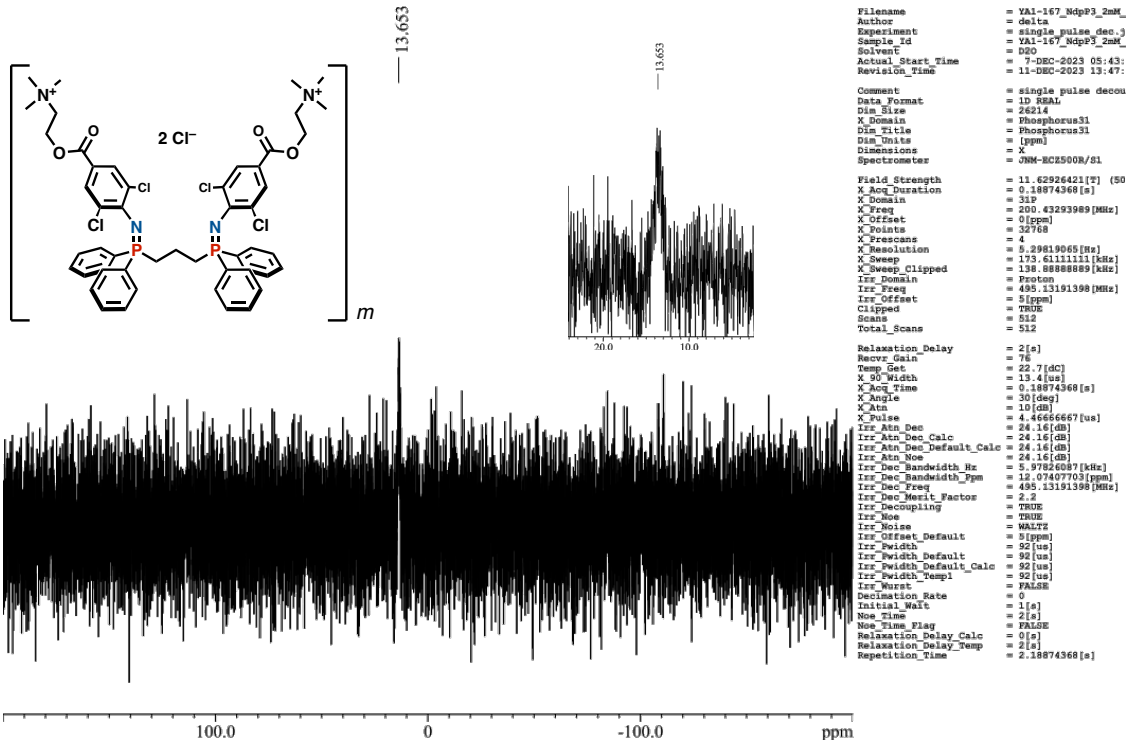

Figure S9. ^{31}P NMR spectrum (202 MHz, D_2O, 298 K, 2.0 mM based on **NdpP3**) of $(\mathbf{NdpP3})_m$.

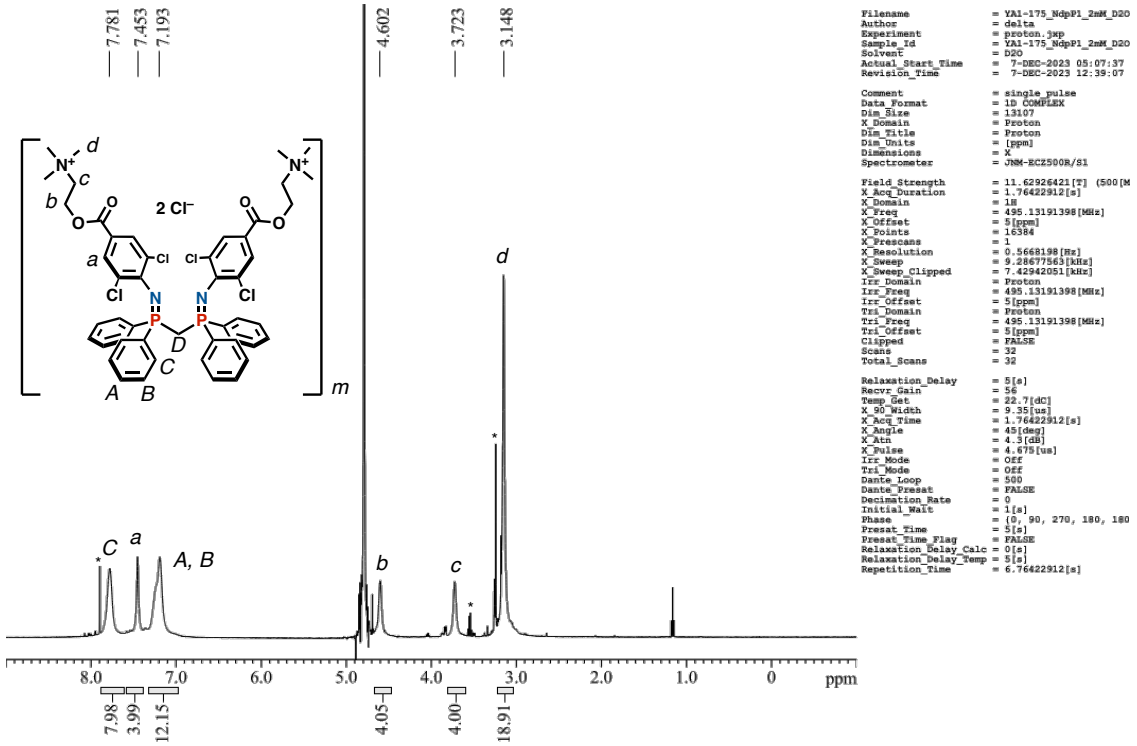

Figure S10. ^{1}H NMR spectrum (500 MHz, D_2O, 298 K, 2.0 mM based on **NdpP1**) of (**NdpP1**)$_m$.

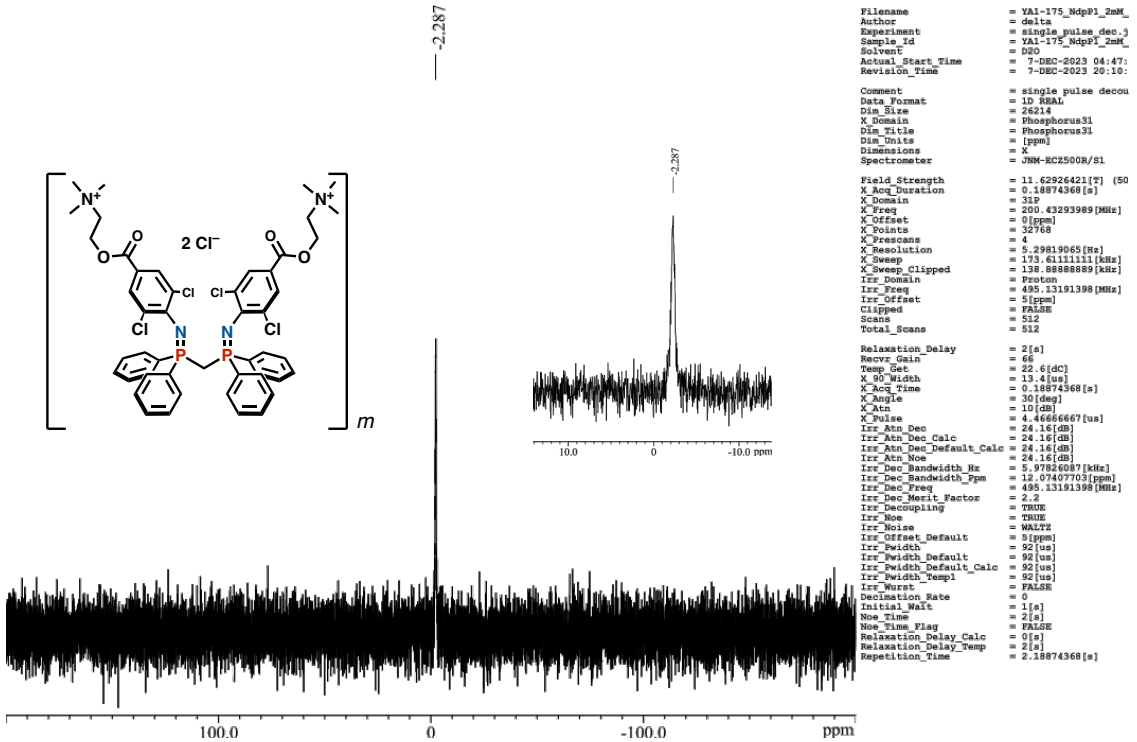

Figure S11. ^{31}P NMR spectrum (202 MHz, D_2O, 298 K, 2.0 mM based on **NdpP1**) of (**NdpP1**)$_m$.

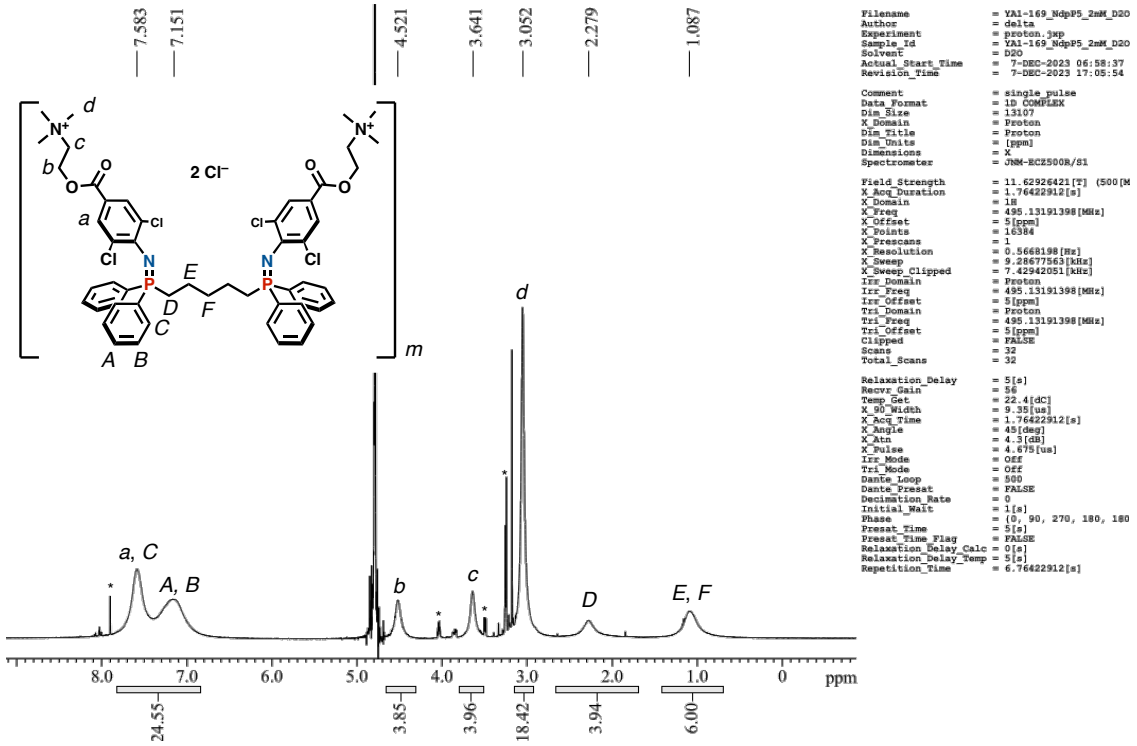

Figure S12. ^{1}H NMR spectrum (500 MHz, D_2O, 298 K, 2.0 mM based on **NdpP5**) of $(\mathbf{NdpP5})_m$.

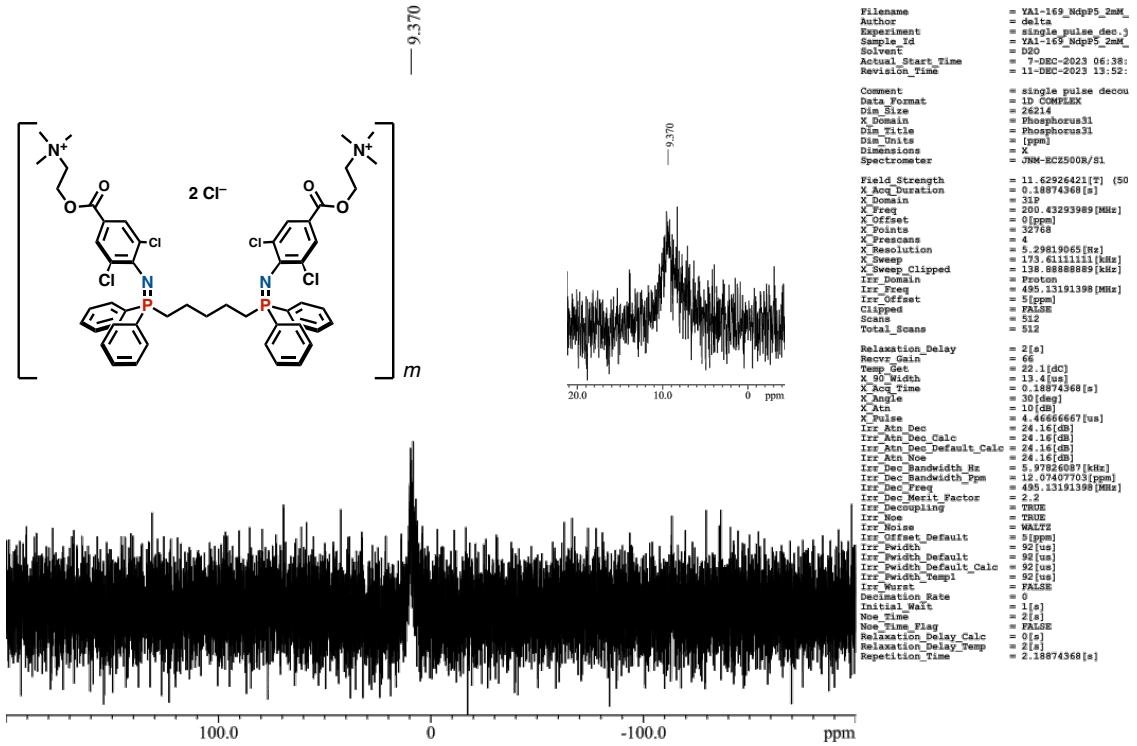

Figure S13. ^{31}P NMR spectrum (202 MHz, D_2O, 298 K, 2.0 mM based on **NdpP5**) of $(\mathbf{NdpP5})_m$.

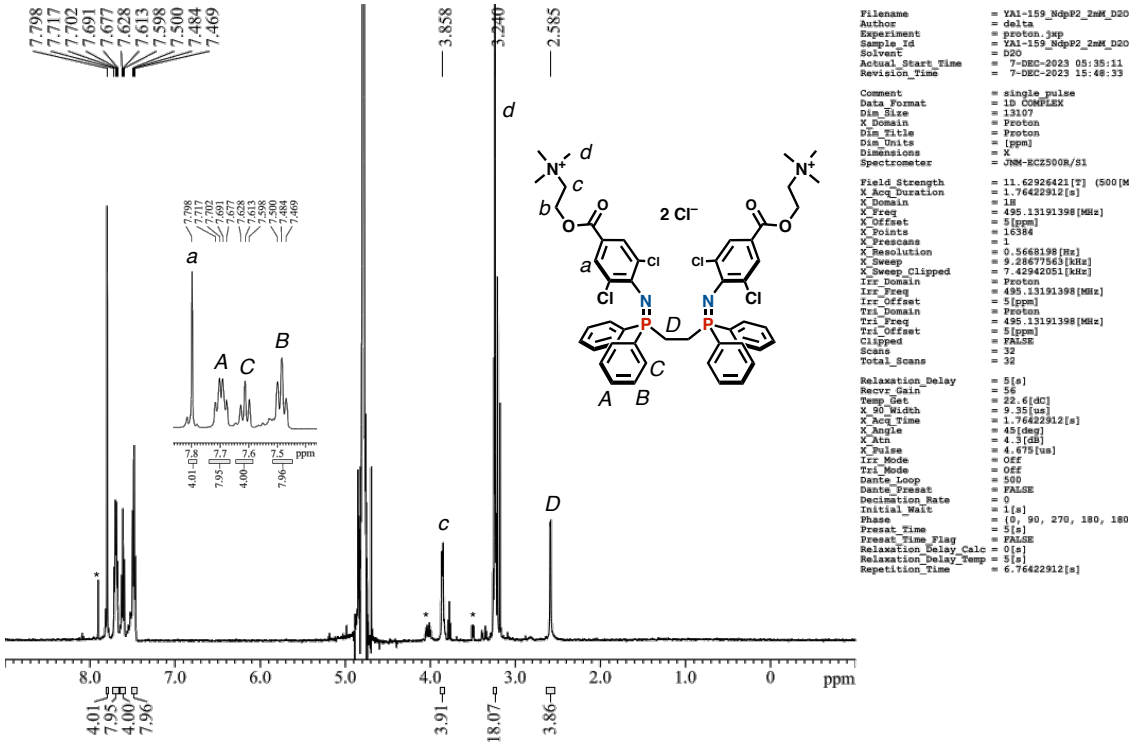

Figure S14. ^{1}H NMR spectrum (500 MHz, D_2O, 298 K, 2.0 mM) of **NdpP2**.

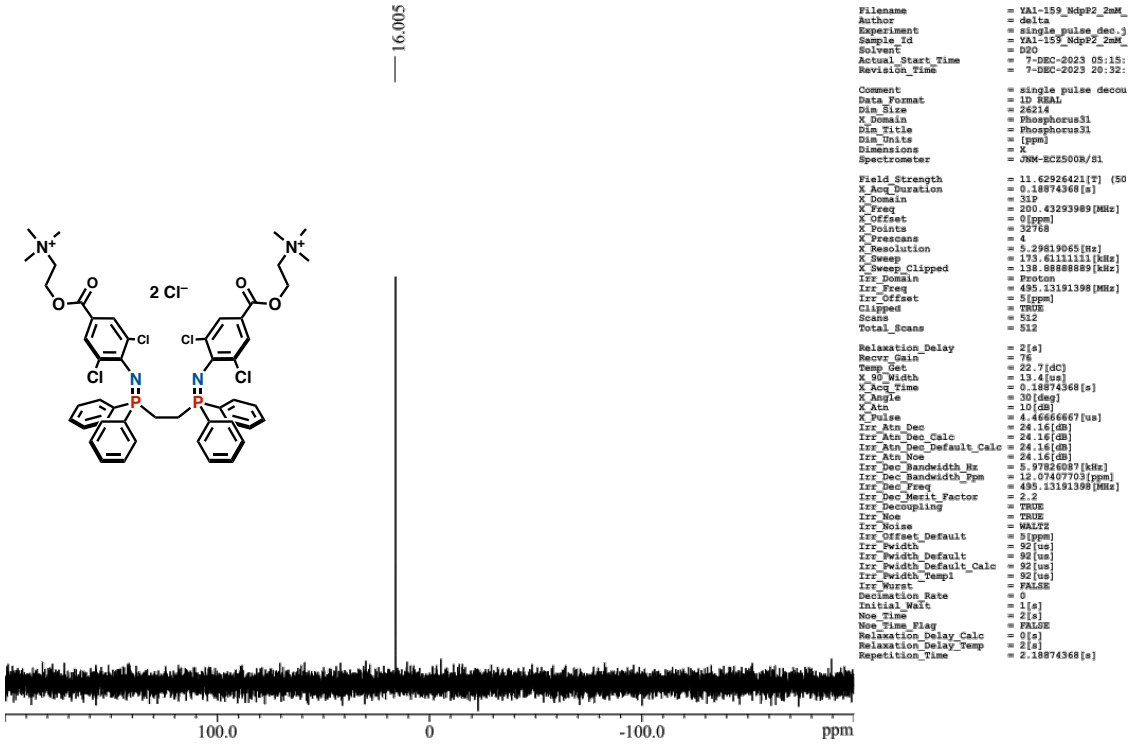

Figure S15. ^{31}P NMR spectrum (202 MHz, D_2O, 298 K, 2.0 mM) of **NdpP2**.

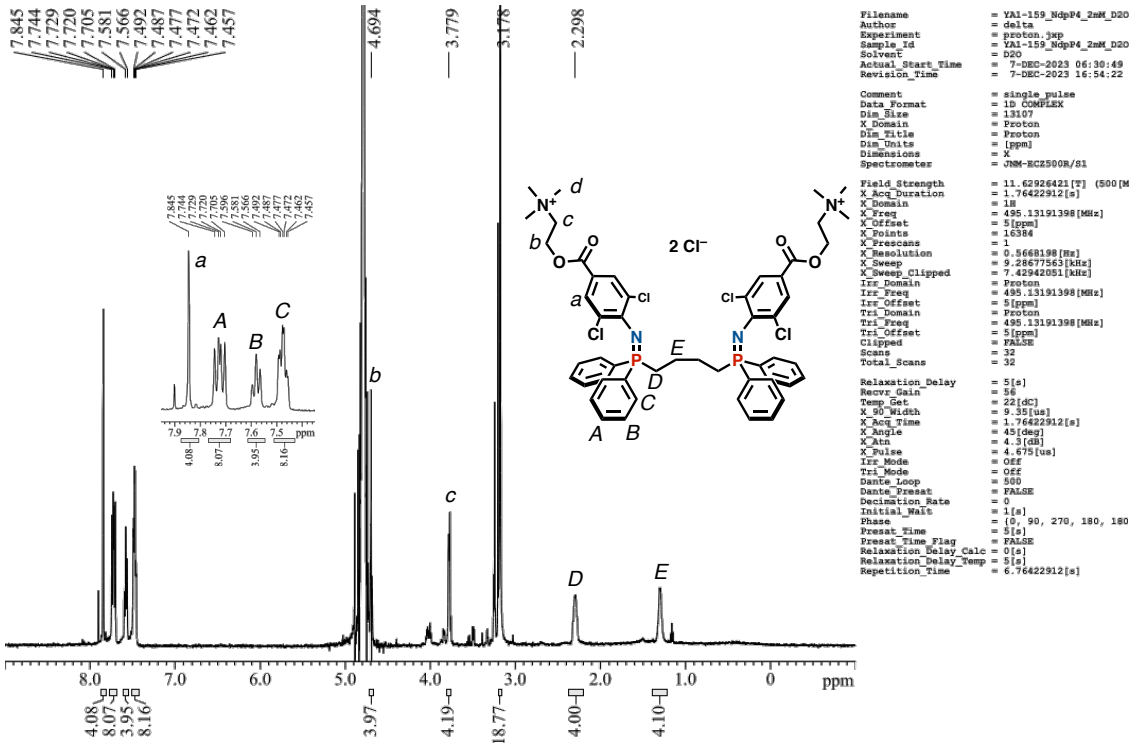

Figure S16. ^{1}H NMR spectrum (500 MHz, D_2O, 298 K, 2.0 mM) of **NdpP4**.

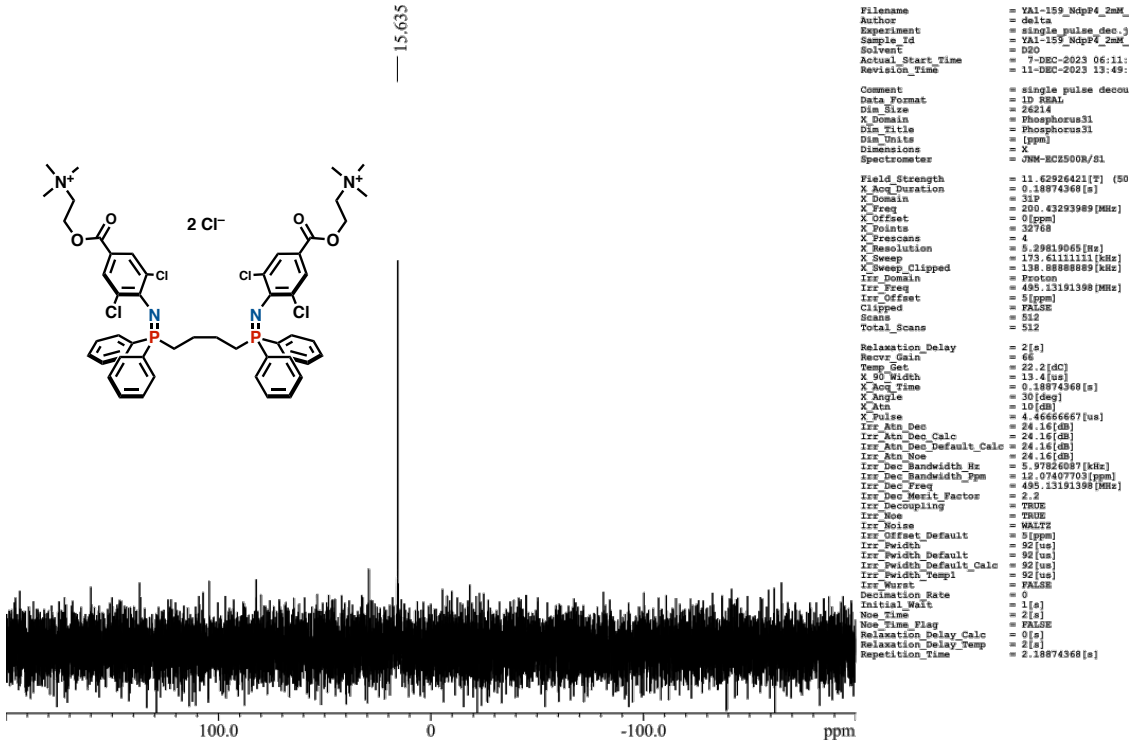

Figure S17. ^{31}P NMR spectrum (202 MHz, D_2O, 298 K, 2.0 mM) of **NdpP4**.

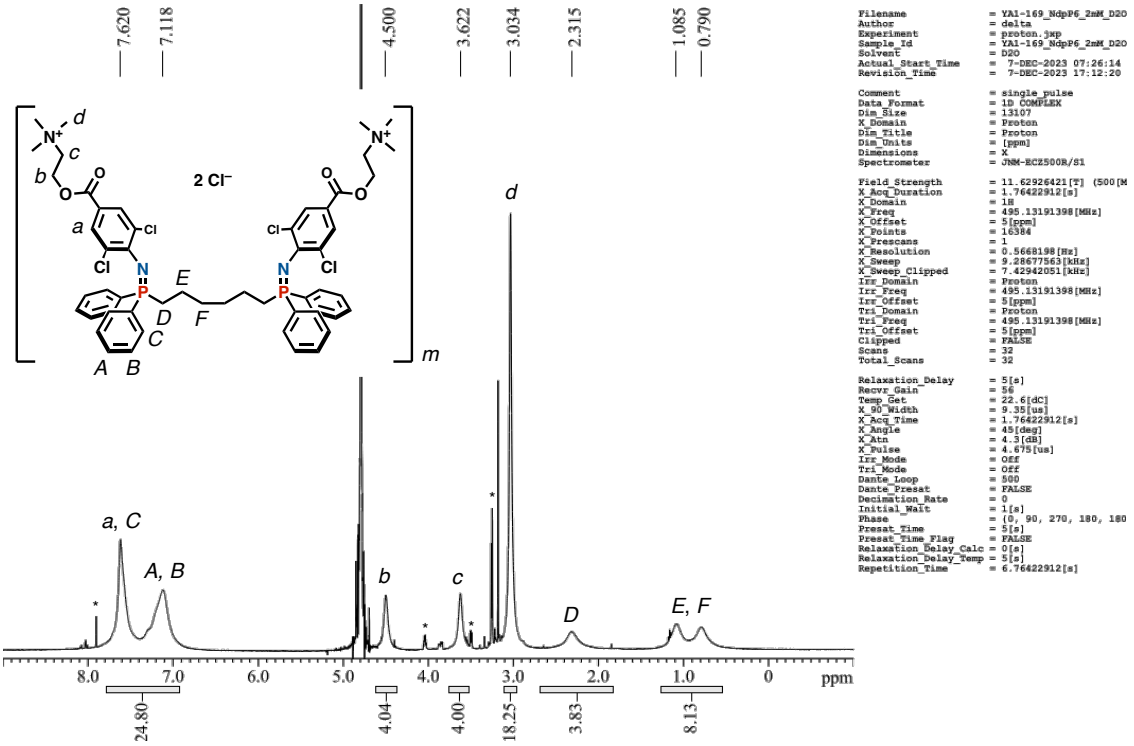

Figure S18. ^{1}H NMR spectrum (500 MHz, D_2O, 298 K, 2.0 mM based on **NdpP6**) of $(\mathbf{NdpP6})_m$.

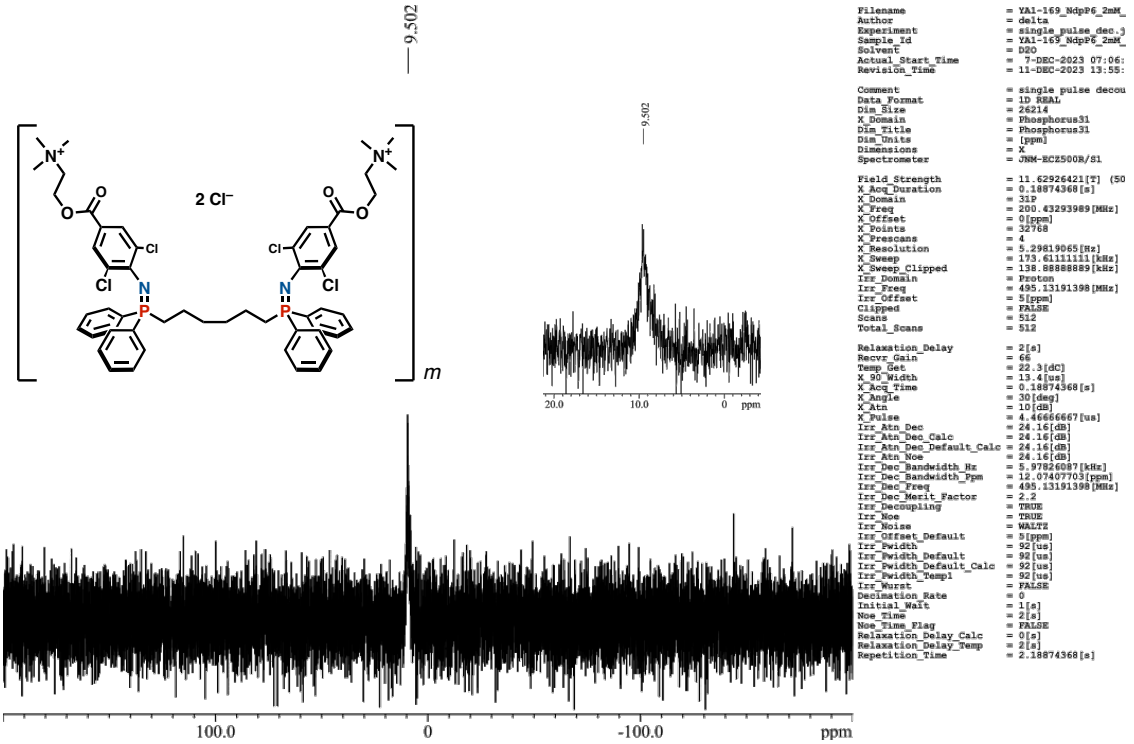

Figure S19. ^{31}P NMR spectrum (202 MHz, D_2O, 298 K, 2.0 mM based on **NdpP6**) of $(\mathbf{NdpP6})_m$.

6.2. ^{1}H DOSY spectra

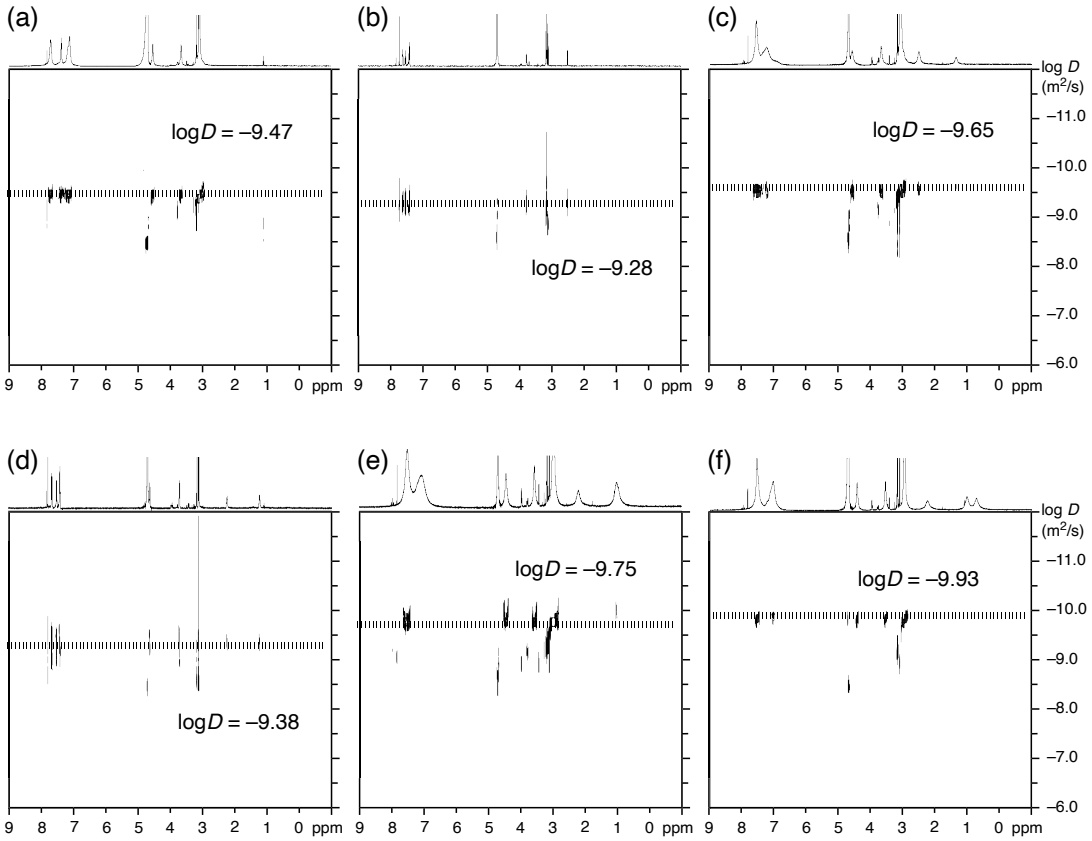

Figure S20. ^{1}H DOSY spectra (600 MHz, D_2O, 298 K, 2.0 mM based on the amphiphiles) and diffusion coefficients of (a) (**NdpP1**)$_m$, (b) (**NdpP2**)$_m$, (c) (**NdpP3**)$_m$, (d) (**NdpP4**)$_m$, (e) (**NdpP5**)$_m$, and (f) (**NdpP6**)$_m$.

6.3. DLS measurements

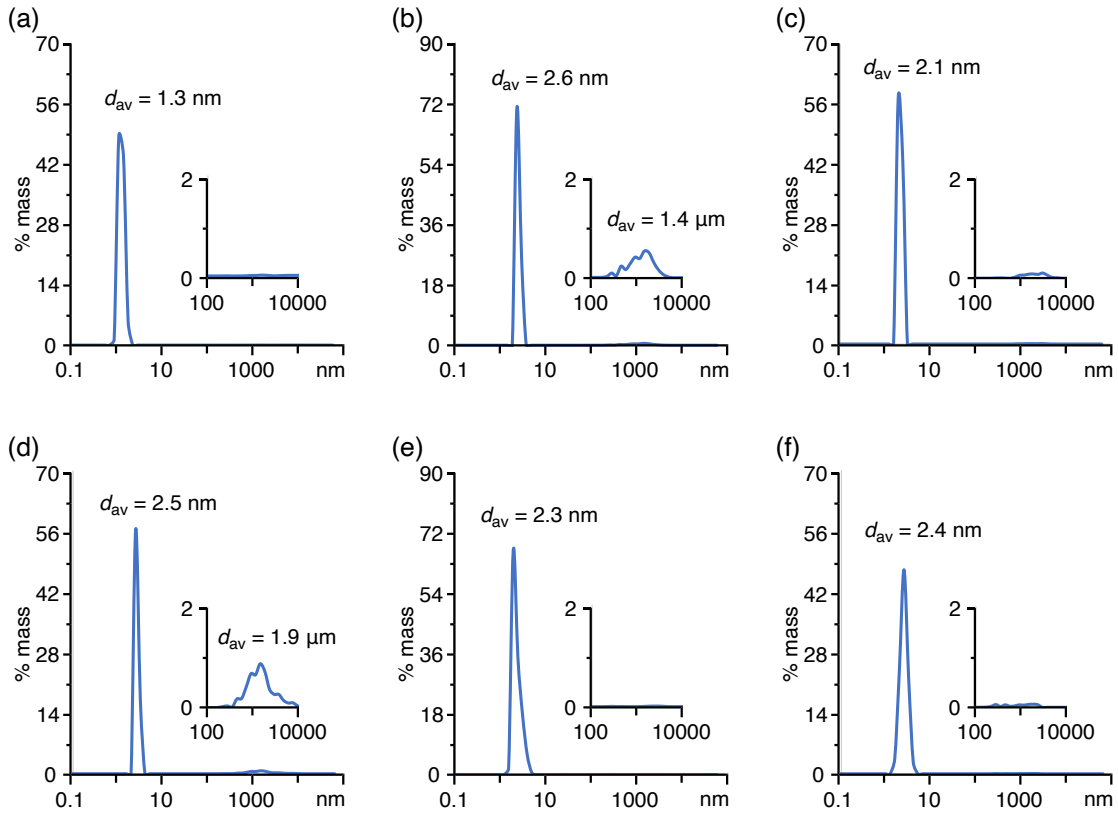

Figure S21. DLS charts (H_2O, 298 K, 2.0 mM based on the amphiphiles) of (a) (**NdpP1**)$_m$, (b) (**NdpP2**)$_m$, (c) (**NdpP3**)$_m$, (d) (**NdpP4**)$_m$, (e) (**NdpP5**)$_m$, and (f) (**NdpP6**)$_m$.

6.4. Optimized structures

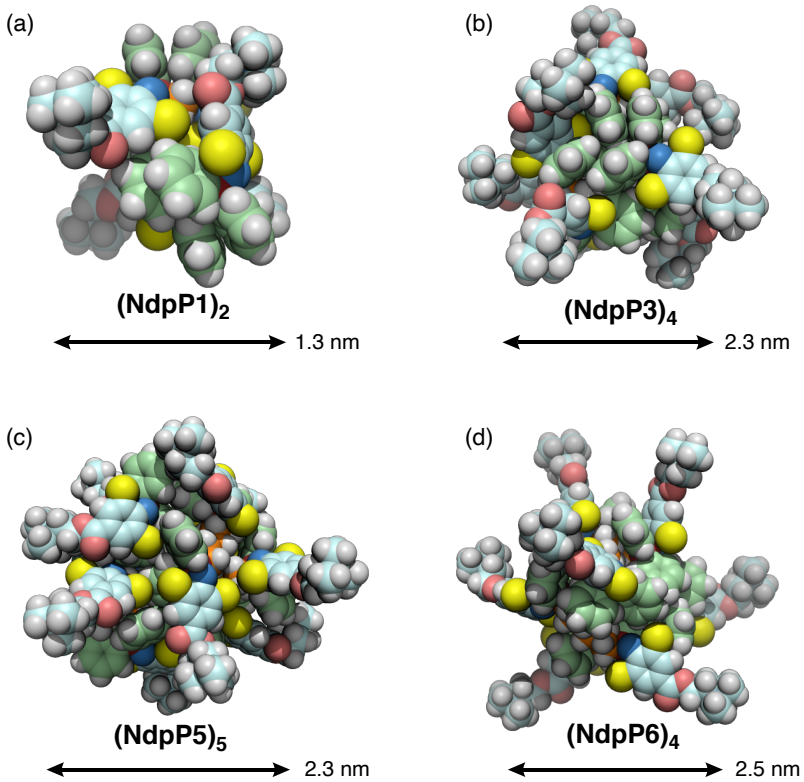

Figure S22. Space-filling representations of optimized structures of (a) (**NdpP1**)$_2$, (b) (**NdpP3**)$_4$, (c) (**NdpP5**)$_5$ and (d) (**NdpP6**)$_4$ (phosphorus (red), nitrogen (blue), oxygen (pink), carbon (green, light blue, and orange), chlorine (yellow).

6.5. Determination of CMC

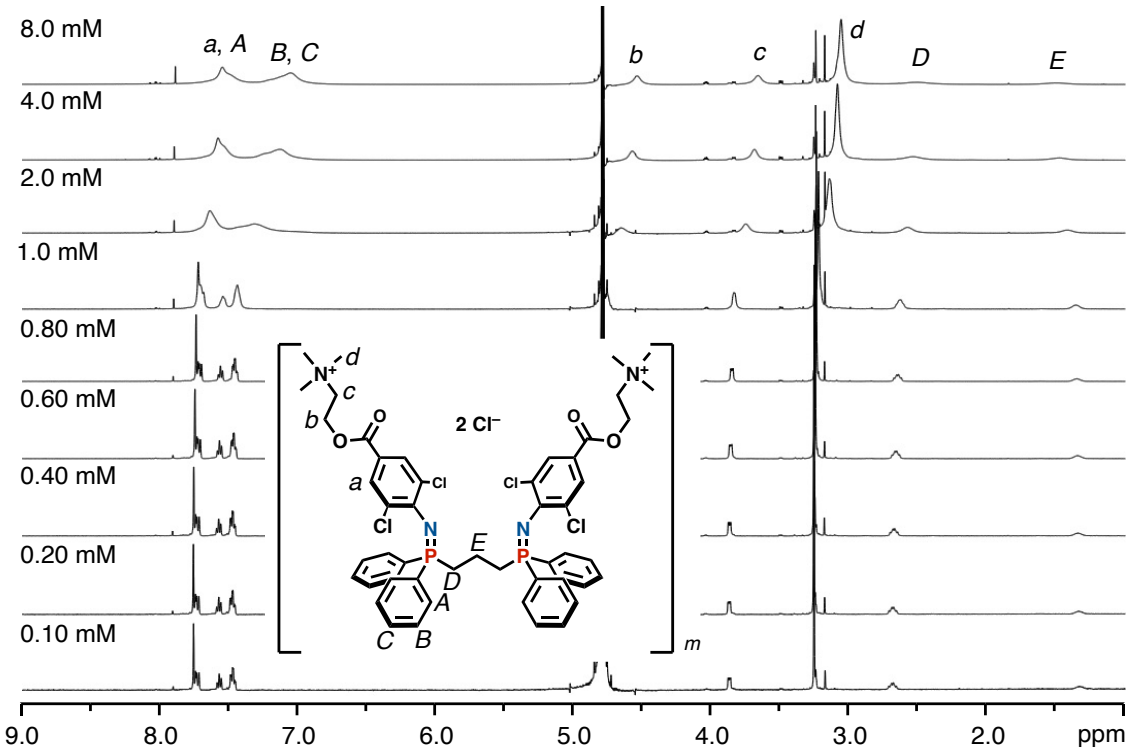

Figure S23. Variable concentration ^{1}H NMR spectra (500 MHz, D_2O, 298 K) of $(\mathbf{NdpP3})_m$.

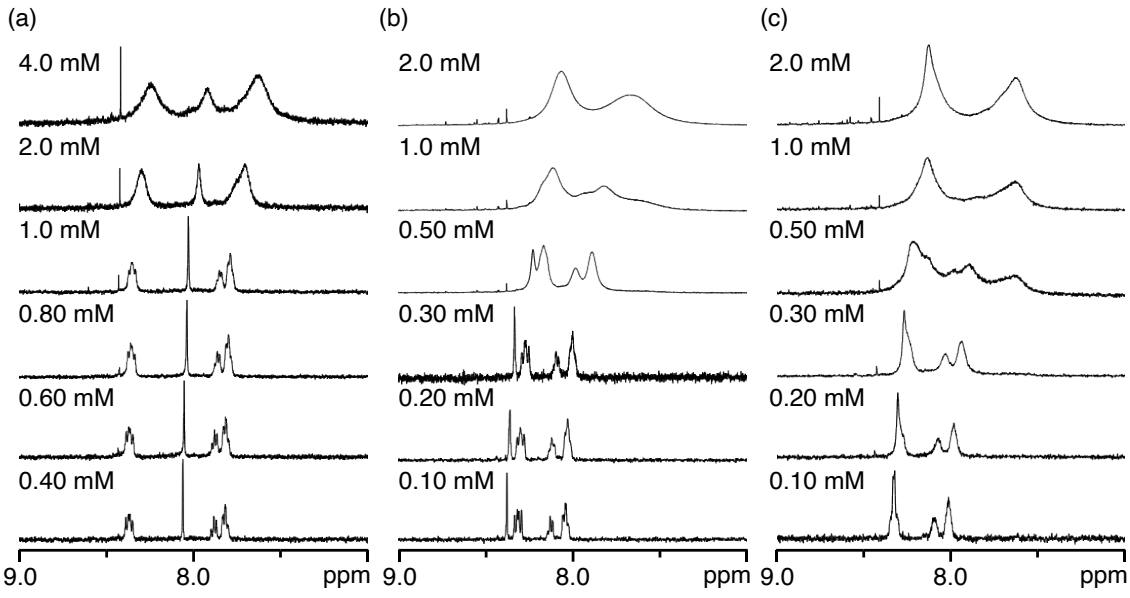

Figure S24. Variable concentration ^{1}H NMR spectra (500 MHz, D_2O, 298 K) of (a) $(\mathbf{NdpP1})_m$, (b) $(\mathbf{NdpP5})_m$, and (c) $(\mathbf{NdpP6})_m$.

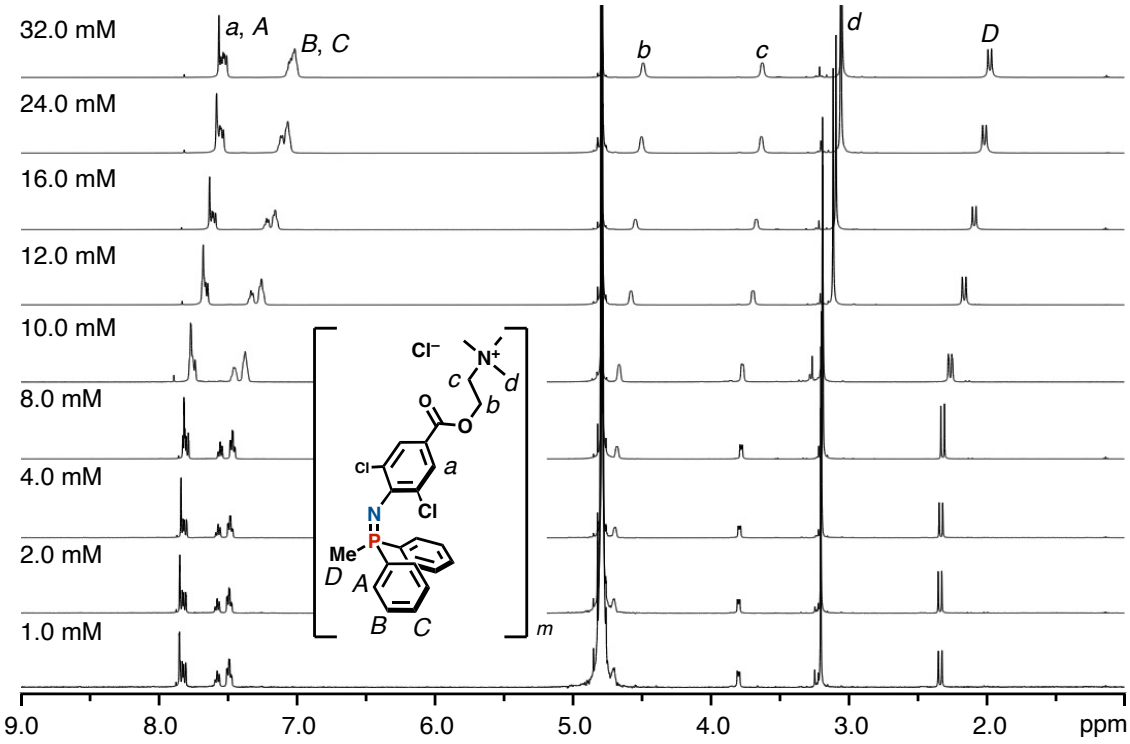

Figure S25. Variable concentration ^{1}H NMR spectra (500 MHz, D_2O, 298 K) of (**NPPh2Me**)$_m$.

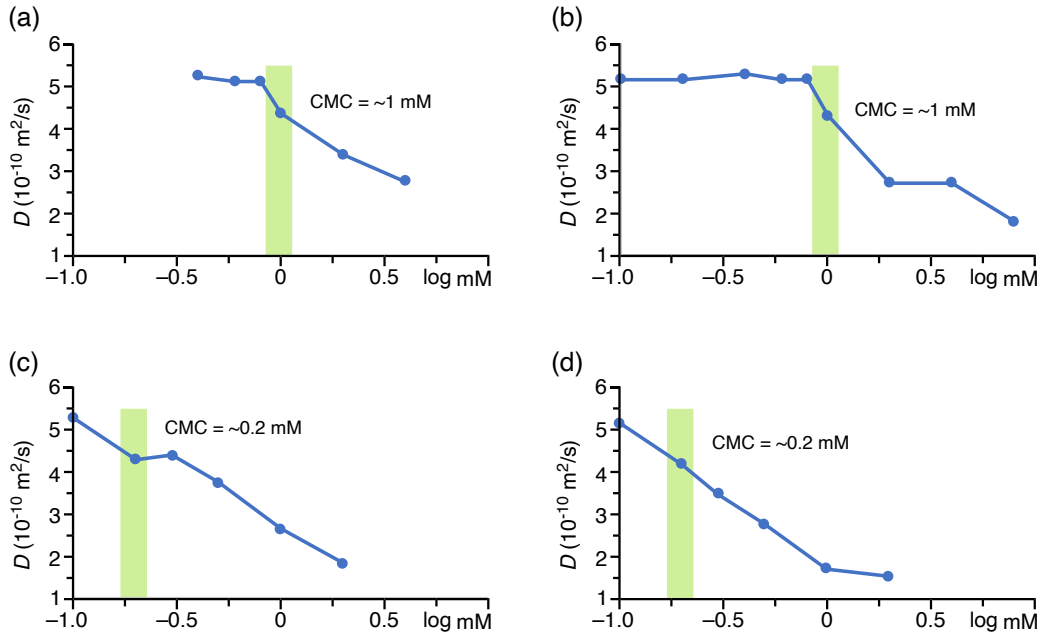

Figure S26. Concentration-dependent diffusion constants (*D*) of (a) **NdpP1**, (b) **NdpP3**, (c) **NdpP5**, and (d) **NdpP6**.

6.6. PXRD analyses

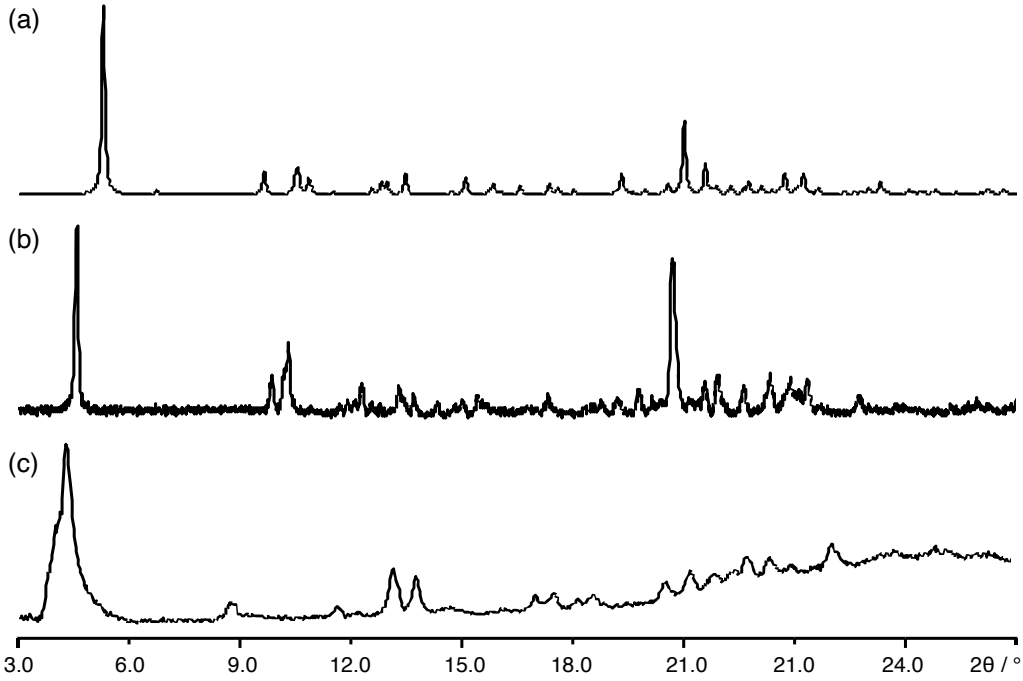

Figure S27. Powder X-ray diffraction (PXRD) patterns of (a) simulation based on the result of single crystal X-ray diffraction (SXRD) of **NdpP2** and white dispersions of (b) **NdpP2** and (c) **NdpP4**.

6.7. AFM and TEM images

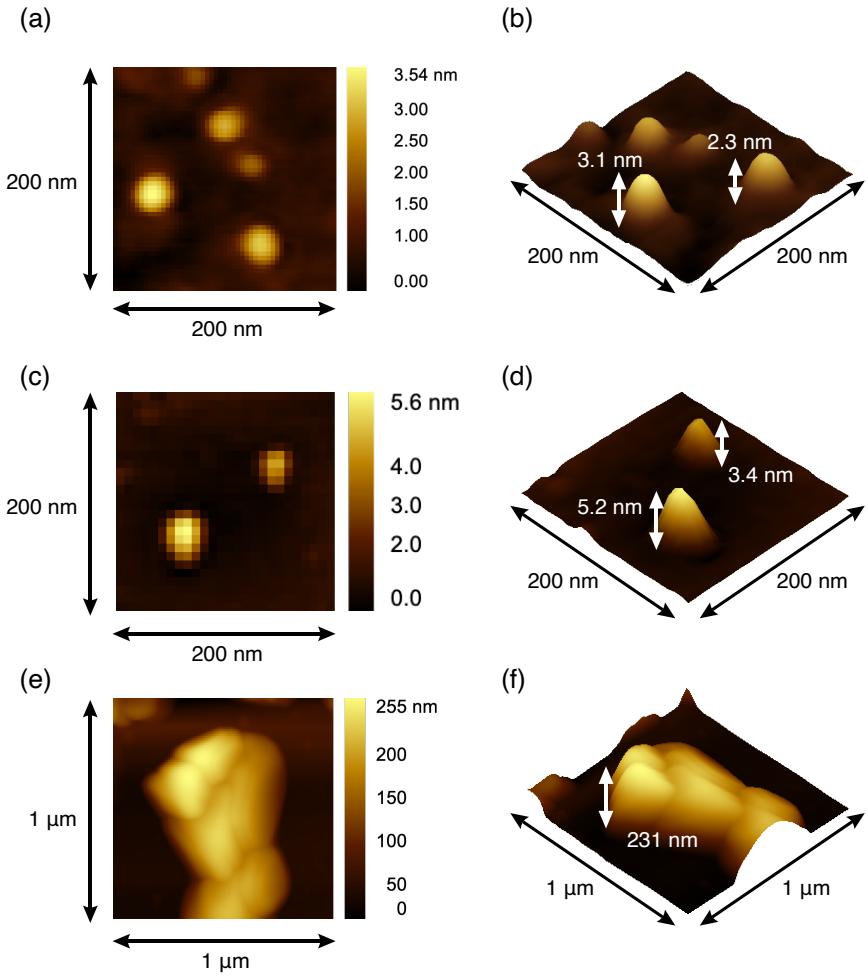

Figure S28. AFM images of (a,b) **NdpP3** and (c–f) white dispersions of **NdpP2**. (c,d) Local and (e,f) wide-area observations.

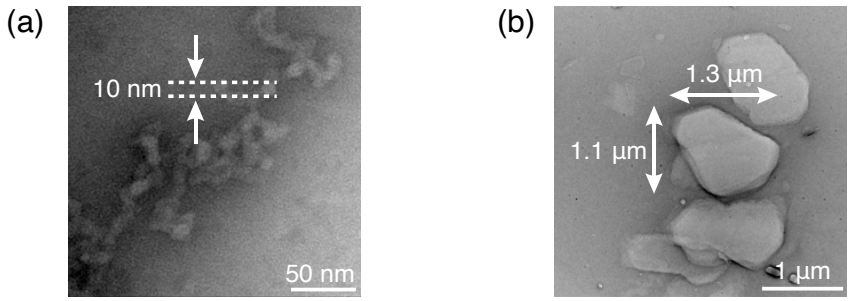

Figure S29. TEM images of white dispersions of **NdpP2**. (a) Local and (b) wide-area observations.

7. Host-guest chemistry

7.1. Encapsulation of hydrophobic organic molecules

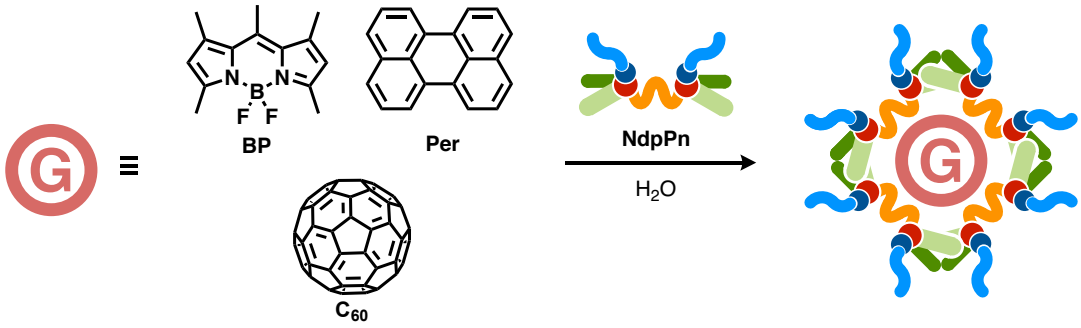

A hydrophobic aromatic compound (4.0 μmol) and gemini amphiphile **NdpPn** (4.0 μmol) or monomeric amphiphile **NPPh2Me** (8.0 μmol) were ground in a mortar for 3 min and subsequently H_2O (2.0 mL) was added. The suspension was vigorously stirred for 1 h at room temperature. The excess of guests was removed by filtration. The formation of host-guest complexes was confirmed by NMR, UV-vis, fluorescence, and DLS analyses with an appropriately diluted solution.

7.2. UV-vis and fluorescence spectra

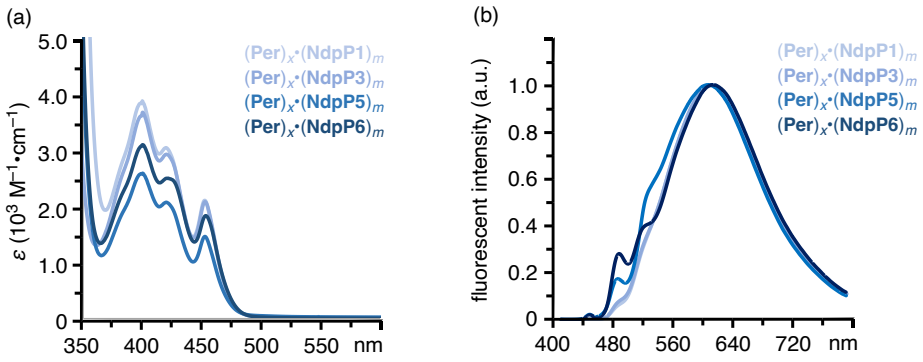

Figure S30. (a) UV-vis and (b) fluorescence spectra (H_2O, 298 K, 2.0 mM based on the amphiphiles) of **(Per)**$_x$**•(NdpP1)**$_m$, **(Per)**$_x$**•(NdpP3)**$_m$, **(Per)**$_x$**•(NdpP5)**$_m$, and **(Per)**$_x$**•(NdpP6)**$_m$.

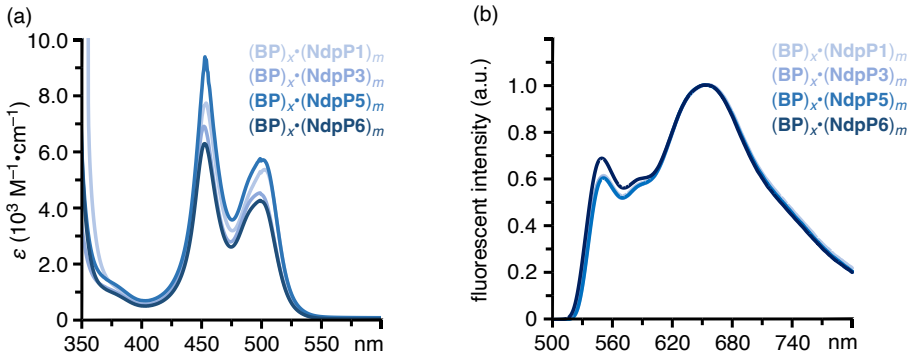

Figure S31. (a) UV-vis and (b) fluorescence spectra (H_2O, 298 K, 2.0 mM based on the amphiphiles) of **(BP)**$_x$**•(NdpP1)**$_m$, **(BP)**$_x$**•(NdpP3)**$_m$, **(BP)**$_x$**•(NdpP5)**$_m$, and **(BP)**$_x$**•(NdpP6)**$_m$.

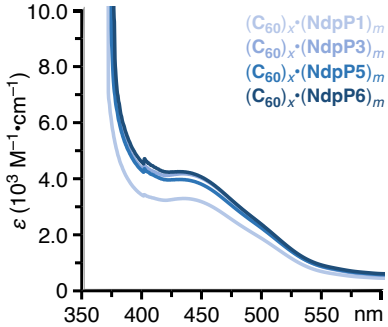

Figure S32. UV-vis spectra (H_2O, 298 K, 2.0 mM based on the amphiphiles) of **(C$_{60}$)**$_x$**•(NdpP1)**$_m$, **(C$_{60}$)**$_x$**•(NdpP3)**$_m$, **(C$_{60}$)**$_x$**•(NdpP5)**$_m$, and **(C$_{60}$)**$_x$**•(NdpP6)**$_m$.

Table S3. Photophysical data of (a) (**Per**)$_x$•(**NdpPn**)$_m$, (b) (**BP**)$_x$•(**NdpPn**)$_m$, and (c) (**C$_{60}$**)$_x$•(**NdpPn**)$_m$ (n = 1, 3, 5, 6) (H_2O, 298 K).

(a)

amphiphile	guest	λ_{max} / nm	λ_{em} / nm
NdpP1	**Per**	401/421/453	608
NdpP3	**Per**	401/421/453	610
NdpP5	**Per**	401/421/453	421/486/605
NdpP6	**Per**	401/422/454	418/487/611

(b)

amphiphile	guest	λ_{max} / nm	λ_{em} / nm
NdpP1	**BP**	455/500	551/655
NdpP3	**BP**	453/500	550/655
NdpP5	**BP**	454/500	551/651
NdpP6	**BP**	453/500	551/638

(c)

amphiphile	guest	λ_{max} / nm	λ_{em} / nm
NdpP1	**C$_{60}$**	433	–
NdpP3	**C$_{60}$**	434	–
NdpP5	**C$_{60}$**	430	–
NdpP6	**C$_{60}$**	429	–

7.3. DLS measurements

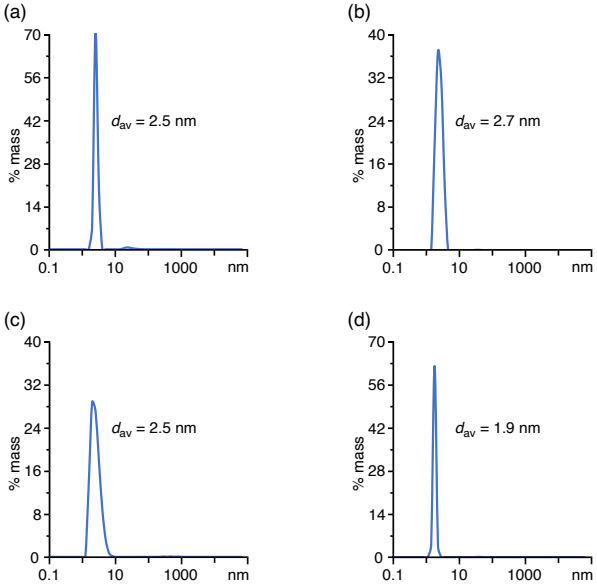

Figure S33. DLS charts (H_2O, 298 K, 2.0 mM based on the amphiphiles) and average diameters of (a) (**Per**)$_x$•(**NdpP1**)$_m$, (b) (**Per**)$_x$•(**NdpP3**)$_m$, (c) (**Per**)$_x$•(**NdpP5**)$_m$, and (d) (**Per**)$_x$•(**NdpP6**)$_m$.

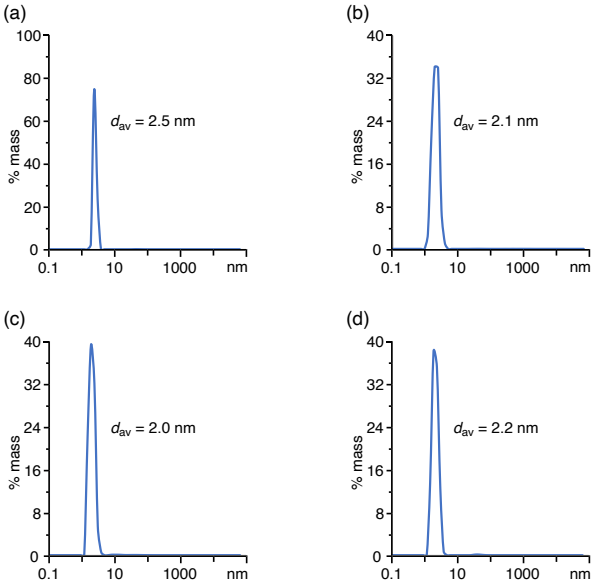

Figure S34. DLS charts (H_2O, 298 K, 2.0 mM based on the amphiphiles) and average diameters of (a) (**BP**)$_x$•(**NdpP1**)$_m$, (b) (**BP**)$_x$•(**NdpP3**)$_m$, (c) (**BP**)$_x$•(**NdpP5**)$_m$, and (d) (**BP**)$_x$•(**NdpP6**)$_m$.

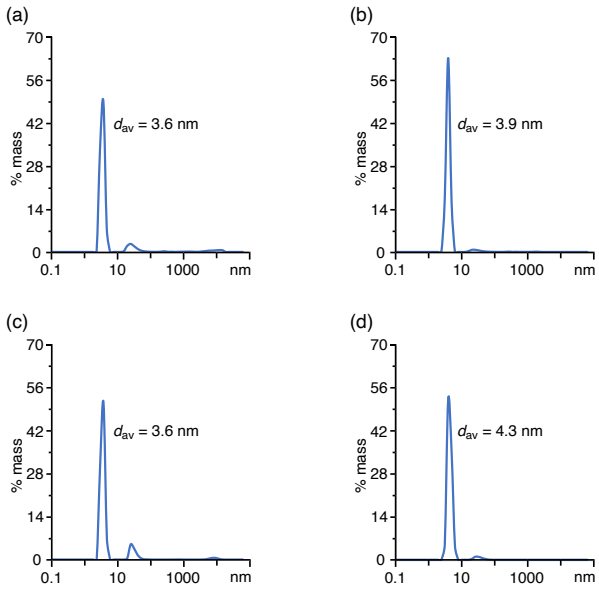

Figure S35. DLS charts (H_2O, 298 K, 2.0 mM based on the amphiphiles) and average diameters of (a) $(\mathbf{C_{60}})_x$•$(\mathbf{NdpP1})_m$, (b) $(\mathbf{C_{60}})_x$•$(\mathbf{NdpP3})_m$, (c) $(\mathbf{C_{60}})_x$•$(\mathbf{NdpP5})_m$, and (d) $(\mathbf{C_{60}})_x$•$(\mathbf{NdpP6})_m$.

7.4. Evaluation of uptake quantity

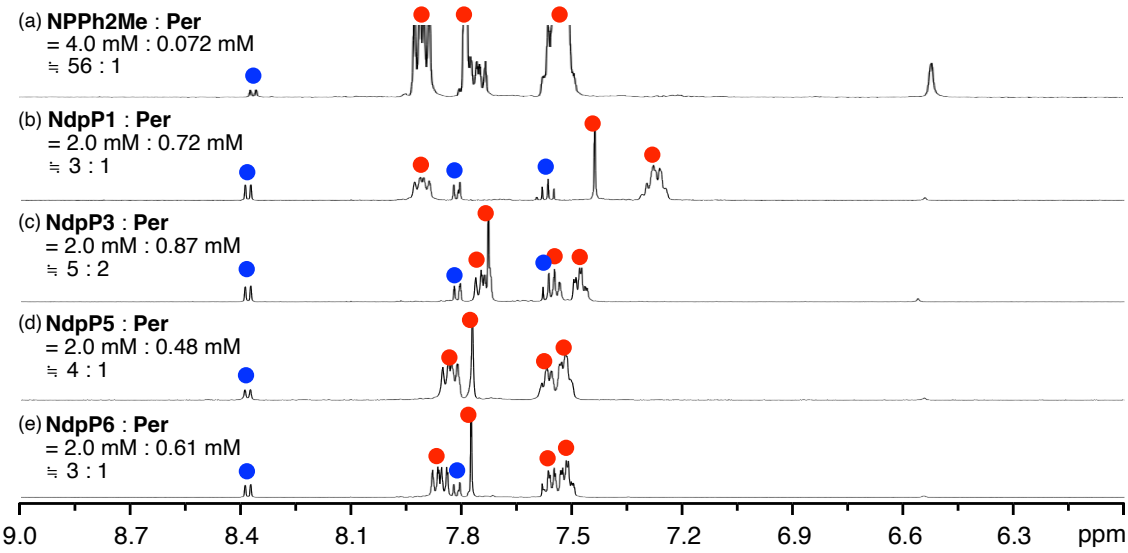

Figure S36. ^{1}H NMR spectra (500 MHz, 298 K, DMSO-d_6) of (a) (**Per**)$_x$•(**NPPh2Me**)$_m$, (b) (**Per**)$_x$•(**NdpP1**)$_m$, (c) (**Per**)$_x$•(**NdpP3**)$_m$, (d) (**Per**)$_x$•(**NdpP5**)$_m$, and (e) (**Per**)$_x$•(**NdpP6**)$_m$. Aqueous solution of host-guest complexes was evaporated and then the residue was dissolved in DMSO-d_6 (red: amphiphiles and blue: **Per**).

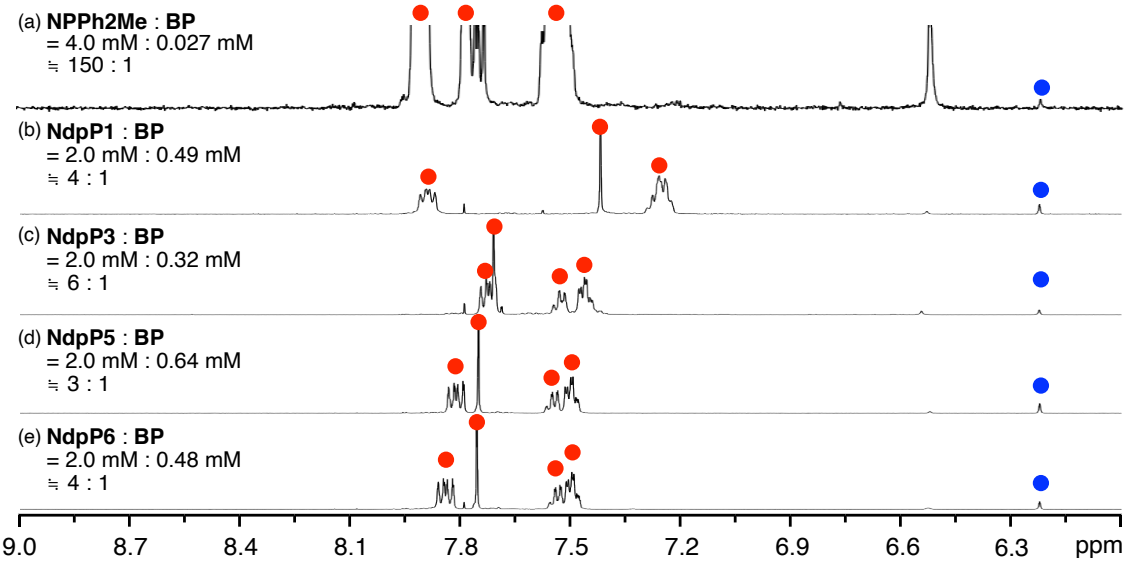

Figure S37. ^{1}H NMR spectra (500 MHz, 298 K, DMSO-d_6) of (a) (**BP**)$_x$•(**NPPh2Me**)$_m$, (b) (**BP**)$_x$•(**NdpP1**)$_m$, (c) (**BP**)$_x$•(**NdpP3**)$_m$, (d) (**BP**)$_x$•(**NdpP5**)$_m$, and (e) (**BP**)$_x$•(**NdpP6**)$_m$. Aqueous solution of host-guest complexes was evaporated and then the residue was dissolved in DMSO-d_6 (red: amphiphiles and blue: **BP**).

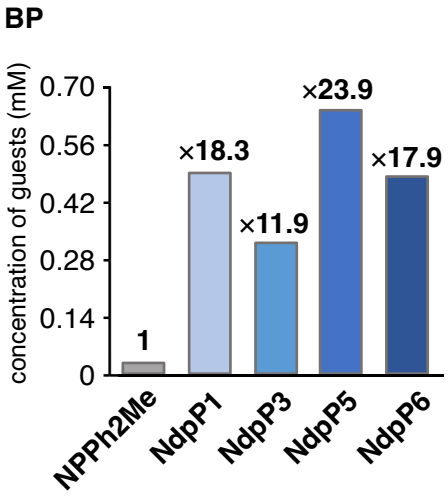

Figure S38. Comparisons of uptake quantity of **BP** by **NPPh2Me** and **NdpPn** (n = 1, 3, 5, 6). The number on the bar indicates relative uptake ratio to **NPPh2Me**.

7.5. Optimized structures

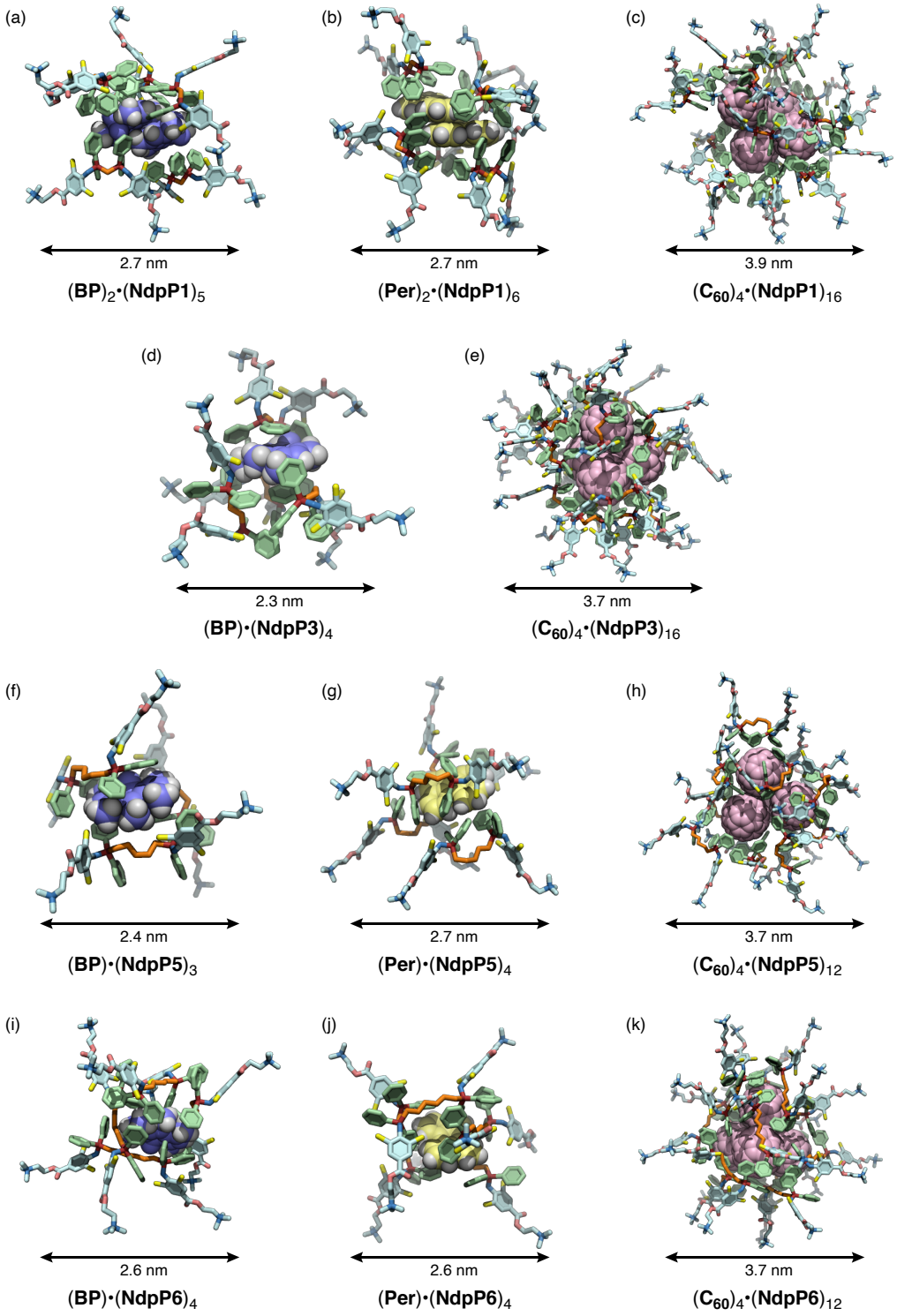

Figure S 39 . Optimized structures of (a) **(BP)**$_2$•**(NdpP1)**$_5$, (b) **(Per)**$_2$•**(NdpP1)**$_6$, (c) **(C$_{60}$)**$_4$•**(NdpP1)**$_{16}$, (d) **(BP)**•**(NdpP3)**$_4$, (e) **(C$_{60}$)**$_4$•**(NdpP3)**$_{16}$, (f) **(BP)**•**(NdpP5)**$_3$, (g) **(Per)**•**(NdpP5)**$_4$, (h) **(C$_{60}$)**$_4$•**(NdpP5)**$_{12}$, (i) **(BP)**•**(NdpP6)**$_4$, (j) **(Per)**•**(NdpP6)**$_4$, (k) **(C$_{60}$)**$_4$•**(NdpP6)**$_{12}$, estimated by molecular mechanics calculation.

8. NMR and MS spectra

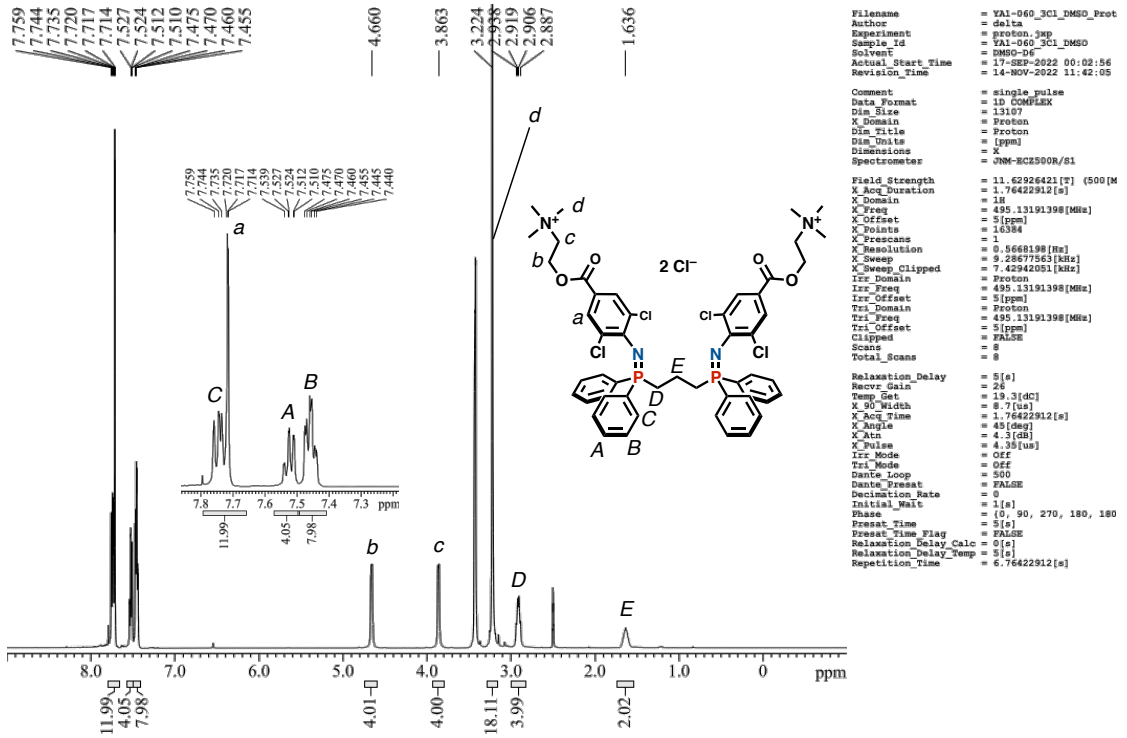

Figure S40. ^{1}H NMR spectrum (500 MHz, DMSO-d_6, 298 K) of **NdpP3**.

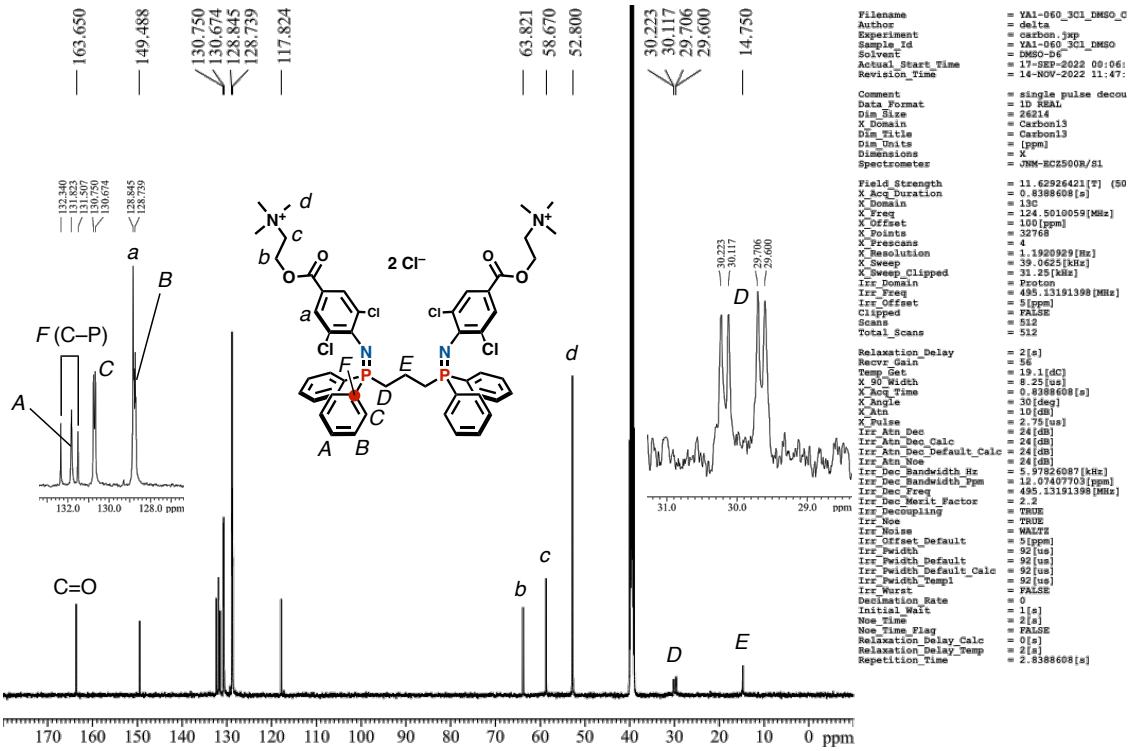

Figure S41. ^{13}C NMR spectrum (125 MHz, DMSO-d_6, 298 K) of **NdpP3**.

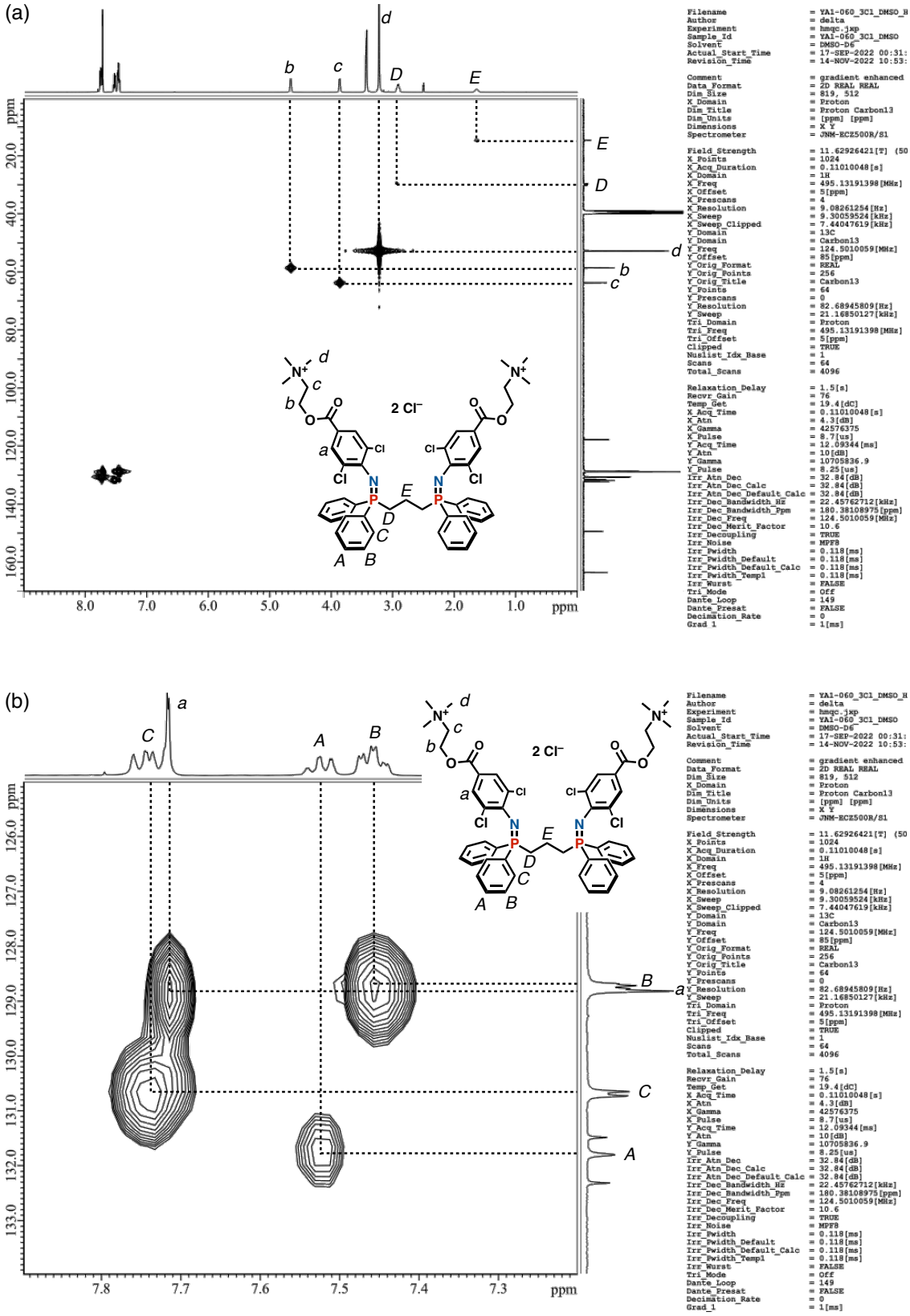

Figure S42. HMQC NMR spectrum (500 MHz, DMSO-d_6, 298 K) of **NdpP3**. (a) Wide region and (b) its aromatic region.

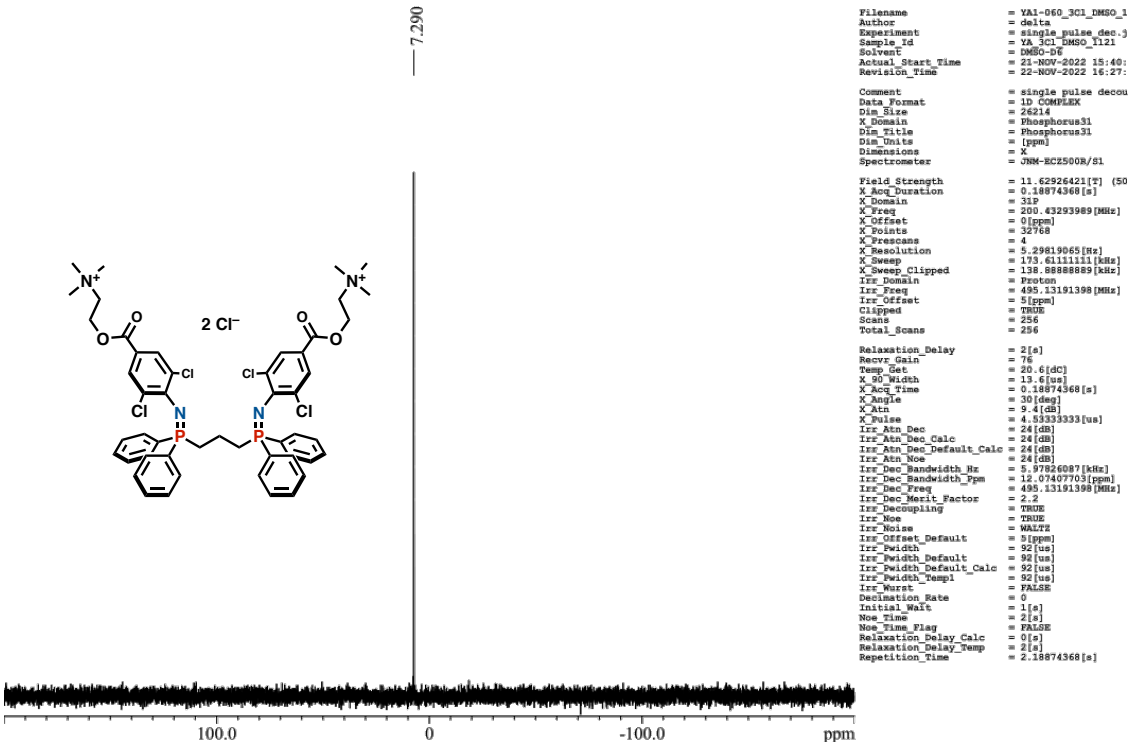

Figure S43. ^{31}P NMR spectrum (202 MHz, DMSO-d_6, 298 K) of **NdpP3**.

Display Report

Analysis Info

Analysis Name	D:\Data\ofcbunseki\irai\2023\toyota_lab\yamashina\231019\NdpP3-000001.d	Acquisition Date	2023/10/19 10:11:25
Method	esi_posi_low.m	Operator	BDAL@DE
Sample Name	NdpP3-	Instrument	micrOTOF 213750.10321
Comment			

Acquisition Parameter

Source Type	ESI	Ion Polarity	Positive	Set Nebulizer	0.3 Bar
Focus	Not active			Set Dry Heater	180 ‹C
Scan Begin	50 m/z	Set Capillary	4500 V	Set Dry Gas	4.0 l/min
Scan End	1500 m/z	Set End Plate Offset	-500 V	Set Divert Valve	Waste

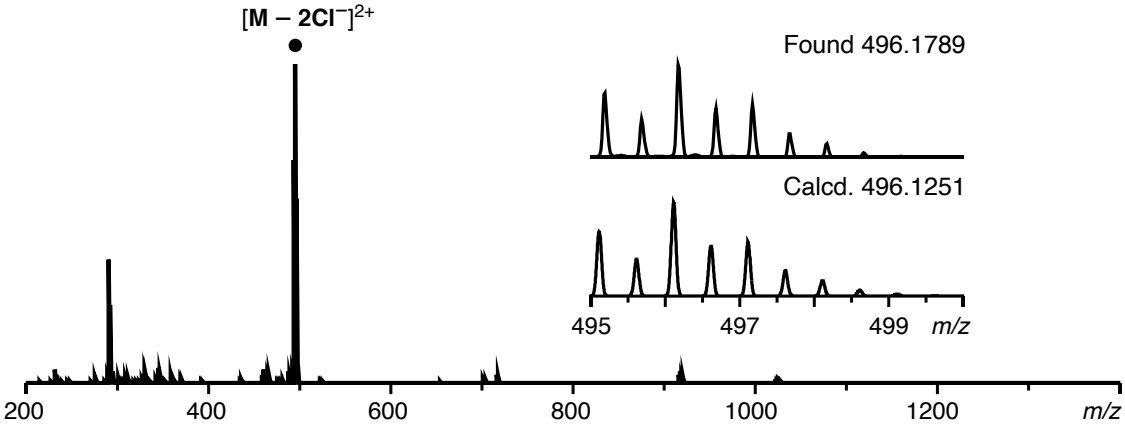

Figure S44. ESI-TOF MS spectrum (CH_3OH/CH_3CN) of **NdpP3**.

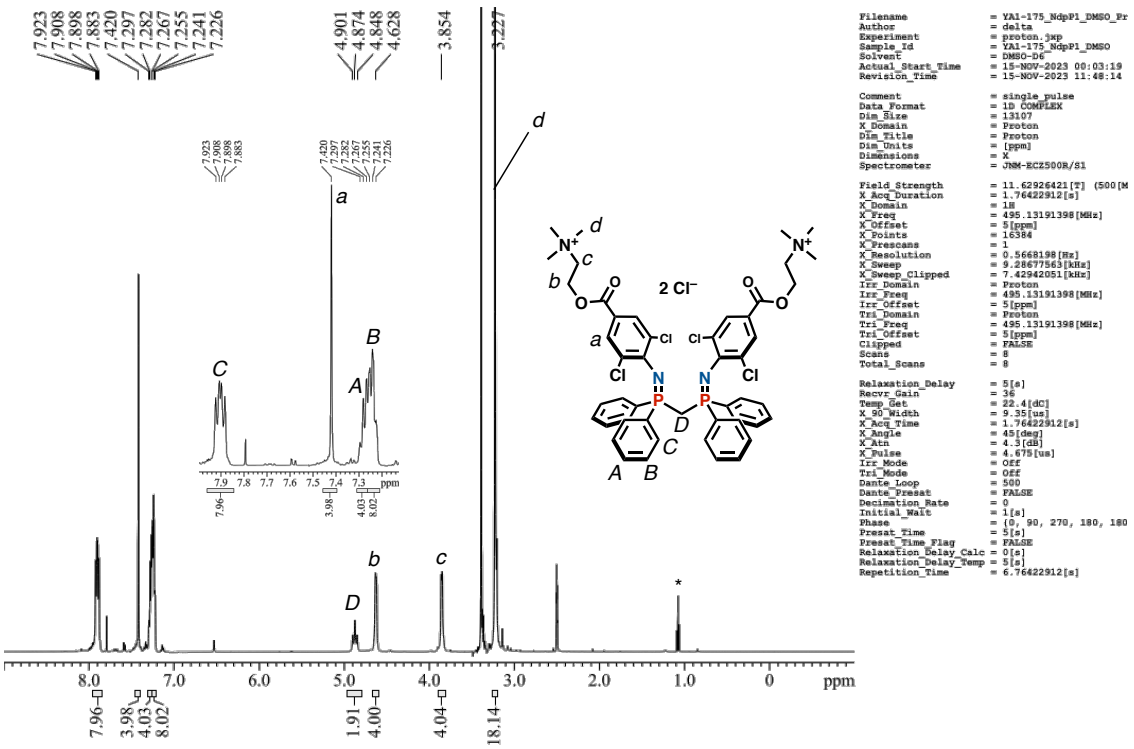

Figure S45. ^{1}H NMR spectrum (500 MHz, DMSO-d_6, 298 K) of **NdpP1** (*: diethyl ether).

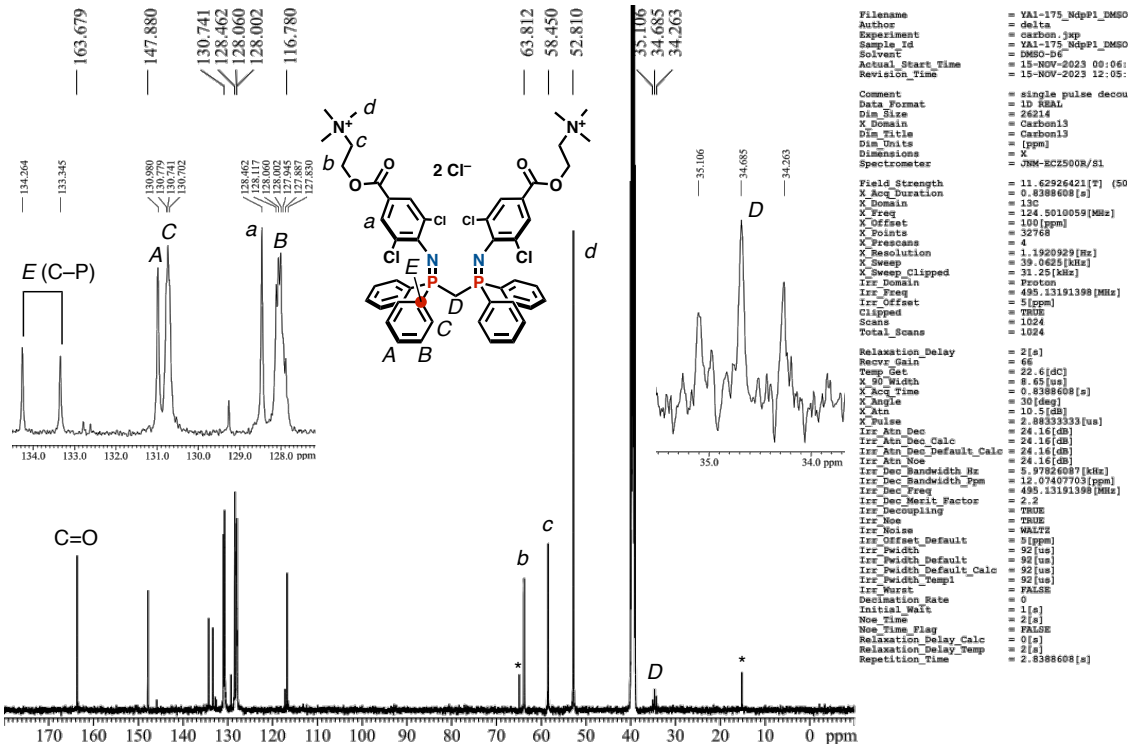

Figure S46. ^{13}C NMR spectrum (125 MHz, DMSO-d_6, 298 K) of **NdpP1** (*: diethyl ether).

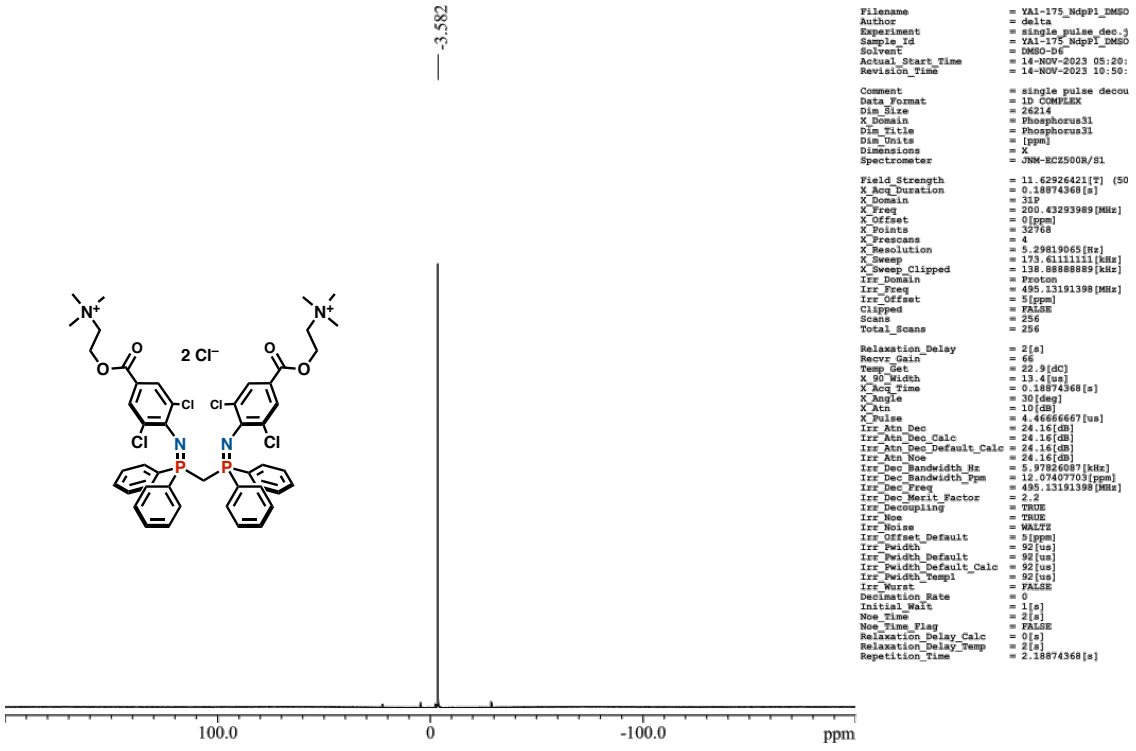

Figure S47. ^{31}P NMR spectrum (202 MHz, DMSO-d_6, 298 K) of **NdpP1**.

Display Report

Analysis Info

Analysis Name	D:\Data\ofcbunseki\irai\2023\toyota_lab\yamashina\231019\NdpP1-000001.d	Acquisition Date	2023/10/19 9:46:36
Method	esi_posi_low.m	Operator	BDAL@DE
Sample Name	NdpP1-	Instrument	micrOTOF 213750.10321
Comment			

Acquisition Parameter

Source Type	ESI	Ion Polarity	Positive	Set Nebulizer	0.3 Bar
Focus	Not active			Set Dry Heater	180 ‹C
Scan Begin	50 m/z	Set Capillary	4500 V	Set Dry Gas	4.0 l/min
Scan End	1500 m/z	Set End Plate Offset	-500 V	Set Divert Valve	Waste

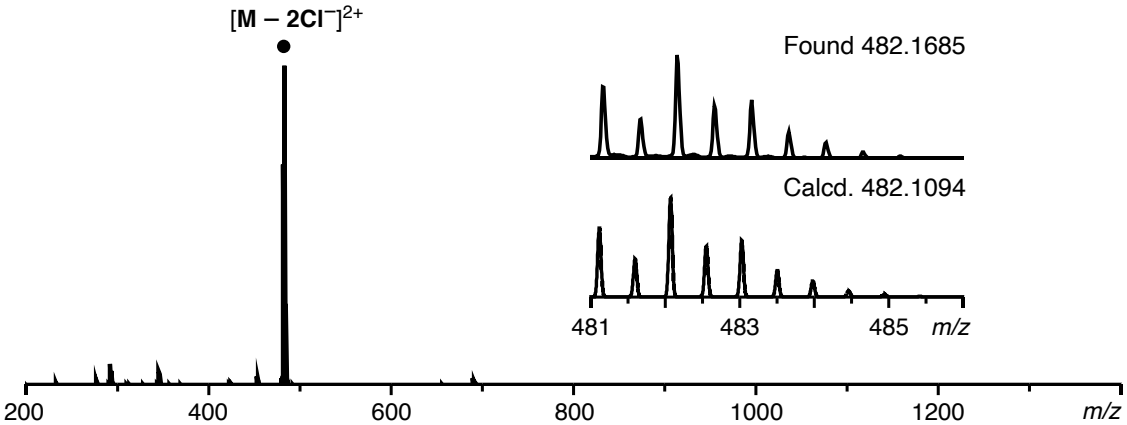

Figure S48. ESI-TOF MS spectrum (CH_3OH/CH_3CN) of **NdpP1**.

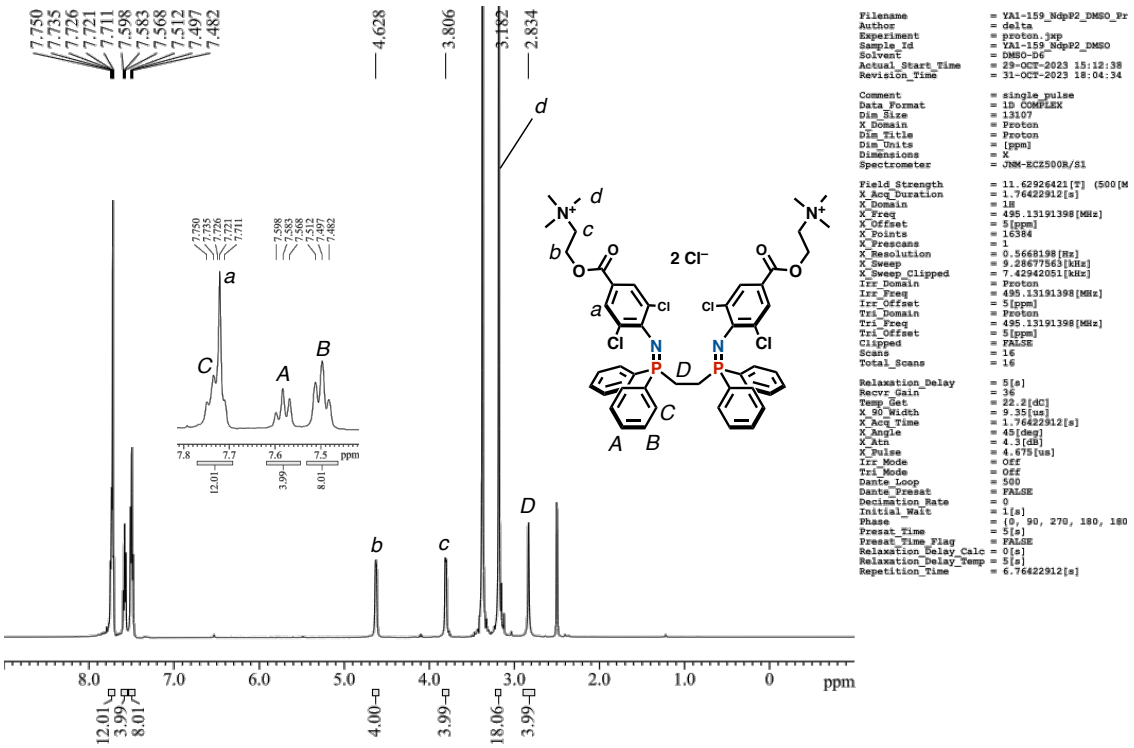

Figure S49. [1]H NMR spectrum (500 MHz, DMSO-d_6, 298 K) of **NdpP2**.

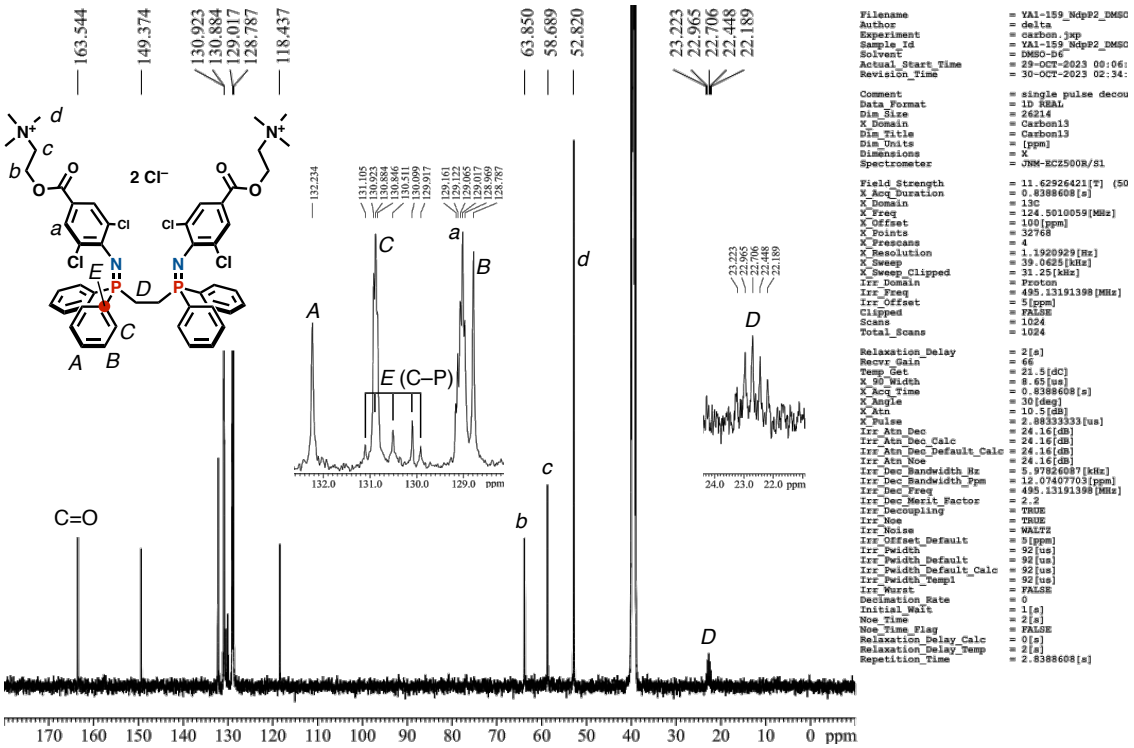

Figure S50. [13]C NMR spectrum (125 MHz, DMSO-d_6, 298 K) of **NdpP2**.

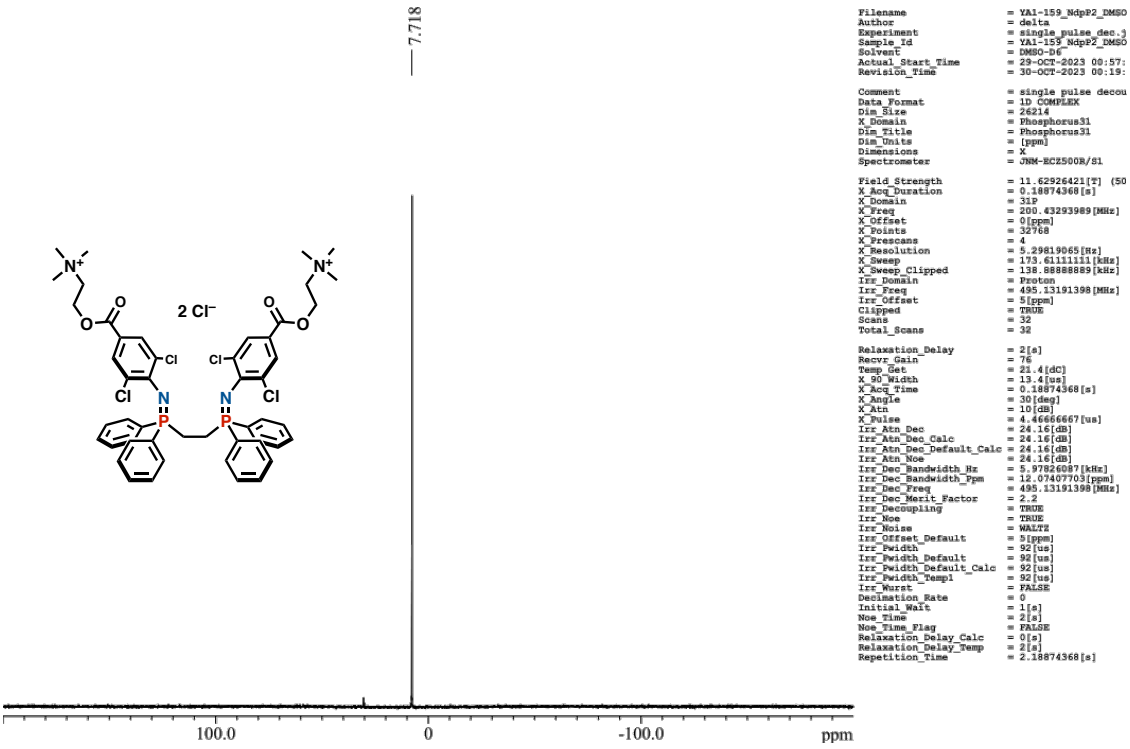

Figure S51. ^{31}P NMR spectrum (202 MHz, DMSO-d_6, 298 K) of **NdpP2**.

Display Report

Analysis Info

Analysis Name	D:\Data\ofcbunseki\irai\2023\toyota_lab\yamashina\231019\NdpP2-000001.d	Acquisition Date	2023/10/19 9:57:22
Method	esi_posi_low.m	Operator	BDAL@DE
Sample Name	NdpP2-	Instrument	micrOTOF 213750.10321
Comment			

Acquisition Parameter

Source Type	ESI	Ion Polarity	Positive	Set Nebulizer	0.3 Bar
Focus	Not active			Set Dry Heater	180 ‹C
Scan Begin	50 m/z	Set Capillary	4500 V	Set Dry Gas	4.0 l/min
Scan End	1500 m/z	Set End Plate Offset	-500 V	Set Divert Valve	Waste

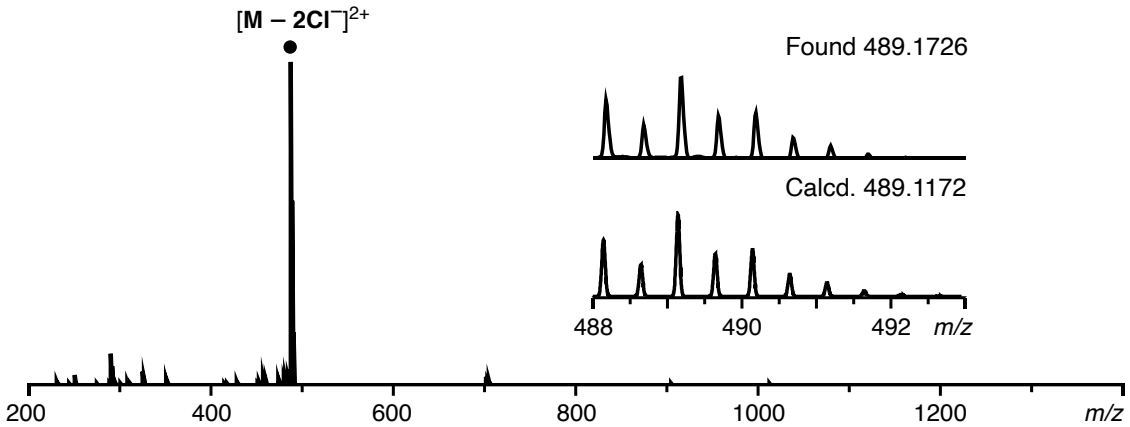

Figure S52. ESI-TOF MS spectrum (CH_3OH/CH_3CN) of **NdpP2**.

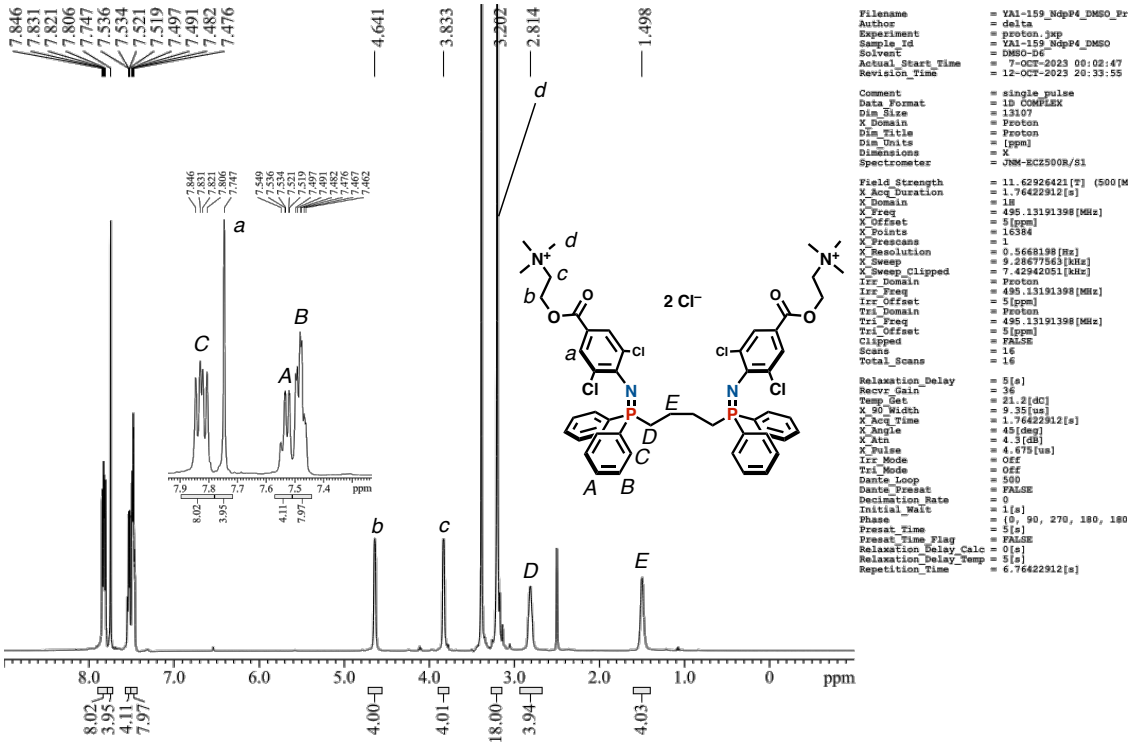

Figure S53. ^{1}H NMR spectrum (500 MHz, DMSO-d_6, 298 K) of **NdpP4**.

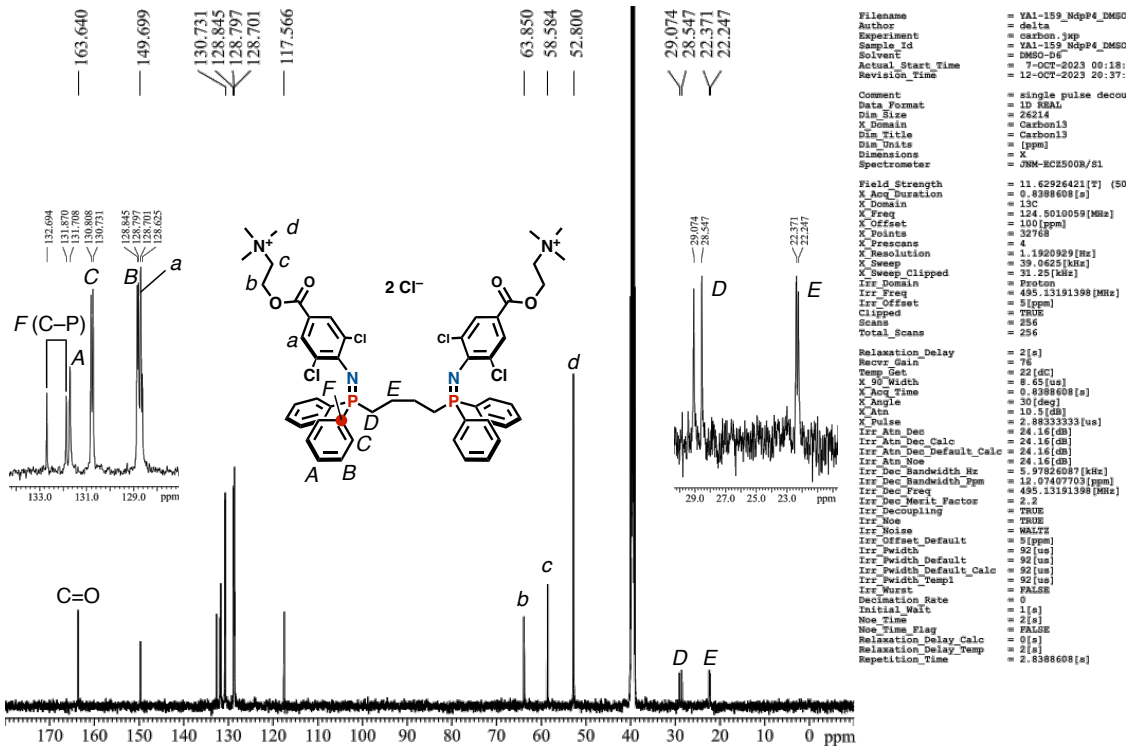

Figure S54. ^{13}C NMR spectrum (125 MHz, DMSO-d_6, 298 K) of **NdpP4**.

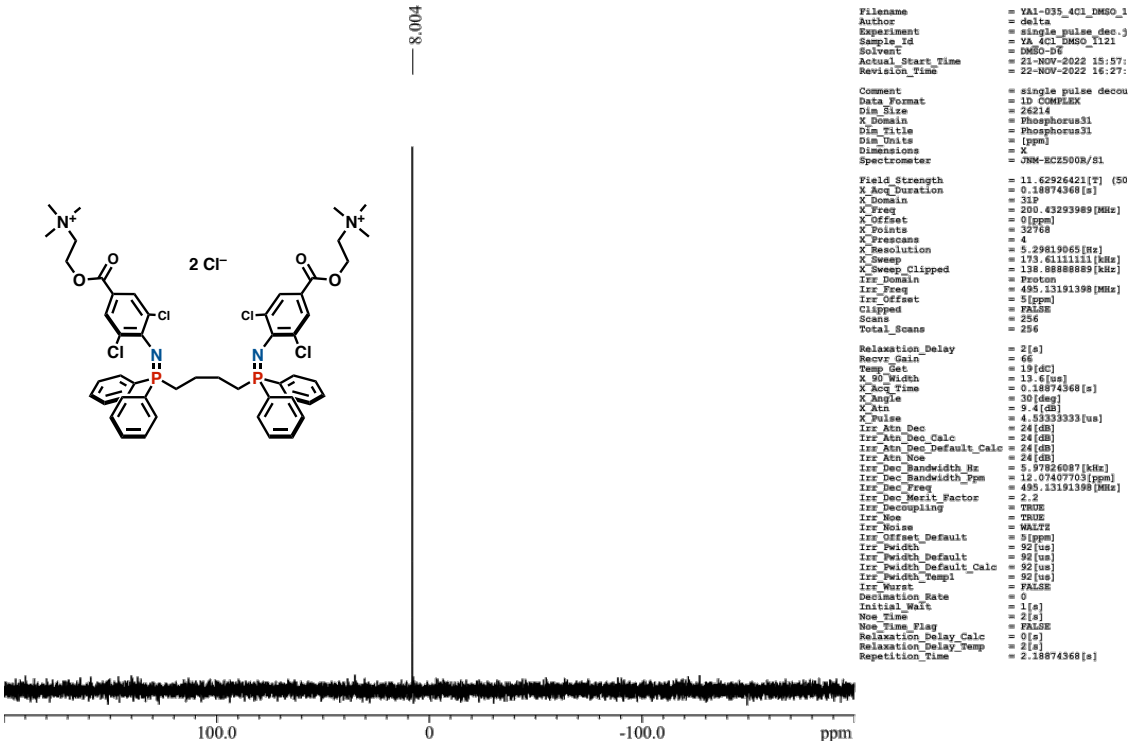

Figure S55. ^{31}P NMR spectrum (202 MHz, DMSO-d_6, 298 K) of **NdpP4**.

Display Report

Analysis Info

Analysis Name	D:\Data\ofcbunseki\irai\2023\toyota_lab\yamashina\231019\NdpP4-000001.d	Acquisition Date	2023/10/19 10:23:25
Method	esi_posi_low.m	Operator	BDAL@DE
Sample Name	NdpP4-	Instrument	micrOTOF 213750.10321
Comment			

Acquisition Parameter

Source Type	ESI	Ion Polarity	Positive	Set Nebulizer	0.3 Bar
Focus	Not active			Set Dry Heater	180 ‹C
Scan Begin	50 m/z	Set Capillary	4500 V	Set Dry Gas	4.0 l/min
Scan End	1500 m/z	Set End Plate Offset	-500 V	Set Divert Valve	Waste

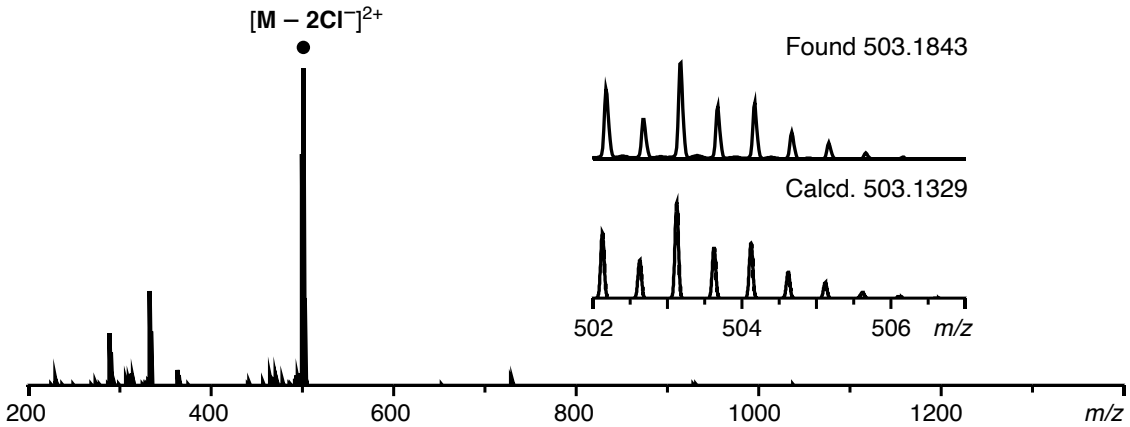

Figure S56. ESI-TOF MS spectrum (CH_3OH/CH_3CN) of **NdpP4**.

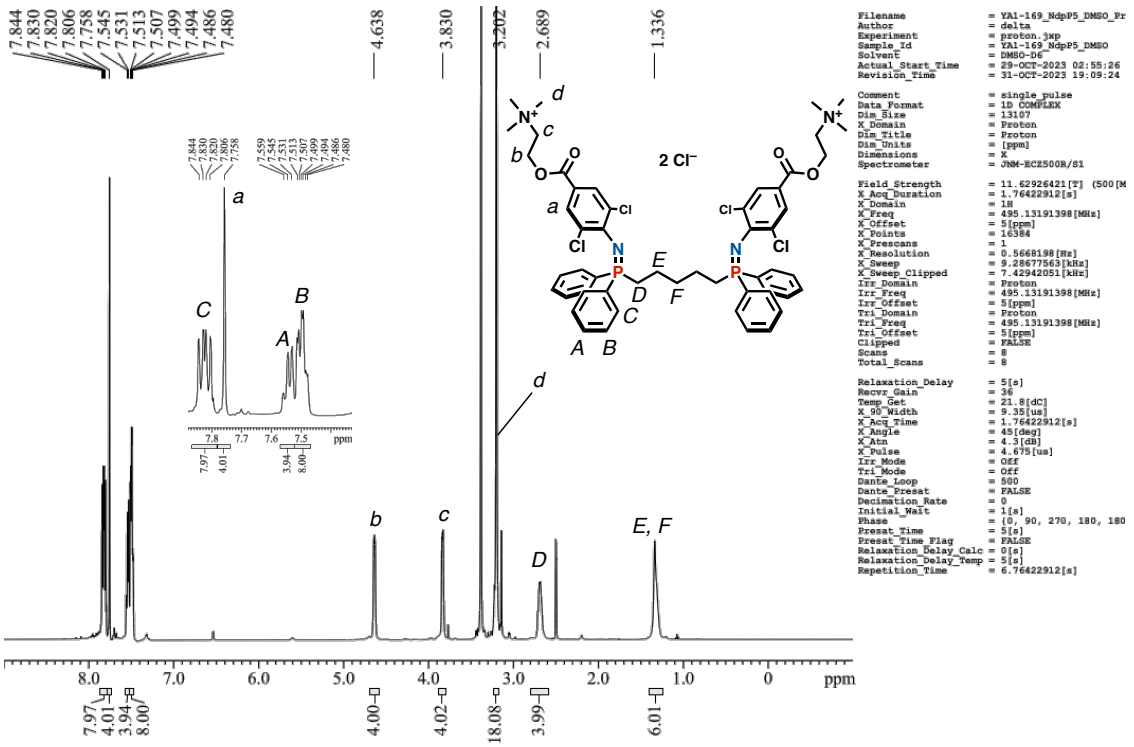

Figure S57. ^{1}H NMR spectrum (500 MHz, DMSO-d_6, 298 K) of **NdpP5**.

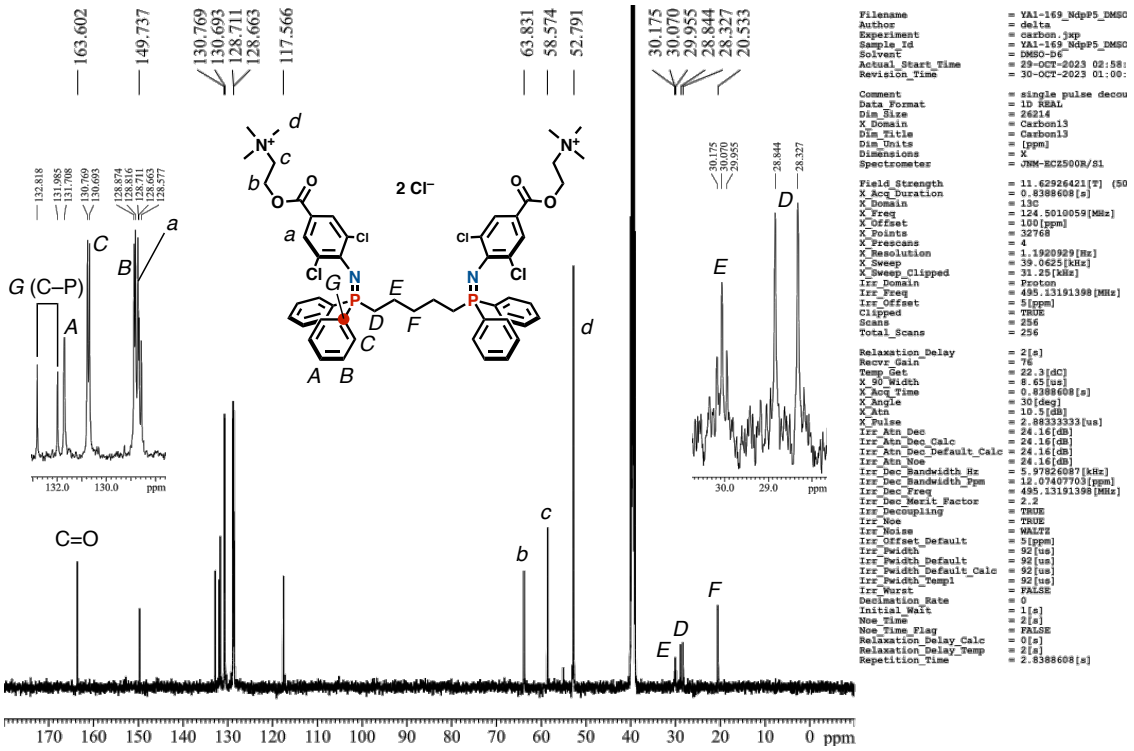

Figure S58. ^{13}C NMR spectrum (125 MHz, DMSO-d_6, 298 K) of **NdpP5**.

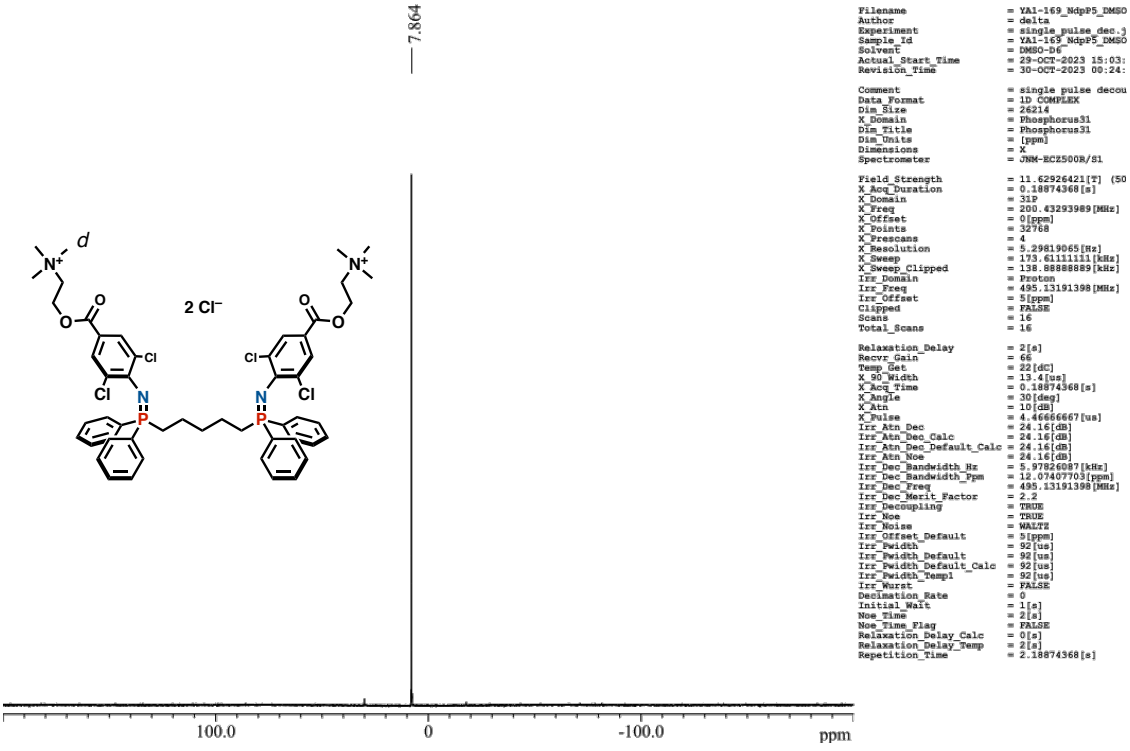

Figure S59. ^{31}P NMR spectrum (202 MHz, DMSO-d_6, 298 K) of **NdpP5**.

Display Report

Analysis Info

Analysis Name	D:\Data\ofcbunseki\irai\2023\toyota_lab\yamashina\231019\NdpP5-000001.d	Acquisition Date	2023/10/19 10:32:59
Method	esi_posi_low.m	Operator	BDAL@DE
Sample Name	NdpP5-	Instrument	micrOTOF 213750.10321
Comment			

Acquisition Parameter

Source Type	ESI	Ion Polarity	Positive	Set Nebulizer	0.3 Bar
Focus	Not active			Set Dry Heater	180 ‹C
Scan Begin	50 m/z	Set Capillary	4500 V	Set Dry Gas	4.0 l/min
Scan End	1500 m/z	Set End Plate Offset	-500 V	Set Divert Valve	Waste

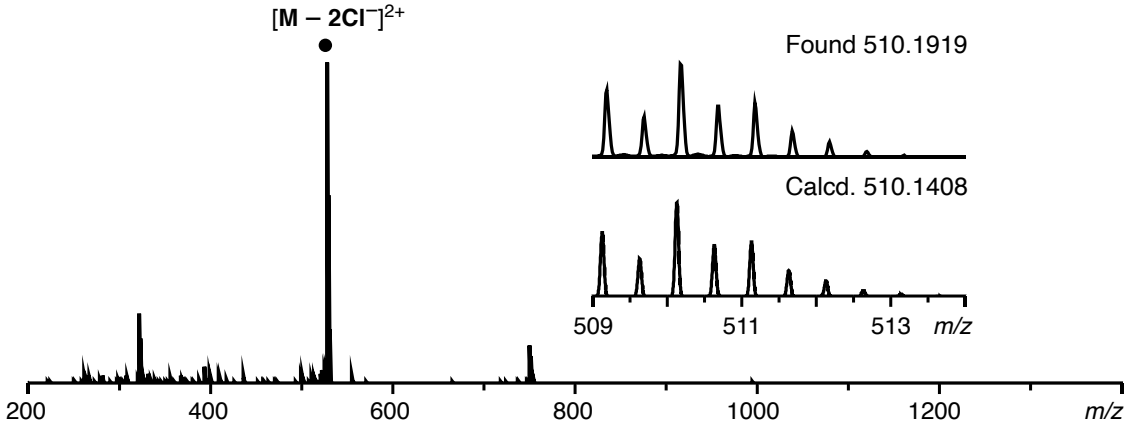

Figure S60. ESI-TOF MS spectrum (CH_3OH/CH_3CN) of **NdpP5**.

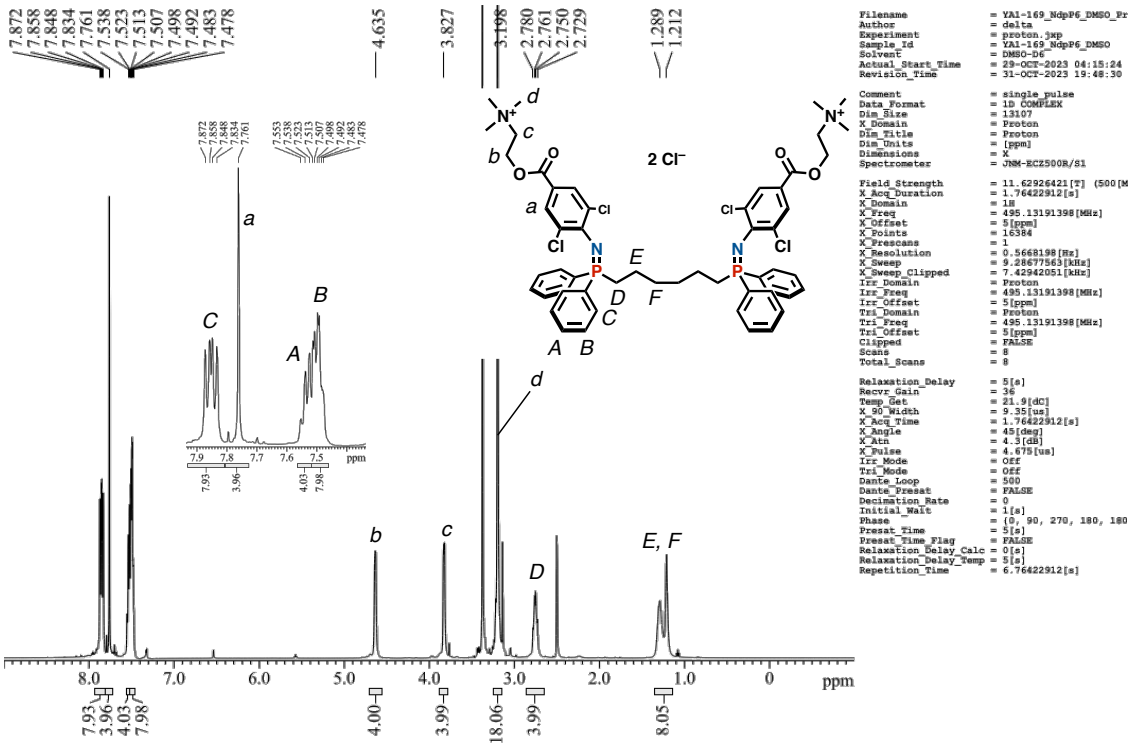

Figure S61. [1]H NMR spectrum (500 MHz, DMSO-d_6, 298 K) of **NdpP6**.

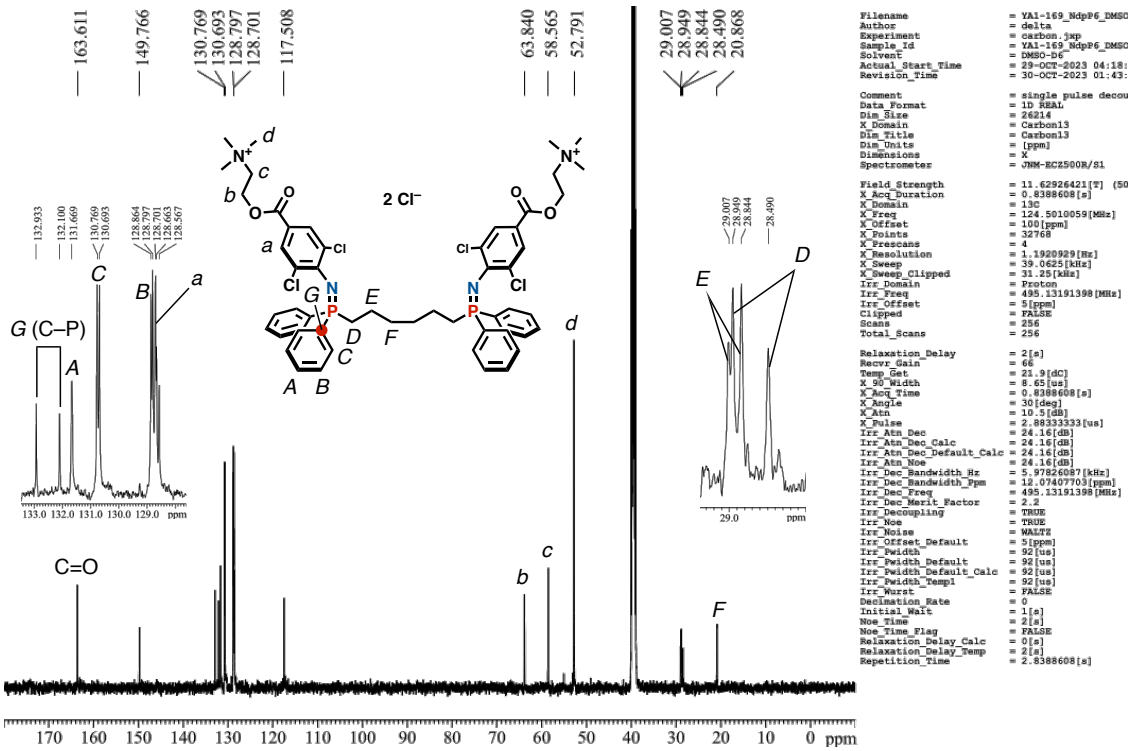

Figure S62. [13]C NMR spectrum (125 MHz, DMSO-d_6, 298 K) of **NdpP6**.

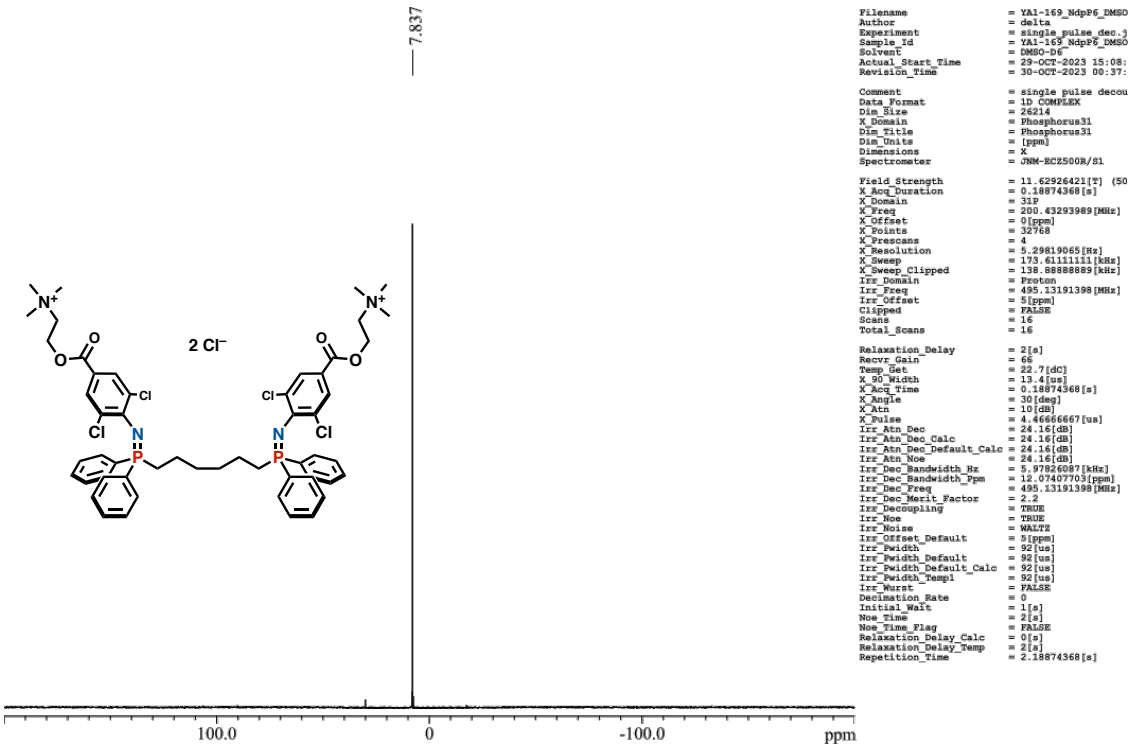

Figure S63. ^{31}P NMR spectrum (202 MHz, DMSO-d_6, 298 K) of **NdpP6**.

Display Report

Analysis Info

Analysis Name	D:\Data\ofcbunseki\irai\2023\toyota_lab\yamashina\231019\NdpP6-000001.d	Acquisition Date	2023/10/19 10:47:12
Method	esi_posi_low.m	Operator	BDAL@DE
Sample Name	NdpP6-	Instrument	micrOTOF 213750.10321
Comment			

Acquisition Parameter

Source Type	ESI	Ion Polarity	Positive	Set Nebulizer	0.3 Bar
Focus	Not active			Set Dry Heater	180 ‹C
Scan Begin	50 m/z	Set Capillary	4500 V	Set Dry Gas	4.0 l/min
Scan End	1500 m/z	Set End Plate Offset	-500 V	Set Divert Valve	Waste

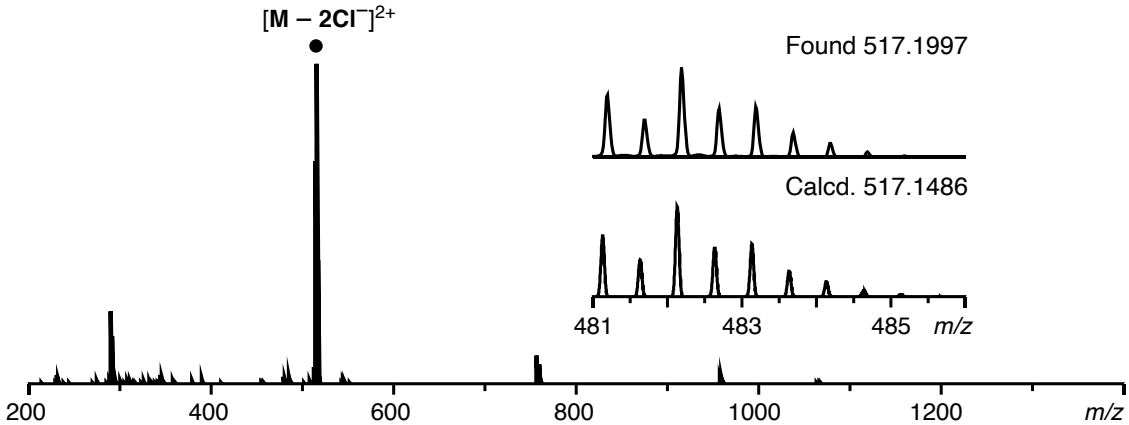

Figure S64. ESI-TOF MS spectrum (CH_3OH/CH_3CN) of **NdpP6**.

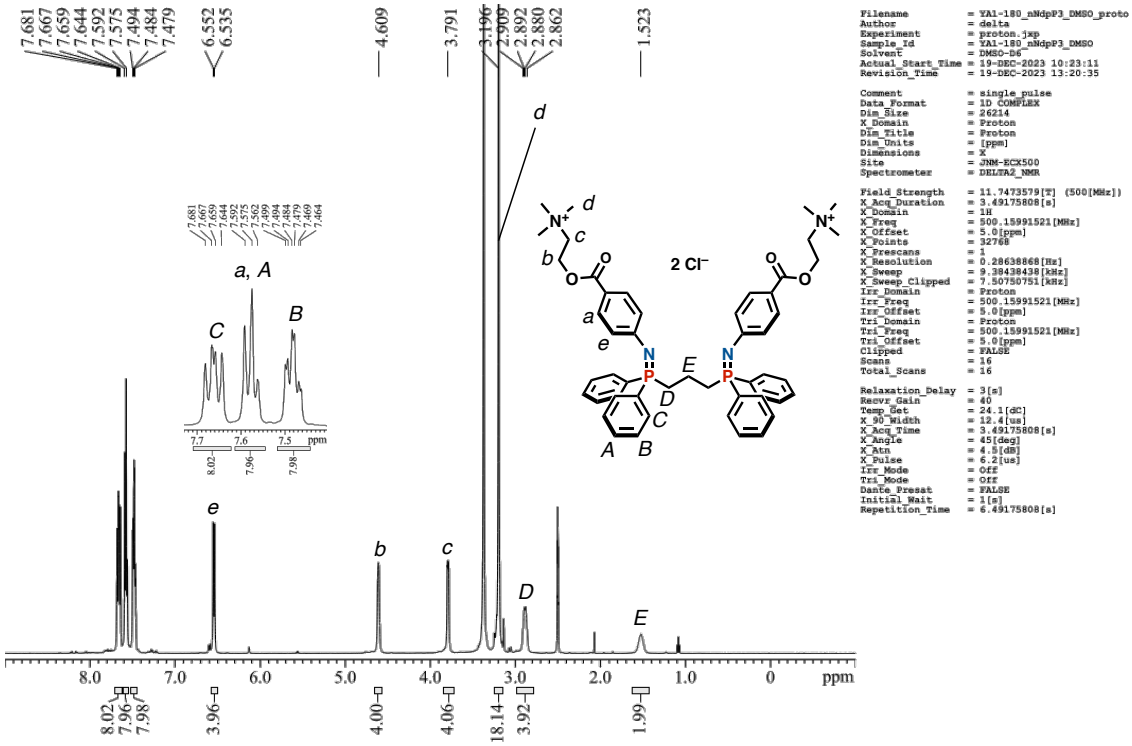

Figure S65. ^{1}H NMR spectrum (500 MHz, DMSO-d_6, 298 K) of **nNdpP3**.

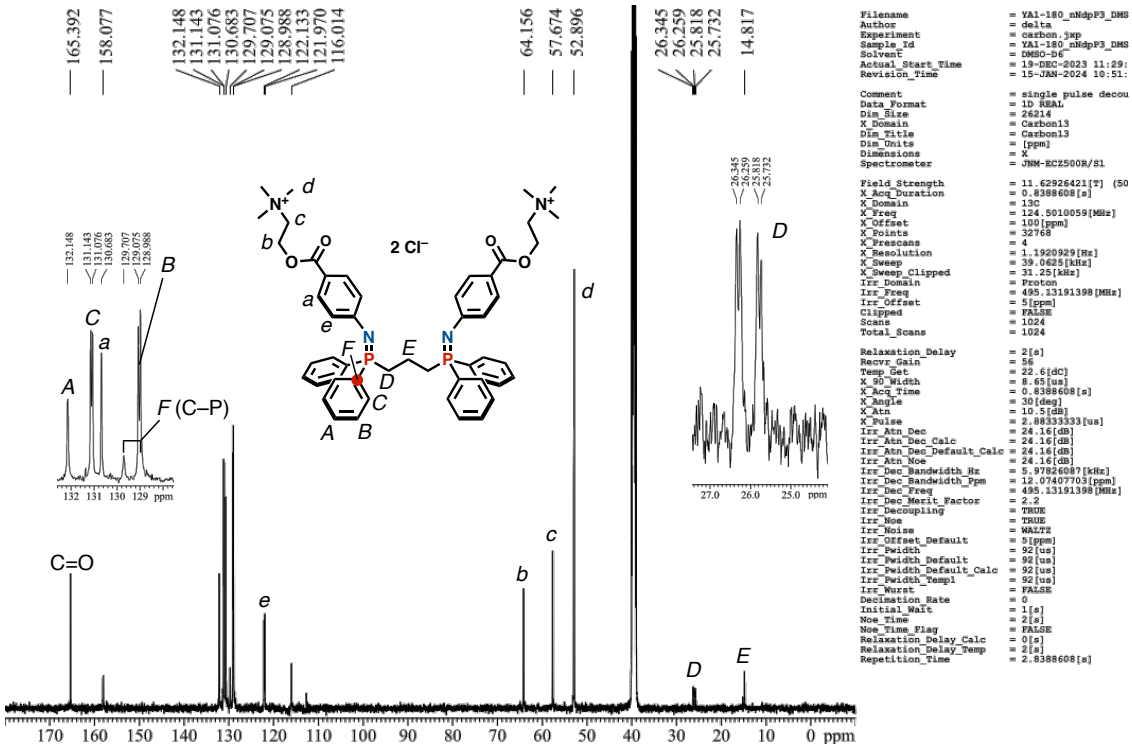

Figure S66. ^{13}C NMR spectrum (125 MHz, DMSO-d_6, 298 K) of **nNdpP3**.

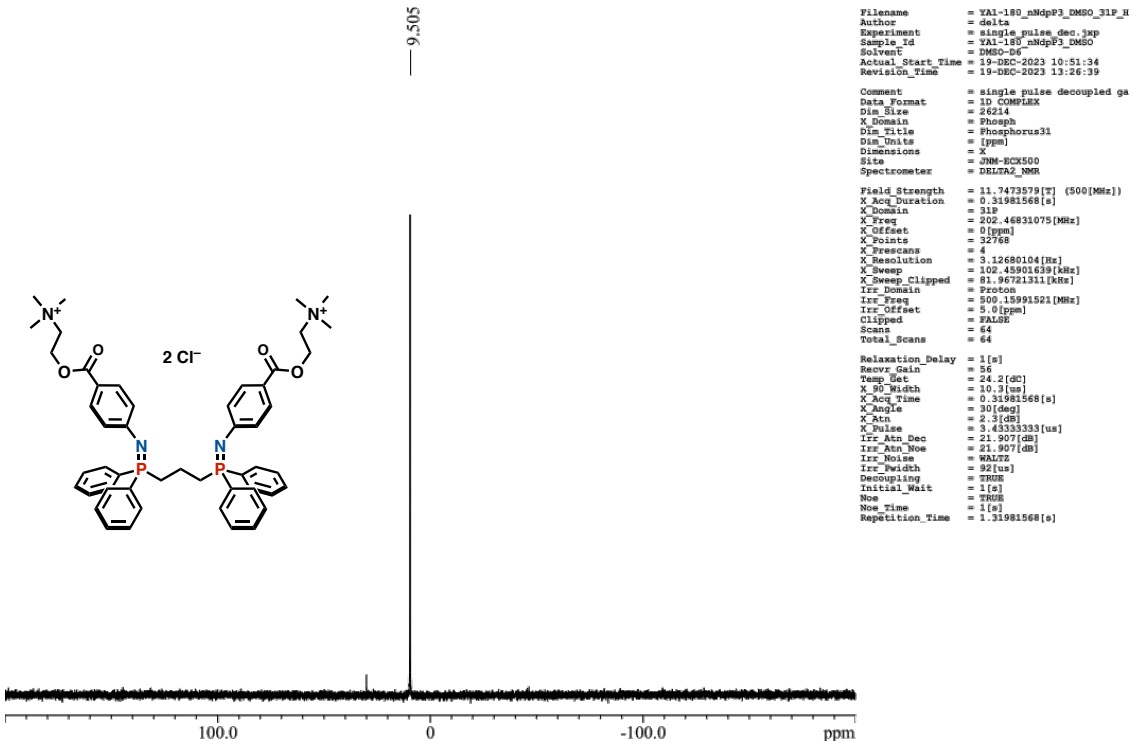

Figure S67. ^{31}P NMR spectrum (202 MHz, DMSO-d_6, 298 K) of **nNdpP3**.

TDCMAS ESI-TOF

Analysis Info			
Analysis Name	D:\Data\ofcbunseki\irai\2023\toyota_lab\akiyama\240119\nNdpP3-000001.d	Acquisition Date	2024/01/18 9:43:54
Method	esi_posi_low.m	Operator	BDAL@DE
Sample Name	nNdpP3-	Instrument / Ser#	micrOTOF 213750.10321
Comment			

Acquisition Parameter					
Source Type	ESI	Ion Polarity	Positive	Set Nebulizer	0.3 Bar
Focus	Not active			Set Dry Heater	180 ‹C
Scan Begin	50 m/z	Set Capillary	4500 V	Set Dry Gas	4.0 l/min
Scan End	1300 m/z	Set End Plate Offset	-500 V	Set Divert Valve	Waste

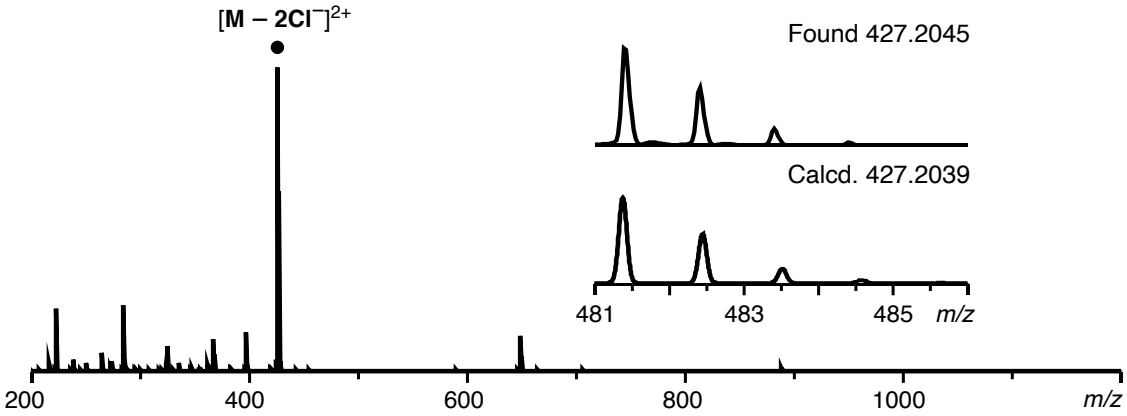

Figure S68. ESI-TOF MS spectrum (CH_3OH/CH_3CN) of **nNdpP3**.

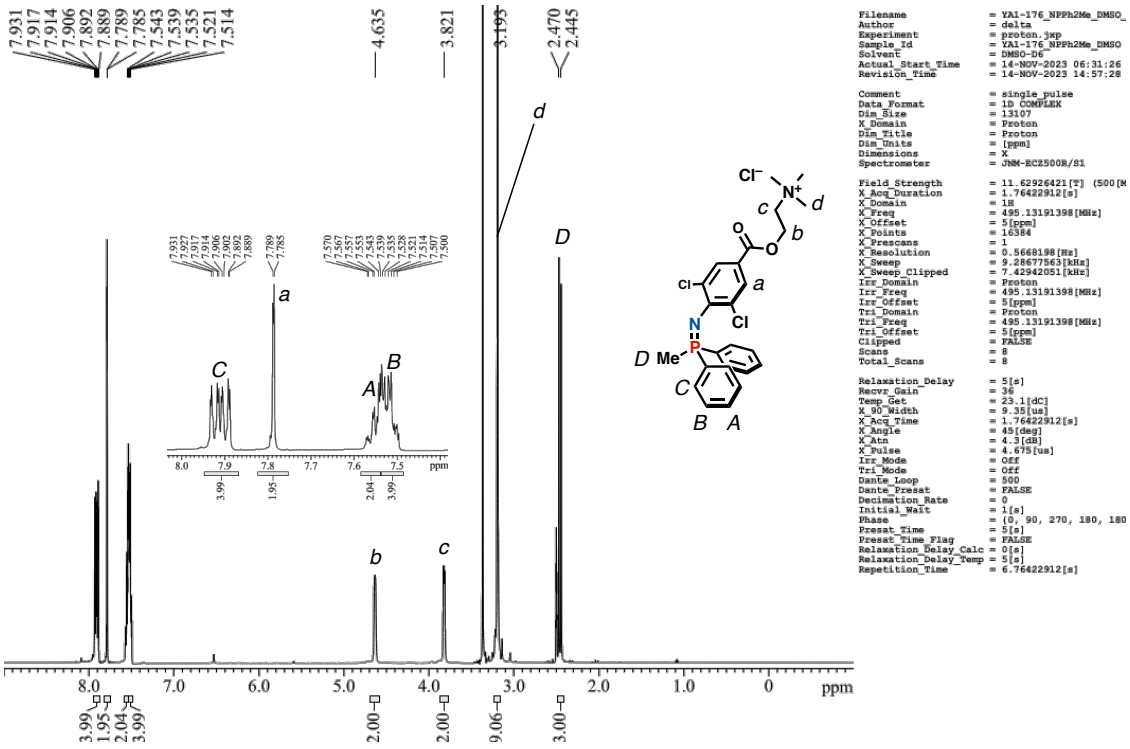

Figure S69. ^{1}H NMR spectrum (500 MHz, DMSO-d_6, 298 K) of **NPPh2Me**.

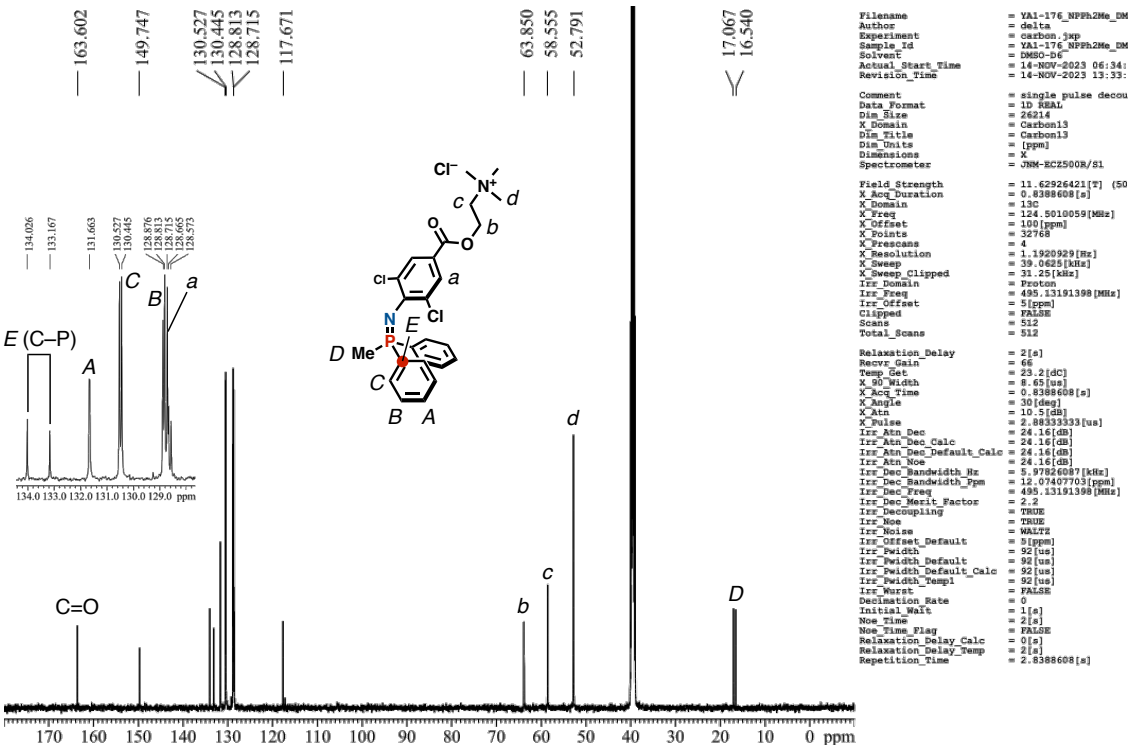

Figure S70. ^{13}C NMR spectrum (125 MHz, DMSO-d_6, 298 K) of **NPPh2Me**.

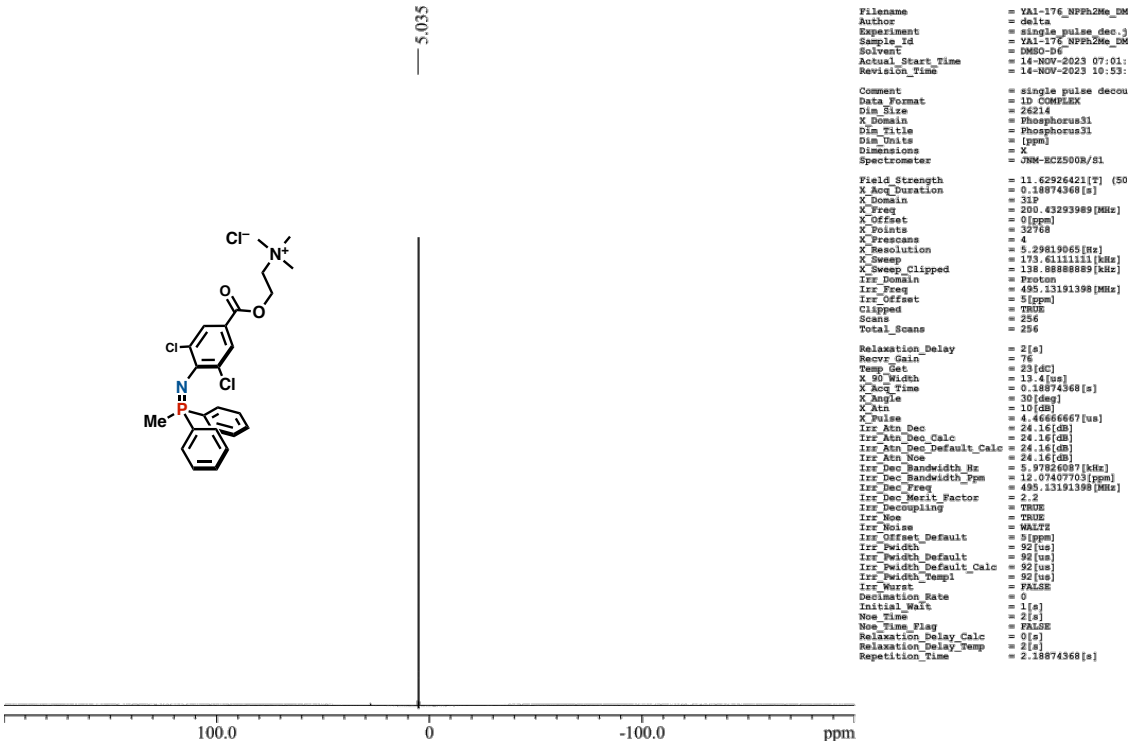

Figure S71. ^{31}P NMR spectrum (202 MHz, DMSO-d_6, 298 K) of **NPPh2Me**.

TDCMAS ESI-TOF

Analysis Info			
Acquisition Date	2024/01/18 9:59:25		
Analysis Name	D:\Data\ofcbunseki\irai\2023\toyota_lab\akiyama\240119\NPPh2Me-000001.d		
Method	esi_posi_low.m	Operator	BDAL@DE
Sample Name	NPPh2Me-	Instrument / Ser#	micrOTOF 213750.10
Comment			321

Acquisition Parameter					
Source Type	ESI	Ion Polarity	Positive	Set Nebulizer	0.3 Bar
Focus	Not active			Set Dry Heater	180 ‹C
Scan Begin	50 m/z	Set Capillary	4500 V	Set Dry Gas	4.0 l/min
Scan End	1300 m/z	Set End Plate Offset	-500 V	Set Divert Valve	Waste

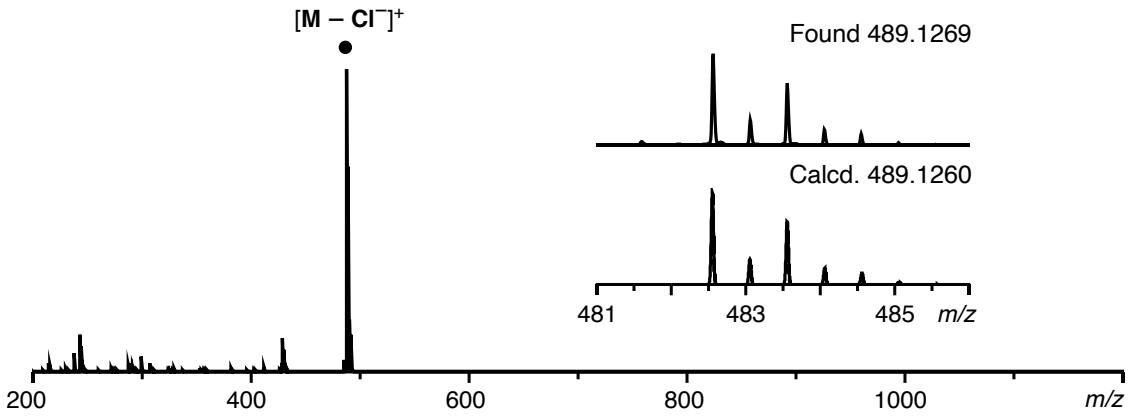

Figure S72. ESI-TOF MS spectrum (CH_3OH/CH_3CN) of **NPPh2Me**.